Charge Transport and Quantum Capacitance of Graphene

by

Jilin Xia

A Dissertation Presented in Partial Fulfillment
of the Requirements for the Degree
Doctor of Philosophy

Approved November 2010 by the
Graduate Supervisory Committee:

N.J. Tao, Chair
David Ferry
Trevor Thornton
Raymond Tsui
Hongbin Yu

ARIZONA STATE UNIVERSITY

December 2010

ABSTRACT

Graphene, a one atomic thick planar sheet of carbon atoms, has a zero gap band structure with a linear dispersion relation. This unique property makes graphene a favorite for physicists and engineers, who are trying to understand the mechanism of charge transport in graphene and using it as channel material for field effect transistor (FET) beyond silicon. Therefore, an in-depth exploring of these electrical properties of graphene is urgent, which is the purpose of this dissertation. In this dissertation, the charge transport and quantum capacitance of graphene were studied.

Firstly, the transport properties of back-gated graphene transistor covering by high dielectric medium were systematically studied. The gate efficiency increased by up to two orders of magnitude in the presence of a high top dielectric medium, but the mobility did not change significantly. The results strongly suggested that the previously reported top dielectric medium-induced charge transport properties of graphene FETs were possibly due to the increase of gate capacitance, rather than enhancement of carrier mobility.

Secondly, a direct measurement of quantum capacitance of graphene was performed. The quantum capacitance displayed a non-zero minimum at the Dirac point and a linear increase on both sides of the minimum with relatively small slopes. The findings - which were not predicted by theory for ideal graphene - suggested that scattering from charged impurities also influences the quantum capacitance. The capacitances in aqueous solutions at different ionic concentrations were also measured, which strongly suggested that the

longstanding puzzle about the interfacial capacitance in carbon-based electrodes had a quantum origin.

Finally, the transport and quantum capacitance of epitaxial graphene were studied simultaneously, the quantum capacitance of epitaxial graphene was extracted, which was similar to that of exfoliated graphene near the Dirac Point, but exhibited a large sub-linear behavior at high carrier density. The self-consistent theory was found to provide a reasonable description of the transport data of the epitaxial graphene device, but a more complete theory was needed to explain both the transport and quantum capacitance data.

DEDICATION

To my beloved parents for their over years' breeding and education.

To my dear wife for her everlasting love and support.

To my little son for the happiness he brings into my life.

ACKNOWLEDGMENTS

First of all, I would like to thank my advisor, Prof. Nongjian Tao, for his continuous guidance, encouragement, and supports. My experience of working as a student of Prof. Nongjian Tao is an invaluable treasure, which will benefit my whole life. His dedication and passion motivated me during the past years and will keep me moving in the future.

Very special thanks to Prof. David Ferry, for providing insightful suggestions and devoting a lot of his precious time to me. He is really a great person to work with and to learn from.

I would also like to thank Profs., David Ferry,Trevor Thornton, Raymond Tsui and Hongbin Yu, for serving on my committee.

It is a great joy to work in Dr. Tao's group, with generous help from them. I would like to thanks Drs. Erica Forzani, Fang Chen, Xiulan Li, Ismael Perez-Diez, Joshua Hihath, Francis Tsow, Kyle Foley, Rodrigo Lglesias, Shaopeng Wang, Lihua Zhang, Xiaojun Xian, Wei Wang, as well as Mr. Xiaonan Shan, Thomas Hines, Christopher Bruot, Chen Cheng, Shaoying Guo, Tianle Gao Miss. Rui Wang and Yan Guan. I will always remember the times working with all of you.

Thanks to my collaborators from navy research lab, Drs. J.L.Tedesco, D.K.Gaskill, for their samples and useful discussions.

Thanks to staffs in CSSER for technical support and helpful suggestions.

TABLE OF CONTENTS

Page

LIST OF TABLES vii

LIST OF FIGURES viii

CHAPTER

1 INTRODUCTION 1

1.1 What is Graphene 1

1.2 Band Structure of Graphene 4

1.3 Graphene Synthesis and Characterization 7

1.4 Graphene Derivatives 16

1.5 Graphene Applications 23

1.6 Milestones of Graphene Development 29

2 THEORIES OF CHARGE TRANSPORT IN GRAPHENE 31

2.1 Diffusive Transport in Graphene 31

2.2 The Self Consistent Theory of Graphene 34

2.3 Ballistic Transport in Graphene 38

3 TRANSPORT OF GRAPHENE WITH TOP HIGH K MEDIUM 41

3.1 Introduction 41

3.2 Mobility Definitions 42

3.3 Experiments, Results and Discussions 44

3.4 Conclusions 53

4 QUANTUM CAPACITANCE OF EXFOLIATED GRAPHENE 54

4.1 Introduction 54

CHAPTER Page

4.2 Experiment Methods 57

4.3 Quantum Capacitance of Single Layer Graphene 59

4.4 Quantum Capacitance of Double Layer Graphene..... 70

4.5 Conclusions..... 74

5 TRANSPORT AND QUANTUM CAPACITANCE PROPERTIES OF EPITAXIAL GRAPHENE..... 76

5.1 Introduction..... 76

5.2 Experiment Methods 78

5.3 Results and Discussions 81

5.4 Conclusions..... 87

6 SUMMARY AND FUTURE 88

6.1 Summary..... 88

6.2 Future 89

REFERENCES 91

APPENDIX

A BOLTZMANN TRANSPORT THEORY 105

B HYSTERESIS IN GRAPHENE 109

LIST OF TABLES

Table Page

1.1. Comparison of different methods for graphene synthesis 12

LIST OF FIGURES

Figure Page

1.1. Schematic of free standing graphene 1

1.2. Graphene: Mother of all graphitic forms 2

1.3. Statistics of papers published related to graphene and bilayer graphene each year on arxiv.org 3

1.4. Band structure of graphene 5

1.5. Quantum Electrodynamics in graphene 7

1.6. Schematic of graphene synthesis methods 12

1.7. Optical Images of graphene with different thickness 13

1.8. Raman spectrum of graphene layers 15

1.9. Graphene characterization using(a)AFM; (b)STM; (c) TEM 16

1.10. Bilayer graphene band gap opening 17

1.11. Graphene Nanoribbons 19

1.12. Graphene Nanomesh 20

1.13. Graphene Doping 23

1.14. Applications of graphene 29

1.15. Milestones of graphene development 30

2.1. (a) Electron Hole Puddles in graphene; (b) Conductivity of graphene as function of carrier density and impurity density 33

2.2. The Self Consistent Theory of graphene transport 37

2.3. Ballistic Transport of Graphene 40

Figure Page

3.1. Screening Effects of top layer dielectric materials on transport properties of graphene FET 46

3.2. Dependence of (a) mobility, (b) residual carrier density and (c) the gate capacitance of graphene FET on NaF concentration 47

3.3. Size effect of top dielectric medium 49

3.4. Simulations of gate capacitance of graphene FET 51

3.5. Real-time transport current of a graphene EFT exposed to a water droplet 52

4.1. Schematic illustration of quantum capacitance measurement setup 58

4.2. Capacitance of graphene as function of gate potential 61

4.3. Theoretical calculation of graphene (a) band structure;(b) carrier density; (c) quantum capacitance 63

4.4 . Dependence of quantum capacitance on potential of graphene 67

4.5. Interfercial Capacitance of graphene in aqueous solution 69

4.6. Capacitance of bilayer graphene as a function of gate potential. 71

4.7. Theoretical calculation of (a) band structure and (b) quantum capacitance of perfect bilayer graphene. 74

5.1. Schematic structure of ideal epitaxial graphene 77

5.2. TEM images of epitaxial graphene and schematic strutures with interlayers 77

Figure Page

5.3. (a) Raman spectrum of single layer epitaxial graphene measured in the channel region after FET device fabrication. (b) Schematic diagram of the experimental setup. 81

Chapter 1

INTRODUCTION

1.1 What is Graphene?

Graphene, named by 'graphite + ene', is a one atomic thick planar sheet of sp^2-bonded carbon atoms arranged in a honeycomb crystal lattice (Fig.1.1). The thickness of graphene is only 0.34nm. Graphene is called the mother of all graphitic forms (Fig. 1.2)[1], can be used as building blocks for three-dimensional graphite(3D), one-dimensional(1D) carbon nanotube, until zero dimensional(0D) fullerene. It is so special for the electrons in it are strictly confined to a two-dimensional (2D) plane, which are so attractive to physicists for exploring properties of 2D electron gas. Theoretical works can be traced back to the early 1940s[2, 3]. However, at that time, it was believed that 2D crystals were thermodynamically unstable and could not exist[4, 5], because the melting temperature of thin films decreases rapidly with decreasing thickness, and the films segregate into islands or decomposes[1]. Consequently, researches in this field was limited to theoretical studies[6].

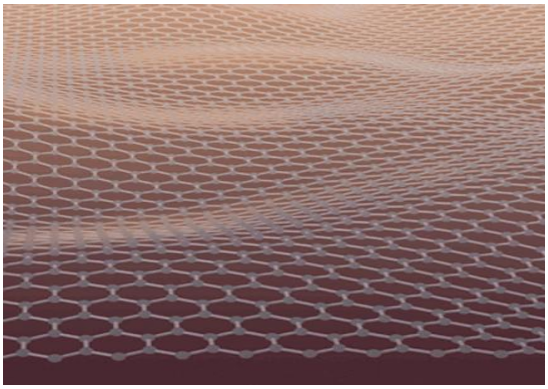

Figure 1.1. Schematic of free standing graphene

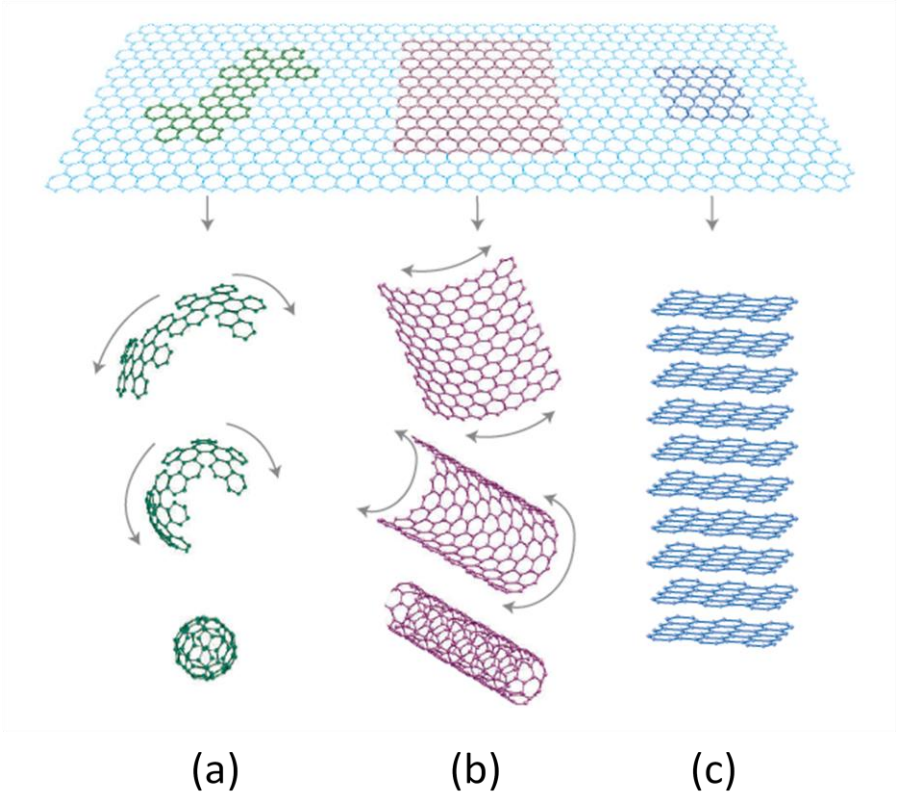

Figure 1.2. Graphene: Mother of all graphitic forms. (a) 0D fullerene; (b) 1D carbon nanotube; (c) 3D graphite [1].

Into 21st century, following the Moore Law, Si-based semiconductor industry has been rapidly developed for more than 50 years, and will soon encounter both scientific and technical limits. This requires the industry to explore new materials and technologies. For the diversity of its allotropes and mass storage in nature, carbon becomes a fascinating candidate. Especially after the successful synthesis of carbon nanotube in 1991 by S. Iijima [7], carbon based electronics has been highly developed[8, 9], and over 1000 papers has been published, attracting attention from physicists, chemists, material scientists, and engineers. Stimulated by the achievement of carbon nanotube, interests on graphene have been regained.

Pioneer work starts from top-down processing method, trying to make the graphite thinner and thinner mechanically [10-13], or chemically[14,15]. Finally, in 2004, Andre Geim and Konstantin Novoselov at Manchester University isolated single layer graphene successfully, by a unbelievable easy mechanical exfoliation method just using scotch tape [16]. It is really a milestone for graphene society, since then, researches on graphene spread out all over the world. Fig. 1.3 shows the statistics of papers published each year related to graphene (single /thicker layers) [17], only on www.arxiv.org. Graphene has attracted interests from researchers majored in physics, electrical engineer, material scientist, chemistry and even biology.

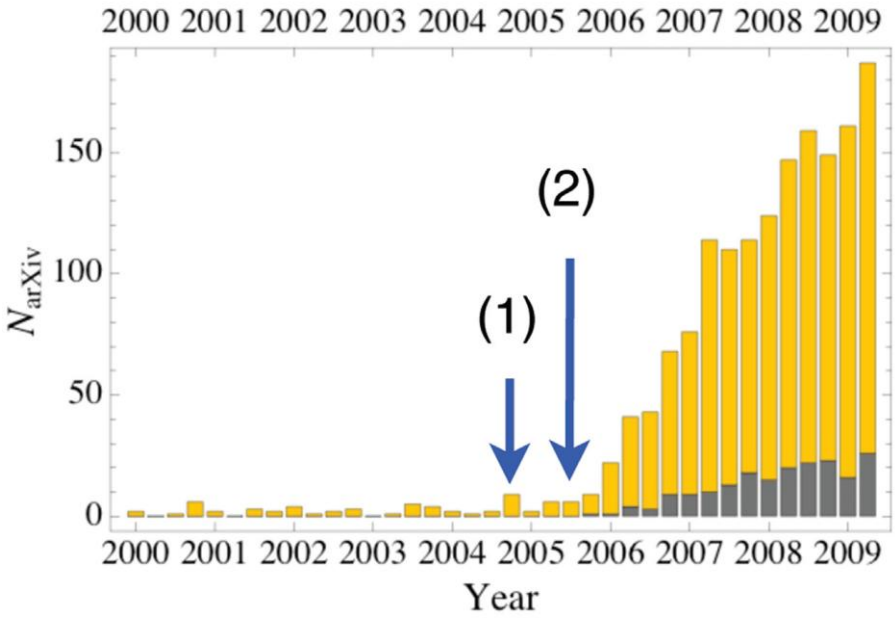

Figure 1.3. Statistics of papers published related to graphene (yellow) and bilayer graphene(gray) each year on arxiv.org. (1) Discovery of graphene; (2) Anomalous QHE measurement. [17]

1.2 Band structure of graphene

At the very beginning of graphene's discovery, it became a favorite of scientists. Why is that? This is because the special property of graphene: a truly 2D electron system with mass less electrons. Back to the end, these properties origin from the unique band structure of graphene, the famous linear dispersion relation.

Fig. 1.4(a) shows the honeycomb lattice of graphene. Each carbon atom is covalent bonded with nearest three carbon atoms through sp^2 hybridization, with carbon-carbon bond length of a_0=0.142nm. The structure can be seen as a triangular lattice with a basis of two atoms per unit cell, which is represented by a_1 and a_2:

$$\vec{a_1} = \frac{a}{2}(3, \sqrt{3}), \vec{a_2} = \frac{a}{2}(3, -\sqrt{3}) \tag{1.1}$$

The corresponding reciprocal lattice is given by:

$$\vec{b_1} = \frac{2\pi}{3a}(1, \sqrt{3}), \vec{b_2} = \frac{2\pi}{3a}(1, -\sqrt{3}) \tag{1.2}$$

A tight bonding approximation is used to calculate the graphene band structure, which is:

$$E(k_x, k_y) = \pm\gamma_0 \sqrt{1 + 4\cos(\frac{\sqrt{3}ak_x}{2})\cos(\frac{k_y a}{2}) + 4\cos^2(\frac{k_y a}{2})} \tag{1.3}$$

Where $a = \sqrt{3}a_0$ and λ_0 is the matrix element between the π orbital of neighboring carbon carbons, which is 2.9eV[2, 18]. The calculated band structure is shown in Fig. 1.4(b) [19, 20] . Especially, at the corners of the Brillouin Zone, or the K(K') points, also called Dirac Point, the Hamiltonian simplifies to:

$$H = \begin{pmatrix} 0 & \gamma(k_x - ik_y) \\ \gamma(k_x + ik_y) & 0 \end{pmatrix} \tag{1.4}$$

which gives the linear dispersion bands:

$$E^{\pm}(k) = \pm\gamma\left|\vec{k}\right| \tag{1.5}$$

shown in Fig. 1.4(c). Here $\gamma = \hbar v_F = \sqrt{3}a\gamma_0 / 2$, v_F is the Fermi group velocity, which is about 1/300 of speed of light.

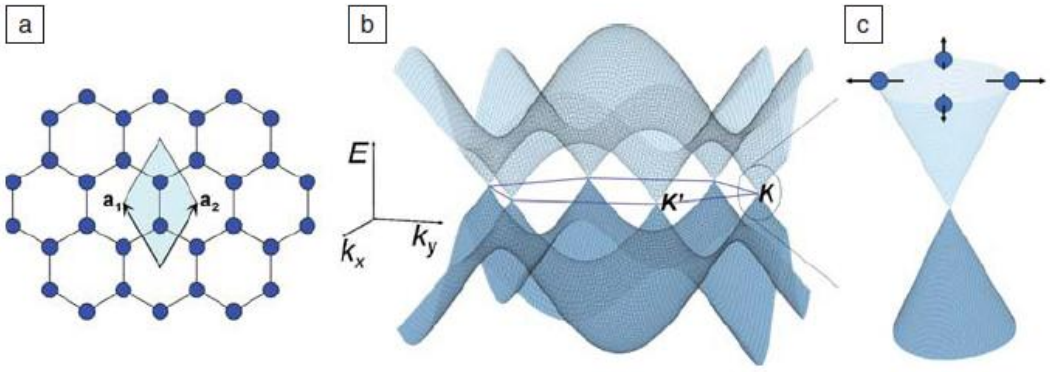

Figure 1.4. Band structure of graphene: (a) Graphene honeycomb lattice. (b) tight-binding band structure of graphene. (c) Band structure close to the Dirac Point. [20]

From the band structure of graphene near Dirac Point, we can know that graphene is a semi-metal without band gap, the conduction band and the valence band touch each other at the K(K') point. This linear relation also indicates that the electrons in it are mass less. As we know, in solid state physics, the electron properties of materials are dominated by the Schrödinger equation, with an

effective mass correspondence to the curvature of the band structure of the material. But this wouldn't apply to graphene, whose band structure is linear with no curvature. In graphene, its charges mimic relativistic particles and are dominated by Dirac Equation rather than Schrödinger Equation, and are therefore called Dirac Fermions. To study and describe the properties, quantum electrodynamics (QED) must be applied. The mass less Dirac fermions in graphene behave as though the speed of light is just 10^6m/s, rather than 3×10^8 m/s, so "Graphene could allow us to investigate the fundamental interactions of matter without the need for huge particle accelerators" [21]. Many phenomena predicted by QED has been observed in graphene, such as non-zero minimum conductivity [22, 23] , anomalous Quantum Hall Effect(QHE) [22, 24, 25], the Klein Paradox [26], and $\pi\alpha$ white light adsorption[27] (α is the fine structure constant) et.al.(Fig.1.5). However, others still remain unsolved. For example, the scattering mechanism that limits the mobility of graphene, the transport properties near Dirac point, as well as the missing π in the minimum conductivity.

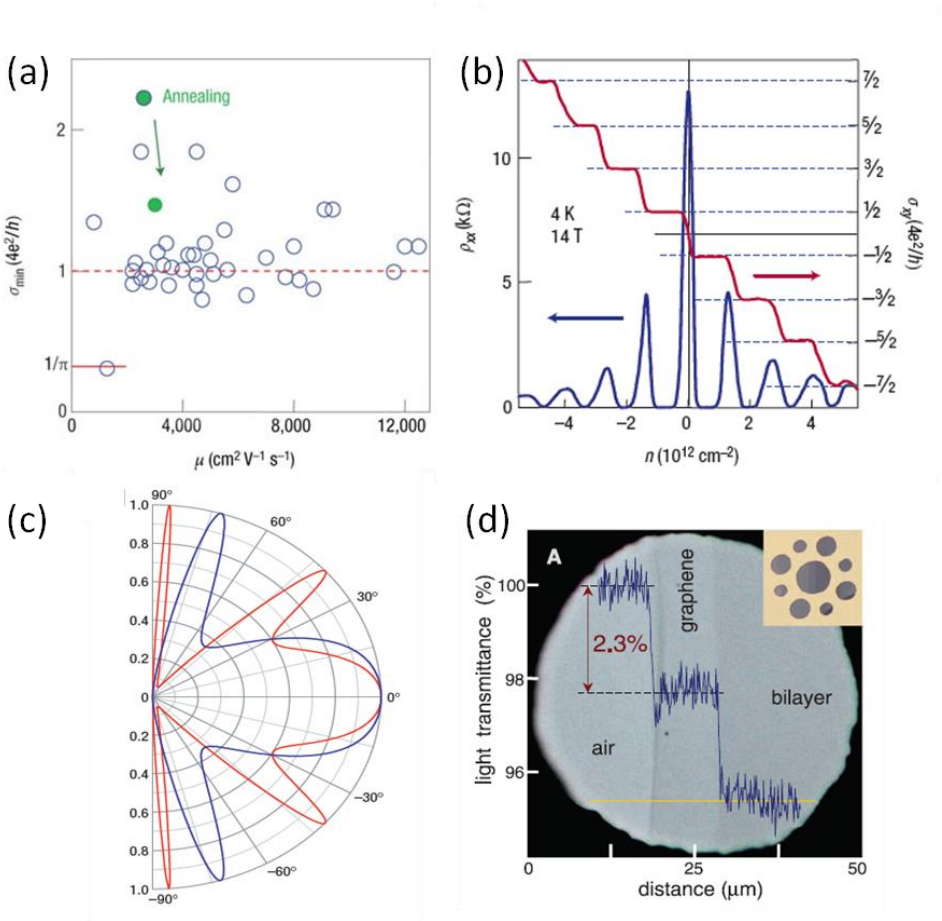

Figure 1.5. Quantum Electrodynamics in graphene (a) non-zero universal minimum conductivity; [28] (b) Unconventional Quantum Hall Effect; [29] (c) Klein Paradox; [30] (d) $\pi\alpha \sim 2.3\%$ white light adsorption. [27]

1.3 Graphene Synthesize and Characterization

As mentioned before, Geim and Novoselov successfully isolated graphene on Si/SiO_2 substrate, using the easy mechanical exfoliation method in 2004. Though the quality of graphene got by this method is nearly perfect, it still has many disadvantages, such as low yield, random distribution, and uncontrollable small size/shape, which restrict its usage only in lab. For application in semiconductor

industry, wafer size, high quality graphene with uniform thickness is in need urgently. Graphene is “calling all chemists”. [31]

Fortunately, to solve this problem, more and more attention has been paid from chemists and material scientists, and there has been a significant progress so far. In the following, I will summarize all the methods for graphene synthesis.

(a) Mechanical Exfoliation

Though the disadvantages mentioned above, mechanical exfoliation is still the most popular method for graphene fabrication, especially for research purpose, because this method is so simple, no extra equipment needed, and the lattice is almost perfect. At the very beginning[16], highly-oriented pyrolytic graphite (HOPG) was used as raw material, stick into a layer of photo-resist, then used scotch tape to peel flakes of graphite off from the HOPG, to make it thinner and thinner, finally released the thin flakes in acetone, and deposited them onto Si/SiO_2 surface by dipping and drying. Graphene with difference thickness and sharp can be observed by optical microscope. Later, this method was modified. Only using scotch tape to peel off small piece of HOPG(or Kish graphite) repeatedly, to get thin layers of graphene on the scotch tape, then use it as stamp, directly attach it to the substrate, press gently, then peel if off, graphene can be left on the surface[32]. This method has become the standard mechanical exfoliation of graphene now, used by different groups around the world.

(b) Chemical Vapor Deposition(CVD)

Actually, single- and few- layer graphene have been grown epitaxial by CVD method even before the mechanical exfoliation method was invented [33-36],

using hydrocarbon gases at high temperature(~1000^0C). However, because CVD graphene can only be formed on metal surface, it is hard to explore the electrical properties, and the thickness are hard to control, usually formed thick graphite crystal rather than graphene films, these are the reasons why not too much attention was paid into this material at that time. Recently development in graphene has re-attracted researchers' interest back to this method, because of its potential in wafer scale synthesis. The first work of few layer graphene synthesis using CVD was reported in 2006 [37], on Ni foil using camphor as precursor. Later on, arrays of macroscopic single-crystalline graphene domains with layer by layer fashion were formed on Ru(0001) surface [38]. Meanwhile, Yu et.al.[39] successfully synthesized high quality 3-4 layers graphene by surface segregation, by dissolving carbon in Ni at high temperature followed by fast cooling down, and what is more, they transferred the epitaxial graphene to insulate substrate for the first time. Activated by this achievement, with more precisely thickness control, single graphene were successfully synthesis on Cooper (Cu) [40, 41] and Nickel(Ni) [42, 43], with size up to centimeters. Most recently[44], 30-inch graphene films were fabricated using so called "roll-to-roll" method, which makes a big step for real application of graphene.

(c) Graphitization of SiC (Epitaxial graphene)

Similar as CVD graphene, formation of graphite on surface of silicon carbide (SiC) by heating SiC to ultra high temperature has been known for a long time, due to the evaporation of Si atoms [45, 46]. It is until 2004 that the 2D electron gas properties of this epitaxial graphene were studied, pioneered by Walt A. de

Heer [47-49] from Georgia Institute of Technology. Removal of Si leaves surface carbons that reconstruct into graphene layers and grow continuously on the flat surface of suitably prepared hexagonal SiC wafer, either on C-face or Si-face. The thickness of the graphene layers depends on annealing time and temperature. Though the properties of epitaxial graphene mimics that of exfoliated graphene, some people consider it as a new material [46], for the coupling between epitaxial graphene and SiC substrate. So far, the properties of the first layer of epitaxial graphene(or called interlayer) is still not clear [50], and it is believed that the comparable low mobility of epitaxial graphene is due to this interaction. Wafer sized epitaxial graphene has been already synthesized[51], for mass fabrication of radio frequency field effect transistors[52]. However, this method takes the disadvantage of high cost, for both synthesis requirements and the SiC substrate, which limits its commercial application.

(d) Chemical Method

Instead of bottom up synthesis such as CVD or epitaxial growth, an alternative method for creating single layer graphene is the top down chemical method. Graphite is first oxidized to produce graphene oxide[53, 54] and then exfoliated to create stable dispersions of individual sheets after deposition on substrate, graphene oxide can be reduced to graphene either chemically[55, 56] or by thermal annealing[57, 58].So many works have been concentrate in this method, by different dispersion solvent[59, 60]or different reductants [61, 62]. Dr. R.S. Ruoff from UT Austin gave a good summary on chemical methods of graphene synthesis[63]. Besides graphene, lots of graphene derivatives or functionalized

graphene can be synthesized by this method.[55, 64] So, chemical method of graphene, takes the advantages of scalable, suitable for mass production, and versatile, for chemical functionalization of graphene, which makes this method especially suitable for application in energy industry, such as super capacitor [65] and Li ions battery[66].

(e) Cross linking

Recently, another bottom up method for graphene synthesis has been promoted, the cross linking method. It is a two-step procedure involving the formation of self-assembled monolayer (SAMs) with highly functionalized monomers followed by chemical cross linkage of the SAMs to from linked monolayer. SAMs were formed on gold surface first, using conjugated carbon molecular species, such as 1,1'-biphenyl-4-thiols(BPT)[67] and 4'-nitro-1,1'-biphenyl-4-thiol(NBPT)[68], then upon irradiation with electrons or other chemical methods [69-70],cross linking is accomplished, to form a mechanical robust monolayer, or so called carbon nanosheet. This nanosheet can be transferred to arbitrary substrate for further application. This cross linking method, not versatile in molecular structure, but also provides a level of molecular control over the structure, can form planar films, as well as balloons, tubes and pleated sheets [71]. These materials are usually insulating initially, but can be conductive after re-crystallization at high temperature [72]. However the lattice is still not perfect even after re-crystallization, which limits its application in electronics.

Fig. 1.6 shows schematic illustrations of graphene synthesis methods [50], while Table 1.1 summarizes the comparisons between these methods.

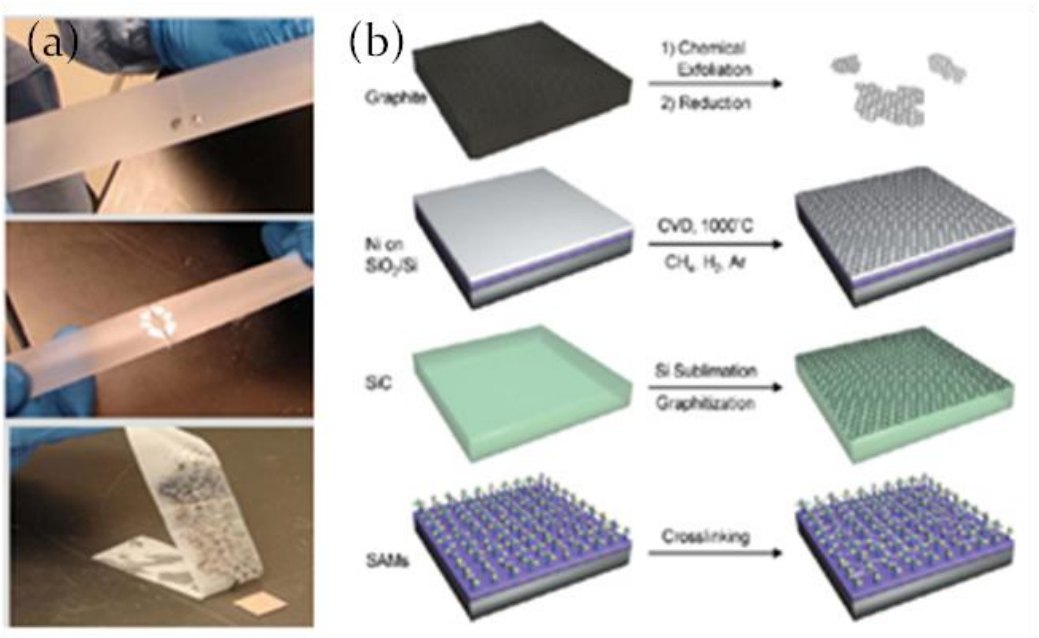

Figure 1.6. Schematics of graphene synthesis methods[50]

	Mass production	Comparable with Semiconductor Processing	Versatility	Quality
Mechanical Exfoliation	NO	NO	NO	Excellent
CVD	Yes	Yes	Yes	Good
Graphitization	Yes	Excellent	NO	Good
Chemical Method	Excellent	NO	Excellent	Good
Cross linking	Yes	NO	Excellent	Bad

Table 1.1. Comparisons of different methods for graphene synthesis

After graphene was synthesized, the next thing is how to characterize it, whether it is single layer, double layer, or even thicker. The first graphene was isolated on a 300nm SiO_2/Si substrate, actually one of the discoverers of graphene,

K.S. Novoselov, said that they were pretty lucky because single layer graphene is visible and can be distinguished from others, just using an optical microscopy. This is approved later by Blake et al.[73] and an optical image of graphene with different layer are illustrated in Fig. 1.7, one can clearly see the color difference between different layers.

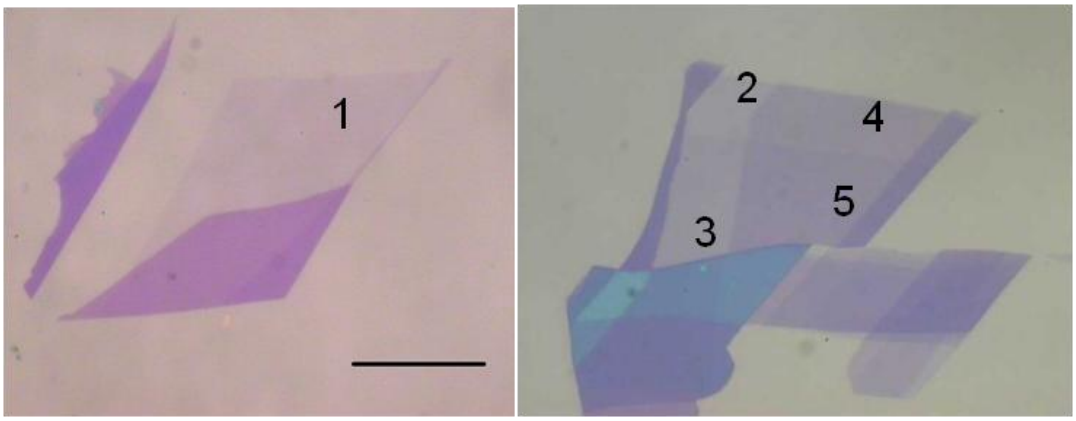

Figure 1.7. Optical Images of graphene with different layers on SiO_2 (300nm)/Si substrate.

Furthermore, Raman spectrum[74] is a good and fast way to characterize graphene. See Fig. 1.8(a) and (b) are Raman Spectrum of single layer graphene and double layer graphene respectively. Usually graphene and graphene layers has two Raman peaks, one around 1600cm^{-1}, named G peak, and another is 2D peak, at ~2700cm^{-1}. The differences are: the 2D peak of single layer graphene can be fitted by a single Lorenz, while that of double layer graphene cannot. Compared with 2D peak of other thicker graphene layers, the significant of double layer graphene is: its 2D peak has a significant secondary peak at ~2650cm^{-1}. Actually, from Raman Spectrum, one can distinguish single layer graphene and double layer graphene from others, but for graphene layers thicker

than 3 layers, the Raman Spectrum are pretty same, which is hard to tell. Raman spectrum is an easy, fast, and nondestructive identification of single and double graphene layers.

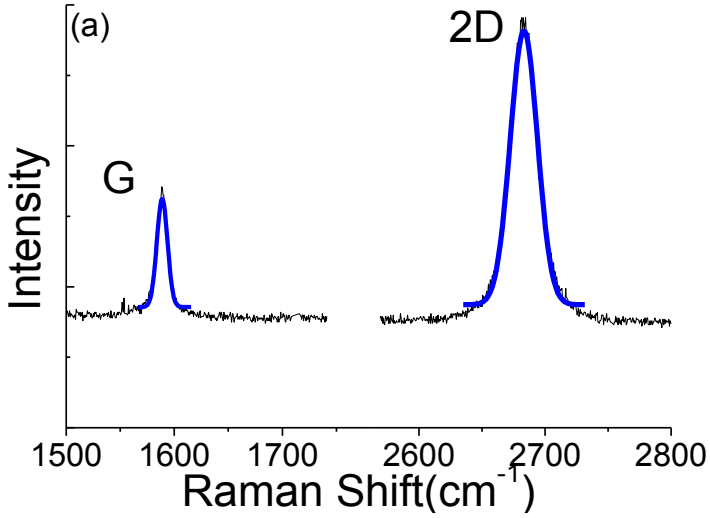

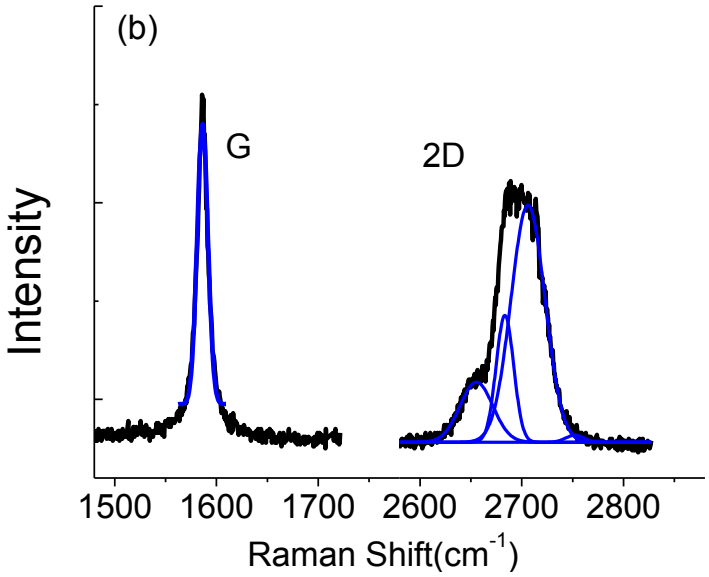

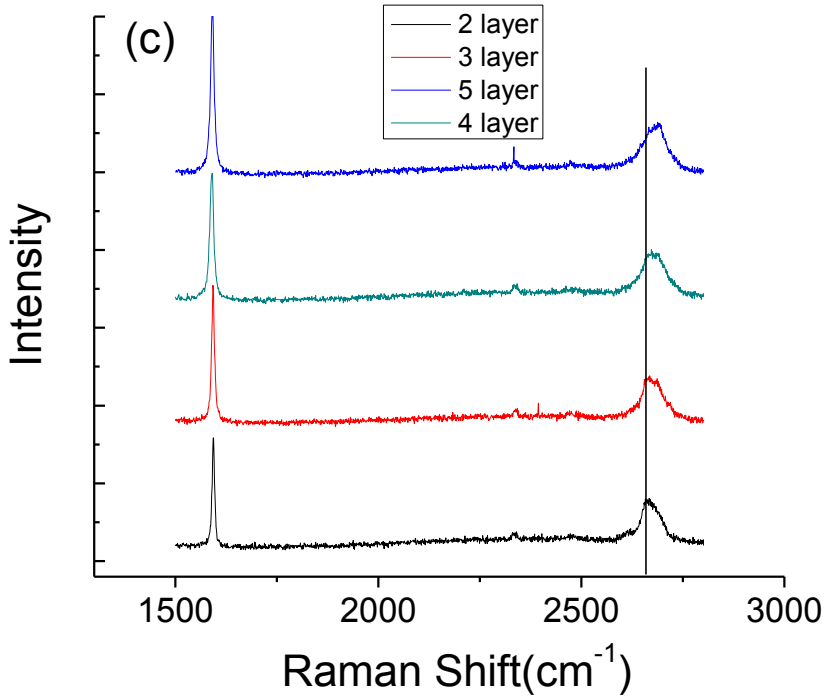

Figure 1.8. Raman Spectrum of (a) single, (b) double, and (c) >3 layers of graphene

There are many other methods to characterize graphene, such as AFM [32], STM [75] and TEM [60] (Fig. 1.9). However, these methods are neither destructive nor need special sample preparation, not good for fast identification of single layer graphene.

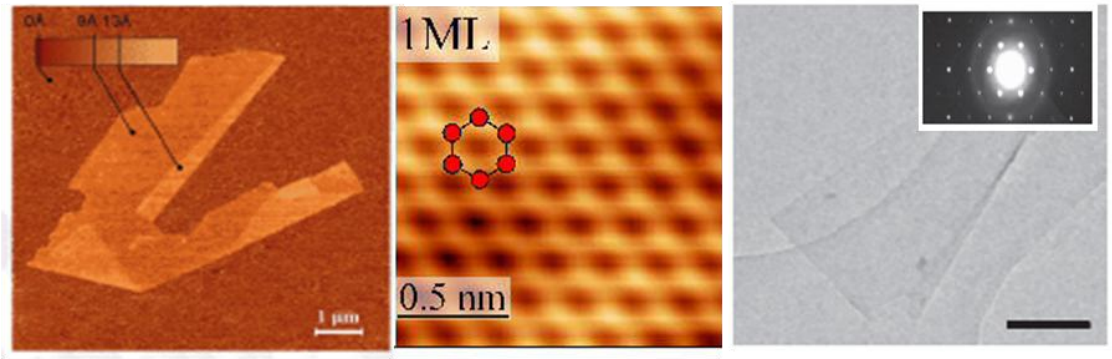

Figure 1.9. Graphene Characterization using (a)AFM; [32] (b)STM; [75] (c)TEM[60]

1.4 Graphene Derivatives

Soon after the discovery of graphene, other graphene derivatives are synthesized and studied. Mainly because graphene is a zero band semi-metal , devices with graphene channel cannot be switched off and therefore not suitable for logic application. Researchers tried to open a bandgap, through modifying graphene. Others tried to further improve the properties of graphene, such as mobility.

(a) Bilayer graphene

Bilayer graphene can be got simultaneously when synthesis graphene using mechanical exfoliated method. Bilayer graphene is also gapless, but different from graphene, its valence and conduction bands have a parabolic shape near the K point, with a overlap of 0.16meV [76]. Through transport of bilayer graphene mimics that of graphene, the quantum hall effect is quite different [29], which makes bilayer graphene also a particular material. What is more, people found that by applying a perpendicular electric field, a band gap can be opened, which

was predicted by theory [77] and confirmed by experiments [78-80]. This Fig. 1.10(a) shows the band structure of bilayer graphene before and after gap opening. The gap is determined and tunable by the strength of the electrical field, and a band gap up to 250meV can be opened by high field(1-3 $\times 10^7$ V cm^{-1}) . Fig. 1.10(b) shows the transport properties of bilayer graphene as a function of top gate voltage while under fixed top gate voltage, which shows the possibility to turn bilayer graphene transistor off by this mechanism.

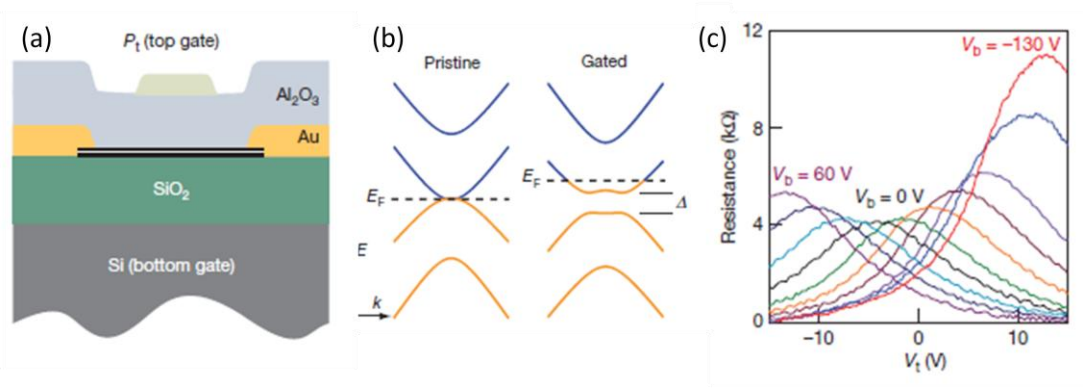

Figure 1.10. Bilayer graphene band gap opening: (a) dual gate bilayer graphene transistor schematic; (b) band structure of bilayer graphene before and after band gap opening; (c) Resistance of bilayer graphene transistor as a function of top gate voltage at different fixed back gate voltage. [80]

(b) Graphene Nanoribbons (GNRs)

Another method to open a band gap in graphene is through electron quantum confinement, by cutting graphene into graphene nanoribbon with width less than 20nm [81], using e-beam technology. GNRs can also be got by other methods, chemically [82, 83] or by unrolling single wall carbon nanotube [84, 85]. GNRs electronics was originally introduced theoretically by Mitsutaka Fujita and co-

workers [86, 87], achieved experimentally firstly by IBM group[81] and Columbia group[88]. There are two kinds of GNRS: armchair or zigzag. Detailed calculation shows that both these two GNRs have band gaps, but with different sources. Band gap of armchair GNRs origins from quantum confinement as well as edge effects[89], while that of zigzag GNRs comes from the staggered sub lattice potential on the hexagonal lattice due to edge magnetization. For experiments, it is hard to distinguish between these two GNRs, but the results[82, 88] correspond to the theoretically calculation of armchair GNRs[90]: the energy gaps increase with decreasing GNR width, with an empirical form of shown in $E_g = \alpha / W$ Fig. 1.11.

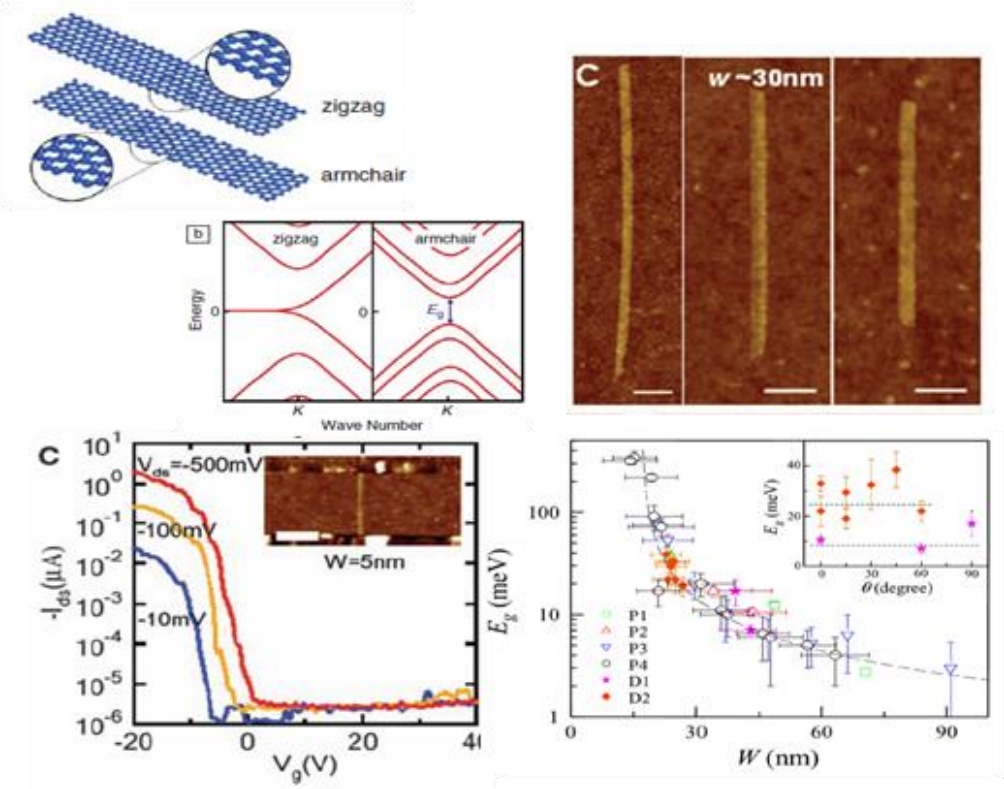

Figure. 1.11. Graphene Nanoribbons (a) structure schematic of armchair and zigzag GNRs and their band structure (b) AFM image of GNRs with different width ; (c) Transport properties of GNRs with a width of 5nm. (d) Band gap of GNRs with different width, as well as a fitting of an empirical form. [82]

(c) Graphene Nanomesh (GNM)

Recently, another mechanism of band gap opening in graphene was proposed, called graphene nanomesh [91], by UCLA group. By etching a high-density array of nanoscale holes into a single layer graphene, using a self assembled block copolymer thin film as mask template, the on/off ratio of the transistor can be enhanced by up to 10 times, compared with that of bulk graphene transistor, which becomes comparable with GNRs. The band gap of GNM depends on the neck width as well as the hole size [92], shown in Fig. 1.12. In fact, people claimed that the mechanism is same as that of GNRs, with a similar relation between the band gap and the neck width [92, 93], the detailed mechanism is unclear yet[94]. The advantage of this GNM is: it can support currents 100 times greater than that of GNRs, but with a similar on/off ration, this is very helpful to increase the trans-conductance of the graphene transistor.

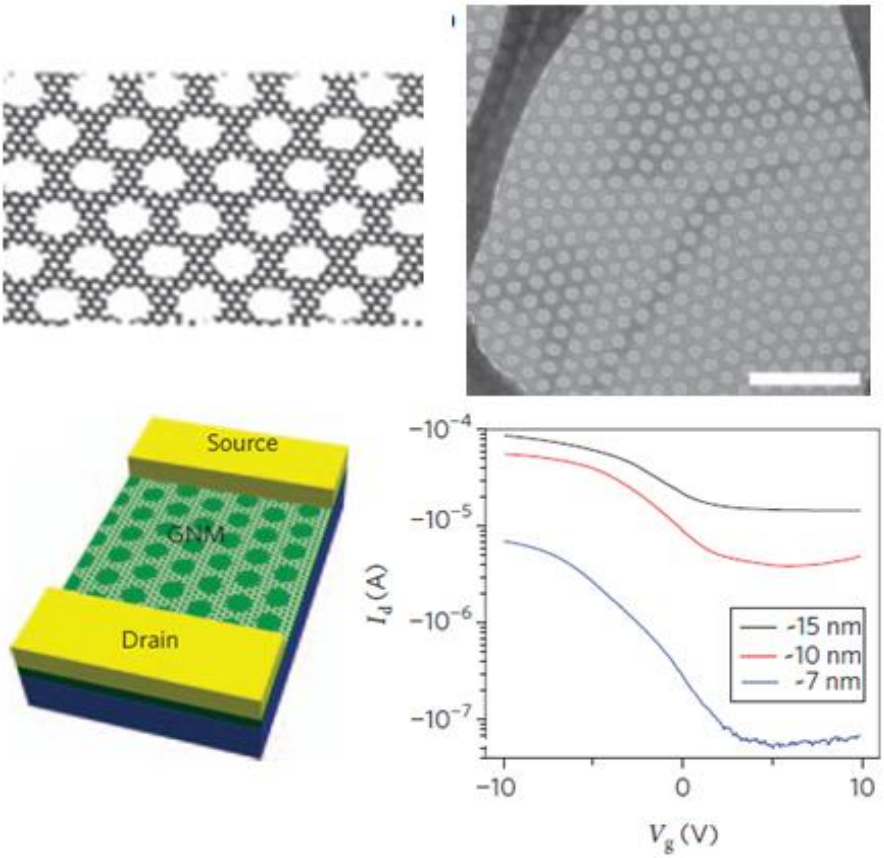

Figure 1.12. Graphene Nanomesh: [91] (a) Structure Schematic ; (b) STM image;(c) Graphene Nanomesh Transistor ; (d) Transport Properties with different width

(d) Doped graphene

Silicon succeeds in semiconductor industry, partially because the easiness to change silicon from conductor to semiconductor, until insulator, by doping or oxidation. Stimulated by this, researchers also want to change the conductivity of graphene by different doping. Three most important doped graphene are: graphene oxide, graphane, and nitrogen doped graphene. Graphene oxide aims to get graphene based insulator, while graphane is graphene in semiconductor form.

Intrinsic graphene is p-type, N/P doping graphene can lead n/p-type graphene transistor, which is important for current CMOS based electronics.

Graphene Oxide (GO) can be synthesized by the chemical method mentioned in section 1.3., and it can be transferred to graphene easily by chemical reduction or annealing. Several good reviews on preparing GO has been published [95, 96]. Actually GO is a compound of carbon, oxygen and hydrogen in variable ratios, with lots of hydroxyl and epoxide functional groups on either side of the sheet. GO itself is an insulator, but become conductive after reduction, the conductivity depends on the level of reduction, but still much smaller (>100 times) than that of graphene even after fully reduction [97-98], which is due to the much more defects in the reduced GO.

Graphane, which is hydrogenated graphene, is a 2-dimensional polymer of carbon and hydrogen with sp^3 carbon bands. Different from GO's strongly disordered structure, idea graphane owns perfect lattice structure, with one hydrogen atom attaching to each site of the graphene lattice. Graphane is a semiconductor with a gap of 3.5eV, predicted by Sofo et.al. theoretically in 2007 [99]. However, making graphane had proven to be kind of difficult, because the hydrogen molecules must first be broken into atoms and the crystal structure of graphene must also be altered or damaged by high temperature. Fortunately, graphane was successfully first achieved by Elias et.al. [100], simply by treating graphene in hydrogen plasma, and the on/off ratio can be enhanced by two orders of magnitudes. What is more, graphane can reversible change back to graphene by

annealing at 450^0C, making it possible to tune the electronic properties of graphene by surface chemical modification.

N/P doping is a common approach to tailor the electronic properties of semiconductor materials, without changing the band structures, which is another key reason for the success of silicon. N/P doping of graphene chemically was observed by exposing graphene to donors (NH_3, CO…) or acceptors(NO_2, H_2O…)[101], without reducing the mobility of graphene. However, this adsorbed molecules can easily release at 150^0C, only good for sensors application. Later, stable n-type graphene nanoribbon was achieved through high power electrical joule heating in ammonia gas, which attributed to the formation of carbon-nitrogen bond at the edge[102]. Moreover, doping of graphene is also demonstrated during CVD process, n doping by introducing NH^3 gas into the quartz tube during synthesis[103], while p doping by HNO_3. [44]

The success of n/p doping of graphene, as well as graphene oxide and graphane, demonstrates that a single material could be modified to cover the entire spectrum needed for electronic application, from insulators to semiconductors to metals, makes all graphene based electronics possible[104].

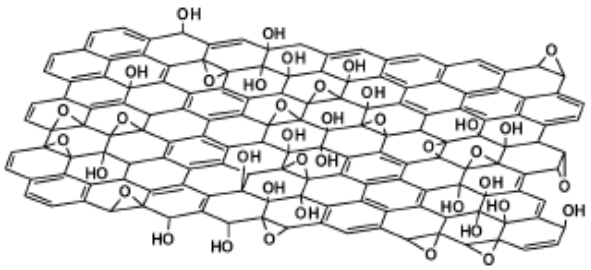

(a)

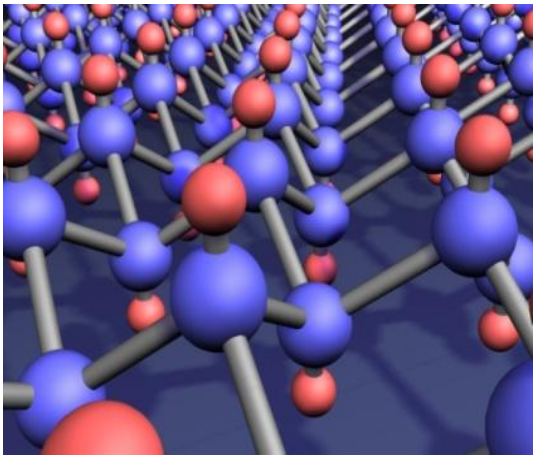

(b)

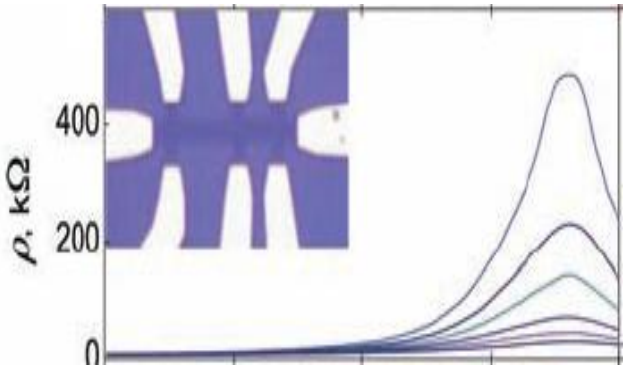

(c)

Figure 1.13. Doping Graphene. (a) Structure of Graphene Oxide; [95] (b) Structure of Graphane and (c) Transport of Graphane.[100]

1.5 Graphene Applications

We have known that, graphene is extremely attractive to solid state physicists, for its unique Dirac fermions in true two dimension. However, graphene is so hot recently, not only because of this quantum electrodynamics, but also for other applications in a wide range, from field effect transistor, chemical/bio sensor, to super capacitor, transparent electrode et.al. .

(a) Field Effect Transistor

As soon as graphene was discovered, the field effect of graphene was studied[16], whose mobility can go as high as 10,000$cm^2V^{-1}s^{-1}$, that is the reason why graphene is attractive for electronics application. Later effect has improved this mobility up to 230,000$cm^2V^{-1}s^{-1}$ by suspending graphene [105] to avoid the scattering from charged impurities and ripples. For these graphene FETs are back gated, which are not suitable for VLSI, top gated graphene FETs have been also fabricated. By optimizing the high k dielectrical material to minimize the interface effect, top-gated graphene FETs with mobility of 6000-7000$cm^2V^{-1}s^{-1}$ have been achieved [106-108]. However, as a semi-metal with zero band gap, graphene FETs are not suitable for logic devices, which requires an on-off ratio between 10^4 and 10^7, corresponding to a band gap of around 0.4 eV [109]. Fortunately, the high mobility of graphene makes it excellent candidate for radiofrequency devices, which don't require FET to switch off either. In this direction, IBM group lead by P. Avouris has made big contributions and progresses. So far, graphene FETs with gigahertz has been achieved either on exfoliated graphene [110, 111] or epitaxial graphene [52, 112, 113], with a record of 100GHz cut-off frequency (240nm gate length), which is higher than that of the best silicon MOSFET with similar gate lengths. However, there is still one thing limiting the radiofrequency performance of graphene FET, the absence of source-drain current saturation[109]. Combined with the uncontrollable mobility, there is still a long way for commercialization of graphene FETs, both for logic device and radiofrequency device.

(b) Nonvolatile memory

Graphene-based atomic scale switches were first observed by Standley et.al. [114], with a simple 2-terminal structure(source and drain). The mechanism is contributed to the formation/breaking of carbon chain within a sub-10nm gap, this switch can be controlled reversely by applying appreciate bias voltage. Remarkably, these switches were extremely robust, with duration up to thousands cycles. In a short period after this phenomena was observed, graphene-based memories were demonstrated[115, 116]. Instead of sweeping, a bias pulse was used to write/erase the memory cell, with writing and erasing voltage of 8V and 6V respectively, and the switching time is around 1us. The on/off ratio was up to 10^7 times, and retention test showed no data loss up to weeks, even with exposition to X-ray(>20Mrad, 8keV), which was significant better than flash memories.

Another kind of graphene based nonvolatile memory was also reported [117], with 3-terminal FET structure, using ferroelectric material as gate material. The writing/erasing is operated through sweeping gate voltage, with an on/off ratio of around 7. The storage mechanism was contributed to the polarization of the ferroelectric gating material. However, this was just a first shot on this kind of memories, lots of work are still in need.

(c) Transparent Electrode

Since Graphene can transmit most of the white light[27], and it has super conductivity, graphene has been considered as a better candidate for transparent electrode, compared with Indium tin oxide(ITO). The challenge is the fabrication

of large scale uniform graphene sheet. CVD method has opened the window for this application. K.Kim et.al. [42] first reported the large scale graphene for stretchable transparent electrode, synthesized by CVD on nickel followed by transferring to PDMS substrate, the sheet resistance is only 280 Ω per square, with a 80% optical transparency, which should be 6-10 graphene layers. Recently, the same group has fabricated 30-inch graphene films on polyethylene terephthalate (PET) substrate[44], with a roll to roll transferring process. The film has a sheet resistance of only 30 Ω per square and ~90% transparency can also remain its conductivity with strain up to 6%, much better than that of ITO. Following by these achievements, many optoelectronic devices has been fabricated and demonstrated using graphene transparent electrode, including solar cell[118-120], flexible liquid crystal display(LCD) [121], organic light emitting diode(OLED) [122], and flexible touch screen [44]. It is believed that the application of graphene will make a breakthrough in this direction.

(d) Energy Storage

For energy storage, graphene is used in two aspects: super-capacitor and Li-ion battery.

As we know, graphene is an one atomic layer material, so the surface area of graphene is pretty large, up to 2630m^2/g, much better than other carbon materials, which makes graphene an idea candidate for super capacitor electrode material. Graphene-based super capacitor was first achieved by R. Ruoff's group of UT Austin[65], using chemical synthesized graphene as electrode material. Specific capacitances of 135 and 99 F/g in aqueous and organic electrolytes were achieved,

respectively. Later on, several groups [123, 124] tried to improve the performance of graphene super capacitor, by different synthesized methods or chemical modification, or using different electrolytes. And others tried to combine graphene with nano crystal MnO_2[125], which is a redox active materials used for pseudo capacitance, however, no significant improvement on specific capacitance has been made so far.

Li-ion battery (LIB) is the most important energy storage device nowadays in portable electronic devices, but the disadvantage of LIB is the low energy, the low power density, and the long charging time. Normally graphite based anode is used as standard electrode in Li-ion battery, for its stability, reversibility and reasonable specific capacity. Recently founds claimed that graphene based anode can increase the performance of LIB for the its super high conductivity, high surface area, and the stability in large potential window. SnO_2/graphene nano-porous electrodes has been synthesized[126], a reversible capacity of 810mAh/g is achieved, much better than that of graphite(372mAh/g), and the cycling performance is drastically enhanced in comparison with that of the bare SnO_2 nano-particle. Now the storage capacity has been enhanced to >2200mAh/g after 50 cycles and >1500mAh/g after 200 cycles, by using silicon nanoparticles/graphene electrode [127]. On the other hand, Wang el.al. [66] found that a nano-structured TiO2-graphene hybrid materials can enhance Li-ion insertion/extraction kinetics in TiO2, especially at high charge/discharge rate. And most recently, Vorbeck Materials Corp. has announced that their graphene-enhanced batteries is already in store, which can charge a cell phone just in 10

minutes. This is the first commercialization of graphene, making graphene into real life, just 6 years after its discovery.

(e) Chemical/Bio sensor

Another promising application of graphene is in chemical/bio sensor. Like single walled carbon nanotubes, every carbon atom in the graphene is a surface atom and can interact or bind to analyte molecules, providing sensitive detection of the molecules. Gas molecules can absorb on the graphene surface and serve as either donors or acceptors, which can be detected by measuring the transport current. The first report on graphene sensing is given by Schedin et.al. in 2007[101], for detecting gas molecules such as NO_2,NH_3, and H_2O. They observed interesting stepwise changes in the Hall resistivity, which was interpreted as the individual adsorption and desorption of NO_2 molecules onto the graphene surface. The adsorption of NO_2 adds holes to graphene but does not significantly affect the carrier mobility, so the stepwise changes were attributed to quantized hole doping and un-doping of the graphene by the individual NO_2 molecule. This remarkable single molecule detection limit was achieved due to the high sensitivity and low noise of the graphene device. Following by this, graphene sensors are explored in detecting vapors(Water, Acetone, Nonanal, Octanoic, Trimthylamine) [128, 129], and protein/DNA biosensors [130, 131]. There are several good reviews on graphene based sensor[132-135]. Through graphene has many advantages in sensor application, it still has several problems unsolved, such as uncontrollable conductivity, weak selectivity, and the controversial sensoring mechanism.

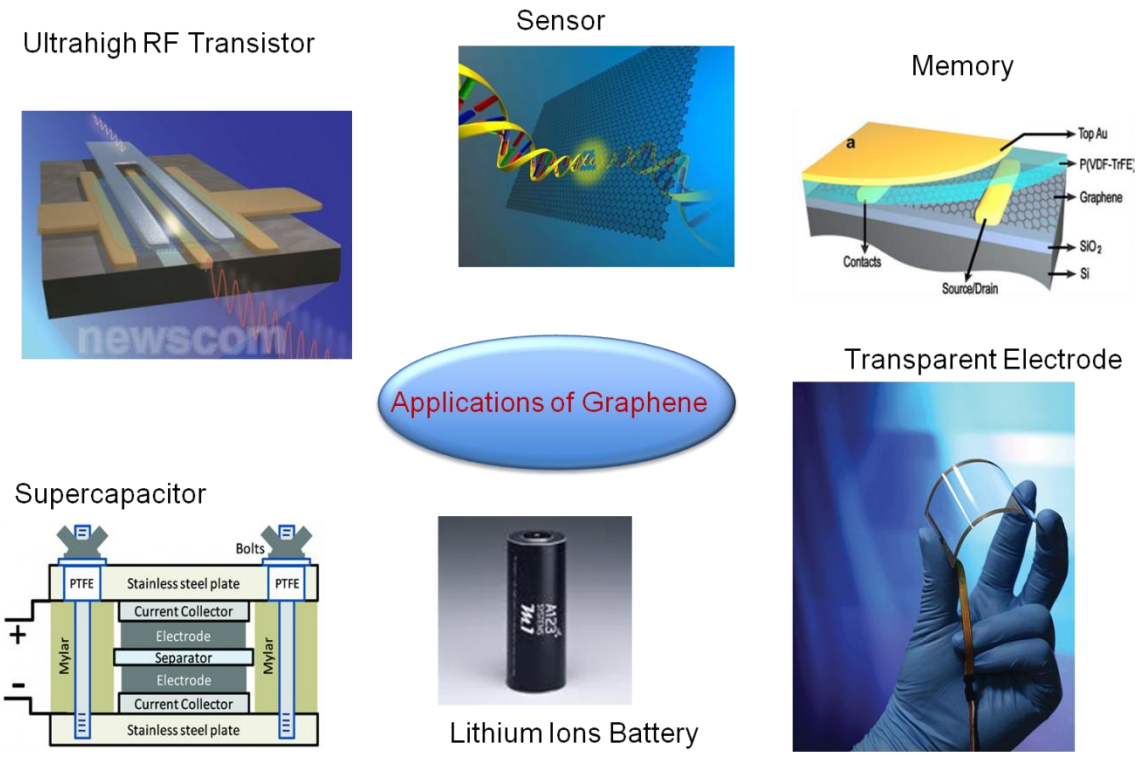

Figure 1.14. Application of Graphene

1.6 Milestone of Graphene Development

First discovery in 2004 by Geim and Novosolev in 2004, graphene has undergone a rapid development, seen in Fig. 1.15. Three years later, in 2007, the first graphene based transistor was demonstrated by PSU group [136], soon after that, IBM group successfully fabricated graphene transistors operating at 26GHz [110], HRL researchers fabricated wafer size graphene devices in early 2009, while IBM group pushed the cutoff frequency of graphene up to 100GHz. In 2010, Korean and Japanese researches demonstrated the first electrical application of graphene, using it as transparent electrode for touch screen. Especially, 2010's Nobel Prize for Physics was award to Geim & Novoselov, the discovery of

graphene, “for groundbreaking experiments regarding the two dimensional material graphene”, which will definitely boost the researches in graphene further.

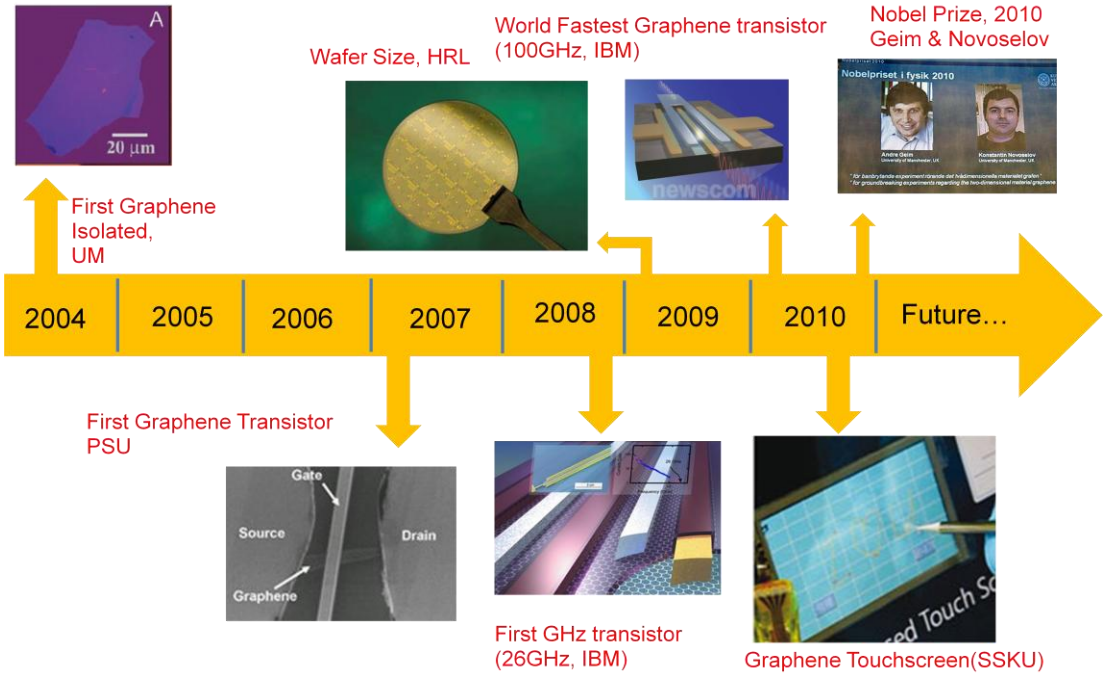

Figure 1.15. Milestones of graphene development

Chapter 2

THEORIES OF CHARGE TRANSPORT IN GRAPHENE

The transport property of graphene is unique, different from any other well known materials, for its unique band structure. As mentioned, there are basically four characteristics in its transport: 1) the linear dependence of conductivity on carrier density, for both hole and electron; 2) the universal non-zero minimum conductivity at zero carrier density (Dirac Point); 3) the shift of Dirac Point; 4) the width of plateau region near Dirac Point. Researchers have made great efforts to explore the mechanism of graphene transport, in mesoscopic transport frame, for graphene under research is usually in micrometer scale. There are three regimes for mesoscopic transport: Ballistic, Diffusive, and Classic, depends on the mean free path and the device size. Usually the transport of graphene falls in to either ballistic or diffusive.

2.1 Diffusive Transport in Graphene

At the very beginning of its discovery, people tried to explain the transport of graphene using Drude Model [16], by $\sigma = \mu ne$. However, this equation can only explain the linear relationship between conductivity and carrier density, no explanation on the universal minimum conductivity, nor the determining parameters on the variety mobility. Then, Chen et al [137] demonstrated that by doping graphene with Potassium ions(K^+), the transport properties can be changed systematically, combined the direct observation of electron-hole puddles in graphene using scanning single electron transistor technology[138], it is believed

that the charged impurities in graphene plays a key role in the transport properties, acting as scattering centers, through Coulomb scattering. Boltzmann transport theory(see Appendix A) then is introduced into graphene transport, with the screening effect by the surrounding environment[139-141].

Hwang[140] et al first considered the scattering from charged impurities, as long range Coulomb scattering, with consideration of the screening effect, the relaxation time is given by:

$$\frac{1}{\tau} = \frac{\pi}{\hbar}\sum_{k'} n_i \left|\frac{v(q)}{\varepsilon(q)}\right|^2 (1-\cos^2\theta)\delta(E_{k'} - E_k) \tag{2.1}$$

where $v(q,d) = 2\pi e^2 \exp(-qd)/(\tilde{\kappa}q)$ is the Fourier transform of bare Coulomb potential at the transfer momentum $q = \left|\vec{k} - \vec{k}'\right| = 2k_F \sin(\theta/2)$, $\varepsilon(q)$ is the dielectric function with screening, d is the distance of between graphene layer and impurity layer. By using Random Phase Approximation (RPA), the dielectric function can be written as:

$$\varepsilon(q) = 1 + \frac{q_s}{q}\begin{cases} 1 - \dfrac{\pi q}{8k_F} & if \quad q < 2k_F \\ 1 - \dfrac{\sqrt{q^2 - 4k_F^2}}{2q} - \dfrac{q\sin^{-1}(2k_F/q)}{4k_F} & if \quad q > 2k_F \end{cases} \tag{2.2}$$

where $q_s = 4e^2 k_F/(\hbar\tilde{\kappa}\gamma)$ is the effective graphene 2D Thomas Fermi wave vector and $\tilde{\kappa} = \kappa(1 + \pi r_s/2)$ is the effective dielectric constant. This theory can explain the experimental data at large carrier density, by fitting two parameters (d,

n_i), which shows the linear relation between conductivity and carrier density, with a experimental reasonable mobility value, shown in Fig.2.1.

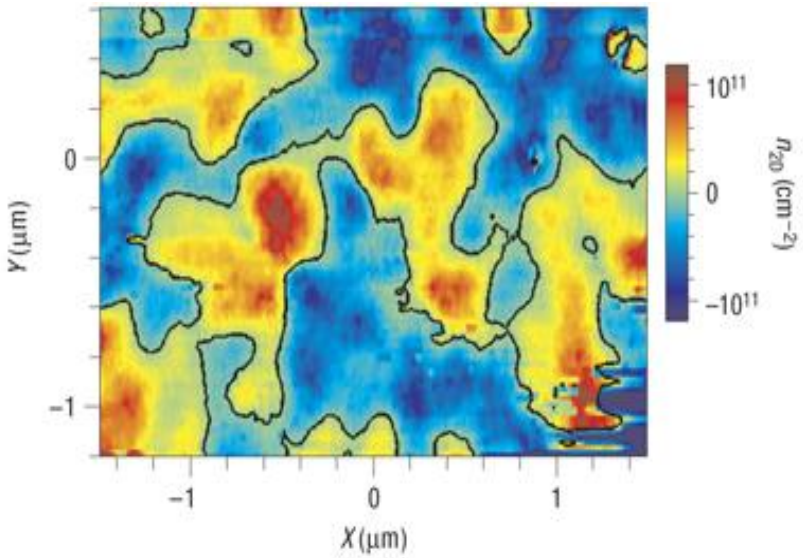

(a)

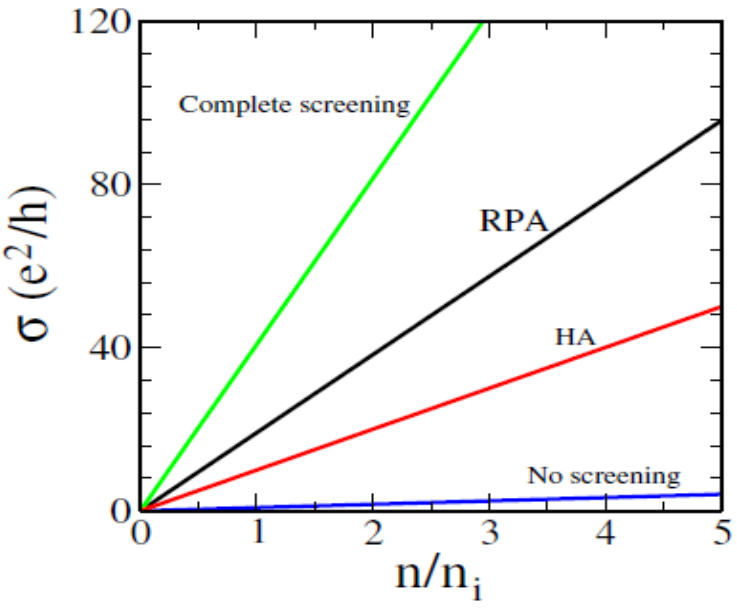

(b)

Figure 2.1. (a) Electron Hole Puddles in graphene; [138] (b) Conductivity of graphene as function of carrier density and impurity density with different screening. [140]

2.2 The self consistent theory of graphene transport

Beside Random Phase Approximation, others approximation are also used to calculate the transport of graphene, such as completely screened approximation [141] and Thomas Fermi Screening [142]. However, as mentioned, these theories can only explain the linear conductivity, other three characters of graphene transport cannot be explained. This problem is solved by the pioneer work by Sarma's group in University of Maryland, named as the self consistent theory for graphene transport [143].

In the self consistent theory, the charged impurities introduces a random voltage fluctuation in the graphene layer, this voltage fluctuation will cause the shift of Dirac Point, and attract extra residual carrier density into the graphene, which response for the minimum conductivity, as well as the plateau near the Dirac Point. At large carrier density, this charged impurities acts as scattering center, which reduces the mobility of intrinsic graphene to a limit value.

For Coulomb scattering, the point charge potential in the graphene layer is $V(r) = -e^2 / 4\pi\varepsilon r$, so the random voltage fluctuations can be calculated by[143, 144]:

$$\overline{\delta V^2} = n_{imp} \int \frac{dq^2}{(2\pi)^2} [\frac{v(q)}{\varepsilon(q)}] \tag{2.3}$$

Where $v(q)$ is the Fourier transform of $V(r)$, $\varepsilon(q)$ is the dielectric function. Using RPA, one can get :

$$\overline{\delta V^2} = 2\pi n_{imp} (\frac{e^2}{\kappa})^2 C_0(r_s, a = 4k_F d) \tag{2.4}$$

$$C_0{}^{RPA}(r_s, a) = -1 + \frac{4E_1(a)}{(2+\pi r_s)^2} + \frac{2e^{-a} r_s}{1+2r_s} + (1+2r_s a)e^{2r_s a}(E_1(2r_s a) - E_1[a(1+2r_s)]) \tag{2.5}$$

Where $E_1(a) = \int_z^\infty t^{-1} e^{-t} dt$ is the exponential integral function.

Then this potential fluctuation will induce extra carrier in graphene, which is called residual carrier density(n*), which can be retrieved by:

$$\overline{\delta V^2} = \hbar^2 v_F{}^2 k_F{}^2 = \hbar^2 v_F{}^2 \pi n^* \tag{2.6}$$

That is $$\frac{n^*}{n_{imp}} = 2(\frac{e^2}{\hbar v_F \kappa})^2 C_0(r_s, a) = 2r_s{}^2 C_0(r_s, a) \tag{2.7}$$

The impurity induced shift of voltage is:

$$\bar{V} = \pi n_{imp} v_F / 2k_F \tag{2.8}$$

which will cause the shift of Dirac Point by[144]:

$$V_{g,\min} = \frac{e\bar{n}}{C_g} \tag{2.9}$$

Where $$\bar{n} = \frac{(\bar{V})^2}{\hbar^2 v_F{}^2 \pi} = \frac{n_{imp}{}^2}{4n^*} \tag{2.10}$$

Finally, the conductivity can be got by BTE(2.15, 2.16) using a simple approximation expression of RPA:

$$\varepsilon(q) = \begin{cases} 1 + q_s / q & if \quad q < 2k_F \\ 1 + \pi r_s / 2 & if \quad q > 2k_F \end{cases} \tag{2.11}$$

which gives

$$\sigma = \frac{e^2 n}{h n_{imp}} \frac{2}{G[2r_s]} \tag{2.12}$$

$$\frac{G[x]}{x^2} = \frac{\pi}{4} + 3x - \frac{3\pi x^2}{2} + \frac{x(3x^2 - 2)\arccos[1/x]}{\sqrt{x^2 - 1}} \tag{2.13}$$

When graphene locates on SiO_2 substrate in air, $G[2r_s] = 0.8$

Then, as a conclusion, the conductivity of graphene as a function of carrier density is given by:

$$\sigma(n) = \begin{cases} \frac{20e^2}{h} \frac{n^*}{n_{imp}} & if \quad n - \bar{n} < n^* \\ \frac{20e^2}{h} \frac{n}{n_{imp}} & if \quad n - \bar{n} > n^* \end{cases} \tag{2.14}$$

which is shown in Fig. 2.2. When graphene is relatively dirty with impurity density $n_{imp} = [250 \times 10^{10} cm^{-2}, 400 \times 10^{10} cm^{-2}]$, the minimum conductivity is indeed $4e^2 / h$, in agreement with experiments. At high carrier density, the conductivity depends linearly on carrier density, with mobility inversed to impurity density.

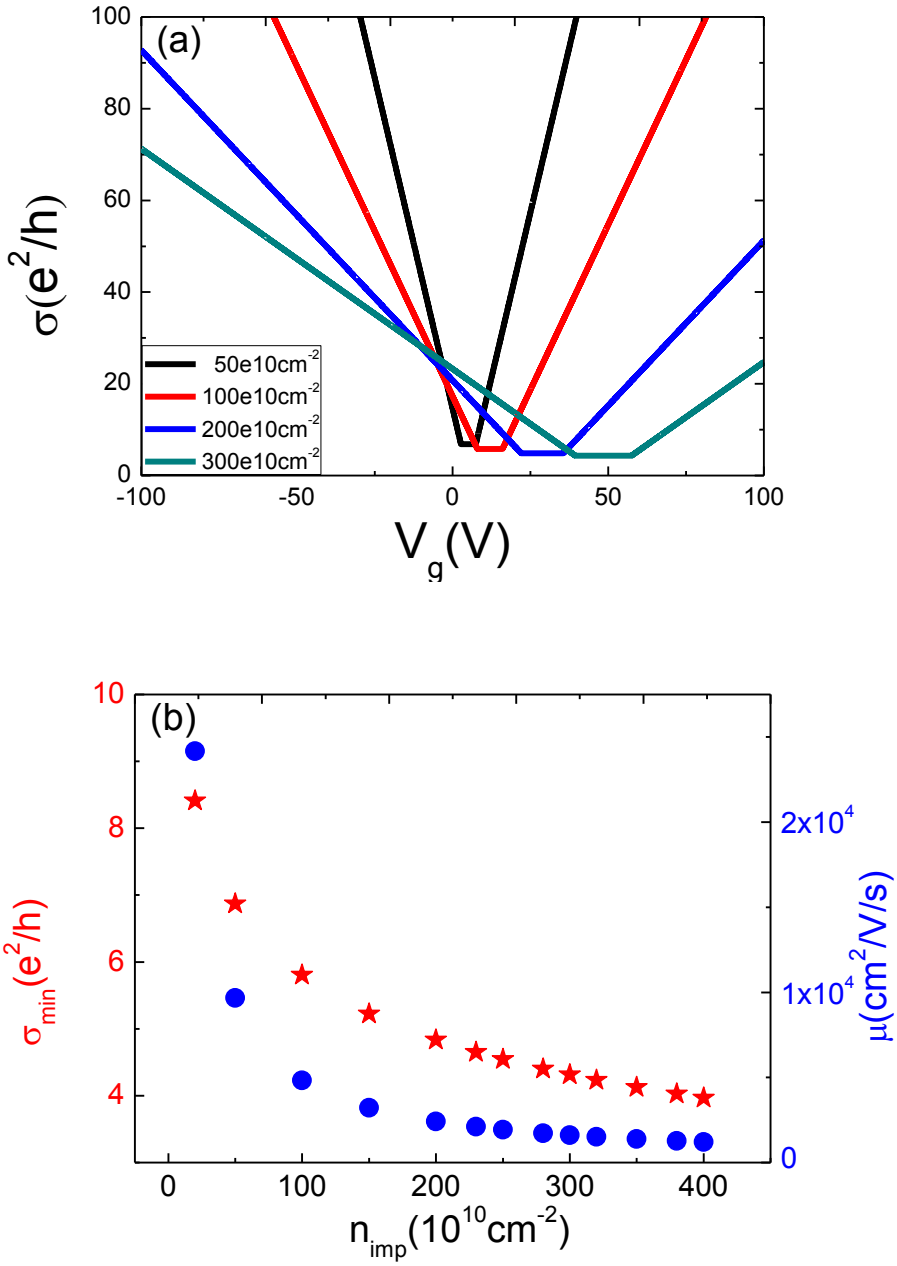

Figure 2.2. The Self Consistent Theory of Graphene Transport: (a) Effect of Charged Impurities (b) Gate dependent Transport properties of the self consistent theory of graphene.(Modified from [143])

As a summary, the self consistent theory can explain most of the transport properties of graphene, especially the mobility and the minimum conductivity. But for the shift of Dirac Point, the theory and the experiment cannot agree quantitative, because later experiment shows that this shift is affected sensitively by adsorbed water molecular, which is not charged impurities. Actually, up to date, there still other arguments that the scattering in graphene is so complicated, not only long range Coulomb scattering, but also others, such as short range defects scattering, corrugation scattering, and resonant scattering with the energy close to the Dirac Point. [145, 146] After all, this self consistent theory is an important step in the right direction.

2.3 Ballistic Transport in Graphene

The charged impurities reduce the mean free path of graphene, which makes graphene diffusive. However, for graphene FET in nanoscale, or suspended graphene after moving impurities, the mean free path becomes comparable, or even longer than the device dimension, ballistic transports were observed[105, 147, 148]. For ballistic graphene, the conductivity is given by Landauer Formula, which is[149, 150]:

$$\sigma = \frac{L}{W}\frac{4e^2}{h}\sum_n T_n \tag{2.15}$$

where Tn is the transmission coefficient, given by[150]:

$$T_n = \left| \frac{k_n}{k_n \cos(k_n L) + i \frac{\mu}{\hbar v_F} \sin(k_n L)} \right|^2 \tag{2.16}$$

with $k_n = \sqrt{(\frac{\mu}{\hbar v_F})^2 - (q_n)^2}$, $q_n = \frac{1}{W}\pi(n + 1/2)$ and W is the width of the FET, Based on it, the minimum conductivity and transport properties of ballistic graphene can be calculated, shown in Fig. 2.3, which correspond to the experiment data[105, 147].

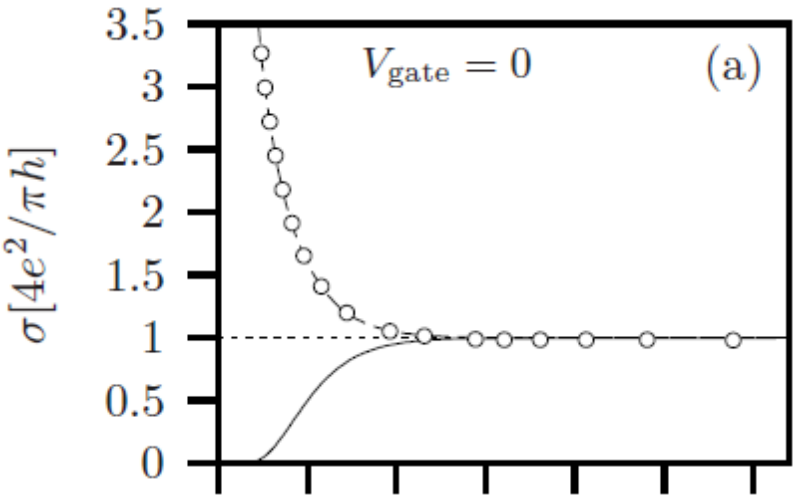

(a)

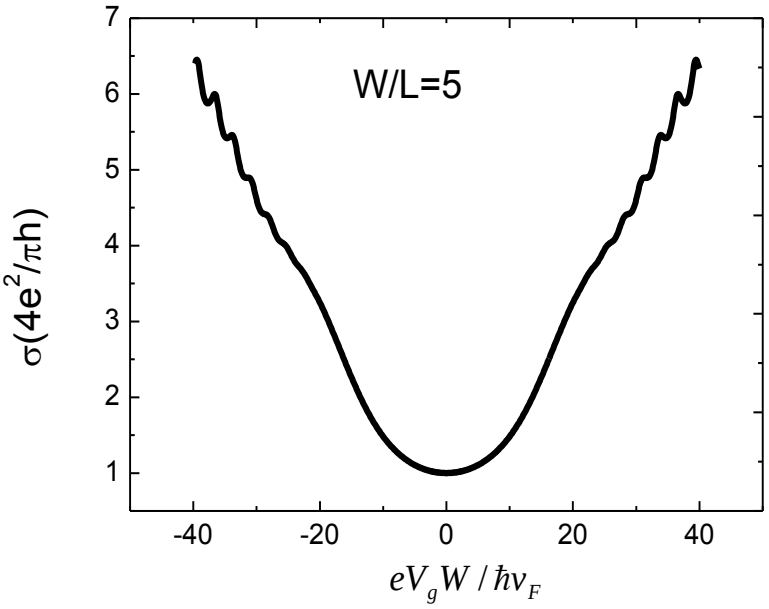

(b)

Figure 2.3. Ballistic Transport of Graphene.(Modified from [150])

Chapter 3

TRANSPORT OF GRAPHENE WITH TOP HIGH K MEDIUM

3.1 Introduction

As we can see in the first chapter, Graphene has attracted much attention because of its unique properties for potential high performance electronics and sensor applications [16, 101, 109]. Recent advances have been rapid, e.g., graphene field effect transistors (FET) with cutoff frequency up to 100 GHz has been demonstrated[151], but several issues remain to be addressed before reaching large scale commercial applications[109]. One of the important issues is the large variability in the mobility of graphene FETs. It is believed that charged impurities trapped between graphene and substrate or on the surface of graphene have profound effects on the mobility of graphene, and also on the location and conductivity value of the Dirac Point[137,140]. Many theoretical works have been devoted to determine the relationship between charged impurities and transport properties[143, 144, 152, 153]. It has been reported that a top dielectric layer can reduce the scattering of carriers by the charged impurities due to screening of the Coulomb potential, and, consequently, significantly increases the graphene mobility[154]. We have also observed large effects of top dielectric media on the current vs. gate voltage curves, and attributed the effects to a large enhancement in the mobility[155,156]. However, these conclusions were drawn based on the assumption that the back-gate capacitance is determined by the gate oxide and does not depend on the top dielectric layer. The validity of this assumption was questioned in a footnote by Ponomarenko et al. (Ref.[145]), although no detailed

supporting data was provided. Because the back-gate capacitance is critically important for correct interpretation of transport measurements, for understanding the transport mechanism, and for chemical and biosensor applications[128, 129], a systematic study of the effect of top dielectric medium on graphene FET back-gate capacitance is required, which is the goal of this chapter.

We performed Hall measurement on graphene FETs in the presence and absence of different top dielectric media. Using a micro-droplet method, we were able to determine the back-gate capacitance as a function of the size of the dielectric medium. We observed that adding a top layer dielectric medium dramatically increases the back-gate capacitance, and the increase is proportional to the size, but it has little effect on the mobility of graphene. These findings are further confirmed by numerical modeling of the back-gate capacitance. Our results do not support the assumption of constant back-gate capacitance that led to the conclusion of dielectric enhancement in graphene mobility [154-156]. In addition, our work indicates that one needs to consider both analyte-induced mobility and gate capacitance changes in the chemical and biosensor applications with graphene FETs[128,129].

3.2 Mobility Definition

We start with a brief clarification of the definition of graphene mobility. Three methods have been used to extract the mobility of graphene from the transport measurements so far. The first one is to select the linear regime of the transport curve $\sigma \sim V_g$, and fit it with $\mu = \Delta\sigma / (C_g \Delta V_g)$[16, 22, 137,157]. This mobility is

independent of carrier density, but the selection of linear regime is somewhat arbitrary because the transport curve is nonlinear. The second method is to calculate the mobility with $\mu = \sigma / ne = \sigma / C_g (V_g - V_{dirac})$ [23,105,145,148]. In this case, the mobility depends on V_g, or carrier density, because of the nonlinearity of the $\sigma \sim V_g$ curve. Near the Dirac Point(conductivity minimum), σ increases weakly with V_g. This regime has been referred to as the puddle regime, in which the carrier density is not well defined due to potential fluctuation[143,158], and the mobility based on the above definition in this regime is meaningless. Moving away from the puddle regime, σ increases rapidly with V_g and the mobility is the highest[105]. Further away from the Dirac Point, it reaches the sub linear regime, where the mobility decreases again, due to short-range scattering. The third definition of mobility is based on the following considerations. The total carrier concentration in graphene channel regions is given by $n_{tot} = \sqrt{n_0^2 + n[V_g]^2}$, so one can obtain the mobility by fitting gate dependent resistance with $R_{tot} = R_{contact} + \frac{L/W}{\sqrt{n_0^2 + n[V_g]^2}\, e\mu}$ [40, 159, 160], where n_0 is the carrier density at the conductivity minimum (referred to as residual carrier density[143]), n[V_g] is gated induced carrier density, R_{tot} and $R_{contact}$ are total resistance and contact resistance, respectively, L and W are the channel length and width, respectively. Note that the elimination of contact resistance is important to extract meaningful mobility with this approach[109]. In this work, we use the third method to extract graphene FET mobility.

3.3 Experiments, Results and Discussions

Single layer graphene FETs with Hall bar structure were fabricated. Briefly, a graphene piece was prepared on SiO_2 (300 nm)/Si substrate by mechanical exfoliation, and identified by color contrast[73] and Raman spectrum[74]. Cr(5nm)/Au(80nm) was used as electrode materials, and all the electrodes were covered by 4.5 μm-thick photoresist in order to eliminate leakage current. A narrow window of 4.3 μm wide is opened to expose graphene, as shown in Fig. 3.1(a). The inset is an AFM image of the FET channel of 9 μm long and 5 μm wide. Resistivity and Hall coefficient were measured at 0 T and 0.5 T at room temperature by applying 1 μA constant current, in air and in 1 mM, 100 mM and 1 M NaF aqueous solutions, respectively (Figs. 3.1(b)-(e). The hall coefficient is fitted by[16],

$$R_H = (n_h \mu_h^{\,2} - n_e \mu_e^{\,2}) / e \cdot (n_e \mu_e + n_h \mu_h)^2 \tag{3.1}$$

where n_e and n_h are the carrier densities of electrons and holes, μ_e and μ_h are the mobilities of electrons and holes, respectively. When one carrier type dominates, $R_H = 1/e \cdot n_{e,h} = 1/C_g(V_g - V_{dirac})$, allowing us to extract the gate capacitance. Also, the resistivity is fitted with the third method [159] mentioned above without including the contact resistance.

$$\rho = R_{tot} \times \frac{W}{L} = \frac{1}{\sqrt{n_0^{\,2} + n[V_g]^2}\, e\mu} \tag{3.2}$$

$$n[V_g] = C_g (V_g - V_{dirac}) / e \tag{3.3}$$

μ, n_0, and C_g in each situation were extracted and shown in Fig.3.2. Exposing the graphene FET to aqueous solutions results in an increase in the mobility by ~20% at 1mM (Fig. 3.2(a)). Increasing the ionic concentration leads to a small decrease in the mobility, this may be attributed to the scattering of carriers by ions adsorbed on graphene. Note this mobility decrease coincides with the increase in the residual carrier density shown in Fig. 3.2(b). Adding aqueous solution causes an increase in the gate capacitance by up to two orders of magnitude. This capacitance change has a profound effect on the change of transport curves. The gate capacitance does not significantly depend on the ionic concentration (we will return to this later), and it appears to depend on the dielectric constant of the medium[145]. We believe that this top dielectric medium-induced transport characteristic changes in other works[154-156] are also largely due to the gate capacitance.

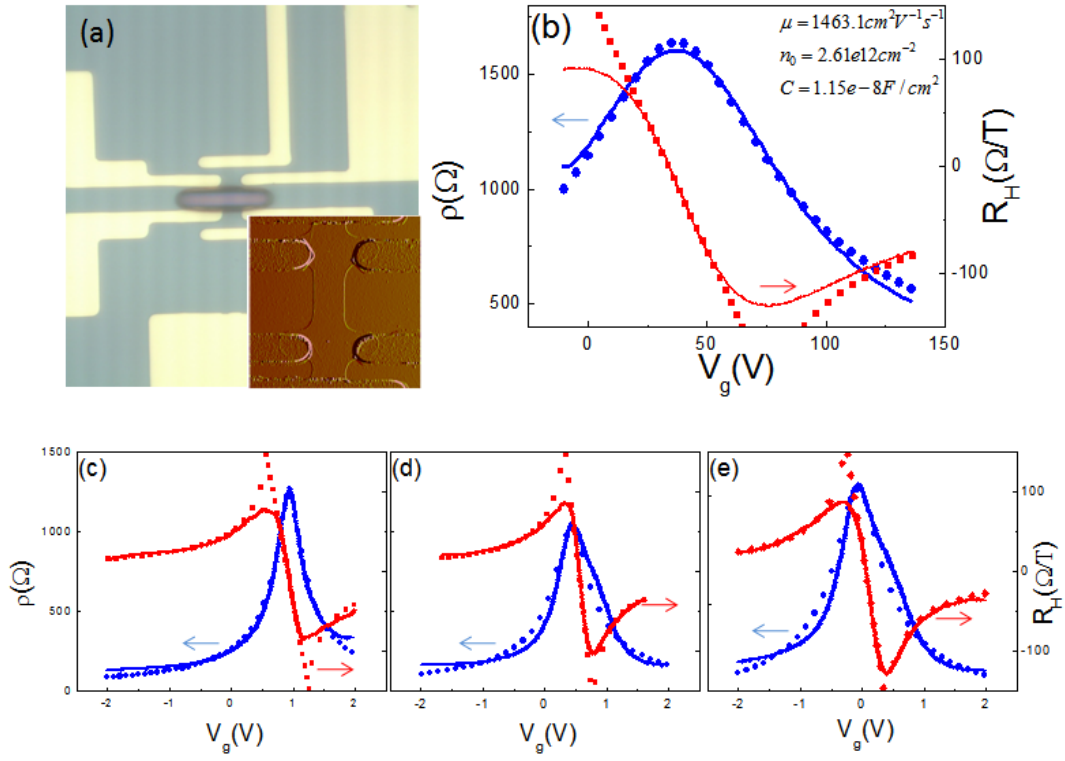

Figure 3.1. Screening Effects of top layer dielectric materials on the transport properties of a graphene FET. (a) Optical micrograph of a 6 pin Hall bar graphene FET. The inset is an AFM image of the channel region with channel width of $5\mu m$. Resistivity (blue curves) and Hall coefficient (red curves) of the graphene FET measured in air (b), 1mM (c), 100mM (d), 1M (e) NaF aqueous solutions, respectively. The symbols are the fittings.

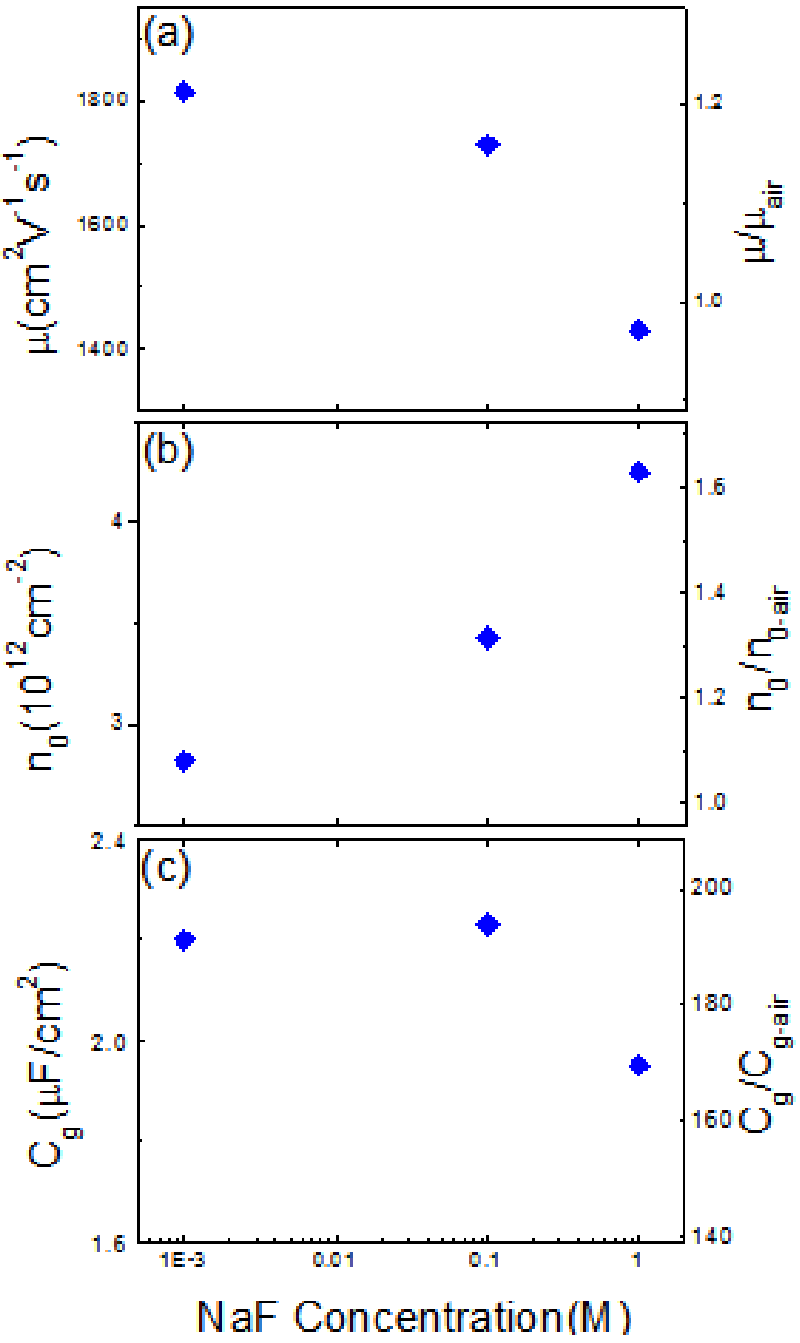
(a)
1800
1600
1400
μ(cm²V⁻¹s⁻¹)
1.2
1.0
μ/μair
(b)
4
3
n0(10¹²cm⁻²)
1.6
1.4
1.2
1.0
n0/n0-air
(c)
2.4
2.0
1.6
Cg(μF/cm²)
200
180
160
140
Cg/Cg-air
1E-3
0.01
0.1
1
NaF Concentration(M)

Figure 3.2. Dependence of (a) mobility μ, (b) residual carrier density n_0, and (c) the gate capacitance, C_g of graphene FET on NaF concentration. The data were extracted from the transport and hall measurements (see text for details).

We have carried out a systematic study of the gate capacitance dependence on the size of the top dielectric medium. To facilitate the study, we used a piezoelectric micropipette that can accurately produce micron-scale water droplets on the FET[161]. After placing a droplet on the FET, we controlled the size of the droplet via controlling water evaporation at a desired temperature (e.g. ~1^0 C). Fig. 3.3(a) shows $I_{sd} - V_g$ curves recorded during controlled evaporation (shrinking size) at $V_{SD} = 10$ mV. All the measurements were carried out with the same parameters, including ramping rate and potential windows, to minimize potential-induced effects[162]. When the size of water droplet decreases, Dirac Point shifts towards positive values (Fig. 3.3(b)). We note that the Dirac Point is the potential at which the conductivity is minimum and the gate induced carrier density neutralizes precisely the impurity induced carrier density[137,143] , which is $V_{dirac} = e\bar{n} / C_g$. For different sizes of water droplet, assuming the impurity density does not change, then the impurity induced carrier density in graphene ($\bar{n}$) should not change either. Then the shift in the Dirac Point potential must come from the change in the gate capacitance, which increases with the size of water droplet.

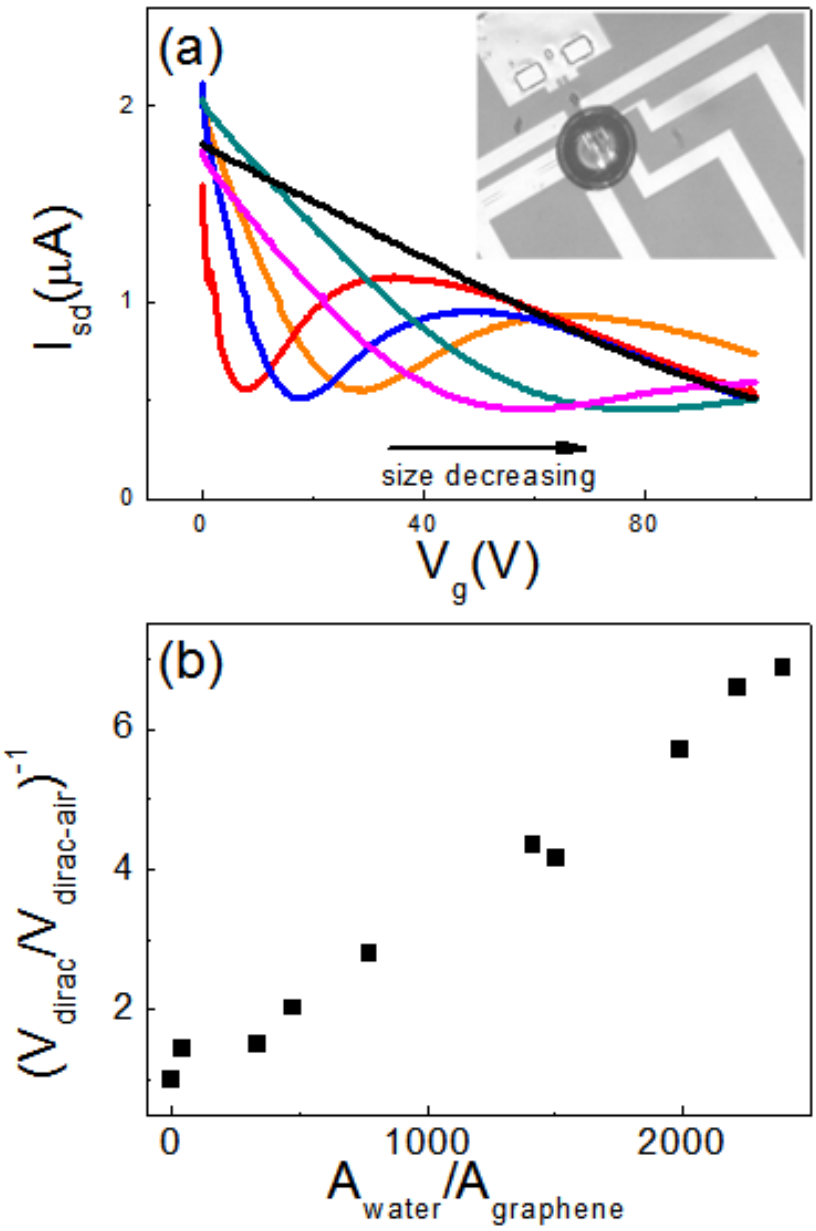

Figure 3.3. Size effect of top dielectric medium: (a) Two-probe transport curves of graphene FET covered by pure water with different sizes, with 10mV source drain bias. The inset is an optical image of measurement configuration. (b)

Relative change of Dirac Point as a function of the area ratio of water droplet and graphene channel.

The next question is what causes this large top dielectric medium-induced change of gate capacitance. In order to address this question, we carried out numerical simulation of gate capacitance using finite element method (FEM) (COMSOL 3.5a AC/DC model). Fig. 3.4(a) is a 3D simulation, showing the effect of top layer media on the gate capacitance, with different dielectric constant (covering the whole surrounding environment). Note that in the model simulation, the graphene dimensions are 1 μm x 1 μm with thickness of 0.34 nm, the SiO_2 layer is 300nm with dielectric constant of 3.9 and the top medium has various κ values. The simulation shows that the gate capacitance increases linearly with the dielectric constant of top medium. For $\kappa = 80$ the gate capacitance increases by about 9 times, which is large but smaller than the experimental value(~200 times). This mismatch could come from the trapped charge in the substrate or the interface charge at the water/graphene interface relocated by the electrical field. To illustrate the size effect of water droplet, 2D FEM simulation is used due to computational limit. Fig. 3.4(c) and (d) show the electrostatic field distributions with and without the water droplet. The calculated gate capacitance increases with the size of the water droplet, in agreement with the experimental finding (Fig. 3.4(b)), it also shows a saturation after certain enhancement.

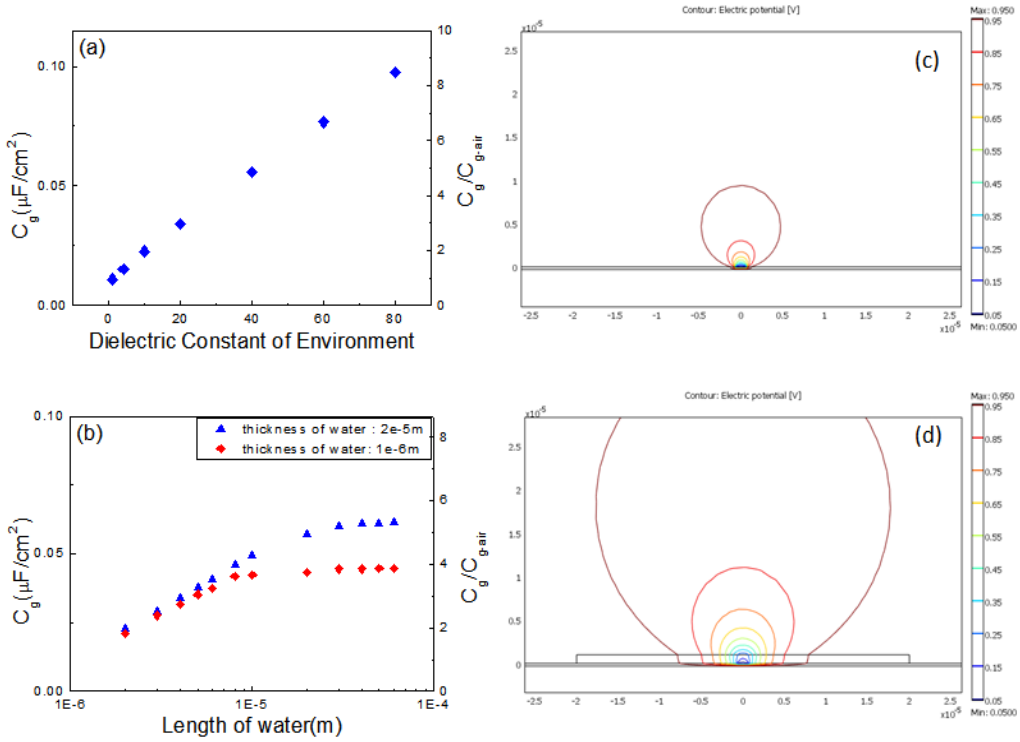

Figure 3.4. Simulations of gate capacitance of graphene FET: (a) 3D simulation of gate capacitance covered by top dielectric media with different dielectric constants. (b) 2D simulation of gate capacitance of a water droplet ($\kappa = 80$) with different sizes. (c) Potential distribution without a water layer. (d) Potential distribution with a water layer($40\mu m \times 6\mu m$). Note that the water layer is simplified as a rectangular shape.

We have also recorded the transport curves of graphene FETs before and after placing a water droplet on top and during the evaporation of the water droplet (Fig. 3.5). Immediately after introducing a water droplet, the source-drain current increases. As the water droplet evaporates, the current decreases, and eventually returns to the origin level when the water droplet completely evaporates. The

current change depends on the size of the water droplet, which, as we have already shown, is due to gate capacitance change. Vapor sensors based on graphene FETs were demonstrated[128-129], for water and other molecules detections, and the observed dependence of the transport properties was attributed to charge transfer between graphene and the adsorbed molecules. An alternative explanation is that the adsorbed molecules act as scattering centers to the carriers, which decreases the mobility[143]. The present work shows that adsorbates may also change the transport curve via changing the gate capacitance. This adsorbates induced capacitance change has also been observed in carbon nanotube(CNT)[163], which was attributed to the limited diameter of CNT. For graphene with even thinner thickness, this effect could be more significant.

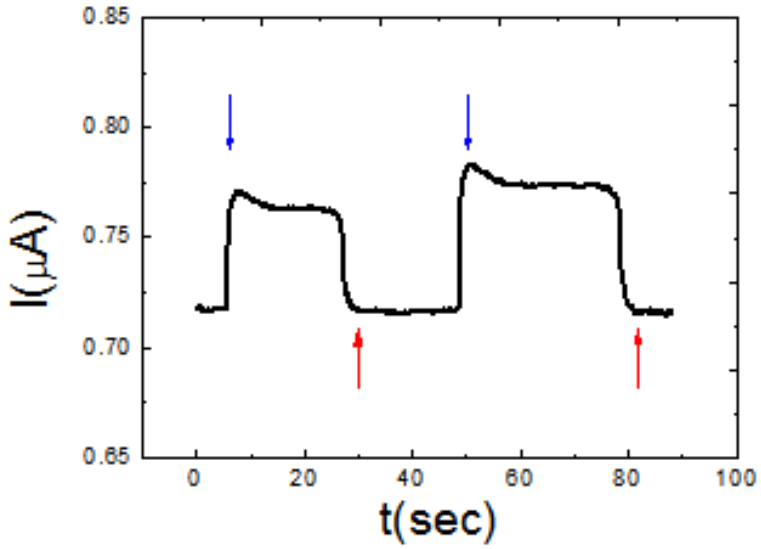

Figure 3.5. Real-time transport current of a graphene FET exposed to a water droplet. Source-drain bias is 10mV without gate potential. Red and blue arrows indicate water injection and complete evaporation, respectively. Two water droplets of different sizes were studied.

3.4 Conclusions

In conclusion, we have measured gate capacitance and mobility of graphene FET with and without top dielectric medium using Hall measurement. We have found that the gate capacitance can increase by up to two orders of magnitude, depending on the size of the top dielectric medium, while the mobility remains nearly constant. We have performed numerical calculations, which support the observation. We have also determined the gate capacitance as a function of the size of the top dielectric medium (water droplet), and observed that the gate capacitance increases with the size. Our work shows that that the previously observed large top dielectric medium effect is large possibly due to the increase in the gate capacitance, rather than enhancement in the graphene mobility. The sensitive dependence of the gate capacitance on the top dielectric medium points to the alternative mechanism of graphene FET-based chemical sensor applications.

Chapter 4

QUANTUM CAPACITANCE OF EXFOLIATED GRAPHENE

4.1 Introduction

The electron transport properties of graphene devices are critical to many applications, but our understanding of these properties is still incomplete despite rapid advance in recent years. One unsolved puzzle is the minimum in the conductivity at the Dirac point, which has stimulated many recent theoretical and experimental efforts [23, 164]. It has been proposed that this minimum is due to charged impurities that induces puddles[138] of electrons and holes in graphene. To fully understand the transport properties, it is important to investigate the scattering of the carriers by the impurities, and also the density of carriers at and near the Dirac point (which is related to the quantum capacitance). Electron transport in graphene has been studied using the field effect transistor (FET) configuration: a graphene sample is placed on an oxidized Si substrate and connected to source and drain electrodes, and the current through the graphene is controlled with a back gate. The capacitance in these devices is dominated by the capacitance of the oxide layer, which makes it difficult to determine the quantum capacitance. However, in order to decrease the operation voltage, it is expected that the oxide layers in future devices will be much thinner and have higher values of k, which means that the quantum capacitance will eventually be the dominant source of capacitance. Chen and Appenzeller[165] reported an effort to extract quantum capacitance of graphene. Due to the large contribution from the gate oxide and trap capacitance contributions in the top gate device, their measured

capacitance is an order of magnitude smaller than the quantum capacitance. In the present work the use electrochemical gate and ionic liquid reduce the Debye ionic screening length to a few Å, which makes the quantum capacitance a dominant component of the measured capacitance. We provide also a simple theory including only one parameter (impurity concentration), to quantitatively explain the measured quantum capacitance.

In addition to electronic applications, graphite and other carbon-based electrodes have already found broad applications in analytical chemistry, electrochemistry, batteries, chemical sensors and biosensors. The interfacial capacitance, a basic quantity in these applications, is unusually small and has a peculiar V-shape comparing with metal electrodes, which has been a longstanding puzzle. Measuring the quantum capacitance of a single and multiple layer graphene in electrolytes will shed new light into the interfacial capacitance puzzle of the carbon electrodes.

The expression of the quantum capacitance for a perfect graphene sheet has been derived [166, 167], but direct measurements that can compare with the theories are still lacking. F.Giannazzo et.al.[168] studied local capacitive properties of graphene using scanning probe microscopy (SPM). Absolute capacitance values per unit area were difficult to obtain because the SPM tip geometry was unknown and variable, and the quantum capacitance contribution was negligibly small comparing to the capacitance contribution from the thick oxide used in the experiment. In the present work, we measure the quantum capacitance of single layer graphene in an ionic liquid electrolyte. The ionic liquid

is chemically inert and stable, and more importantly, its Debye ionic screening length is virtually zero which makes the quantum capacitance a dominant source of the measured capacitance. We are thus able to determine the absolute values of graphene capacitance as a function of voltage, and compare the experimental results with the theoretical predictions. In order to resolve the peculiar interfacial capacitance of carbon electrodes, we also study the capacitance of graphene in aqueous solutions at different ionic concentrations.

First of all, what is quantum capacitance? General speaking, quantum capacitance is a physical concept first introduced by Serge Luryi in 1988[169], to describe the properties of 2D electron gas, which is defined as:

$$C_Q = \frac{\partial Q}{\partial V_{ch}} \tag{4.1}$$

where V_{ch} is the potential of 2D electron gas.

For normal 2D electron gas, we know that its density of state can be described by:

$$g(E) = \frac{m^*}{\pi\hbar^2} \tag{4.2}$$

And $$k_F = [2\pi n]^{1/2} \tag{4.3}$$

So, the quantum capacitance can be calculated:

$$C_Q = \frac{m^* e^2}{\pi\hbar^2} \tag{4.4}$$

This means that for traditional 2D electron gas, the quantum capacitance is constant.

Actually we can consider quantum capacitance like this, assuming a piece of metal, above what there is an electron charge, which will introduce electrical field around it. But due to total screening effect, in the space below the metal, no electrical field can be sensed from the single charge. However, when the piece of metal becomes thinner and thinner, until forms a 2D electron gas system, then there is no enough electrons in it to screen out the electrical field from the single charge, electrical field can be sensed underneath the 2D metal. This phenomenon is just because of quantum capacitance of 2D gas.

4.2 Experiments Methods

Graphene was obtained by mechanical exfoliation of Kish graphite using electronic grade dicing tape to reduce contaminations.[170] Si chip coated with a 290 nm thick SiO_2 layer was used as substrate because single layer graphene is known to develop a distinct color contrast that can be easily identified under an optical microscope[73, 171]. Electrochemical gate potential was applied to the graphene with respect to a Pt quasi-reference electrode inserted in the electrolyte and controlled by a potential-stat (Model 283, Princeton Applied Research). The potential in the case of aqueous electrolytes was calibrated vs. the widely used Ag/AgCl electrode. In order to control the gate voltage precisely, a Pt counter electrode was included to form the standard 3-electrode electrochemical configuration.[172] A small AC modulation (100Hz, 0.01V) is superimposed to the sweeping gate potential (10mV/s), and the AC current response was measured by a lock-in amplifier (SR850 DSP, Stanford Research Systems), from which the

capacitance was determined. In the setup, the dimensions of the connection electrodes were minimized, all the cables and sample holder were carefully shielded to minimize background capacitance. A small residual background capacitance (~1pF) was determined using a control experiment in which no graphene was present.

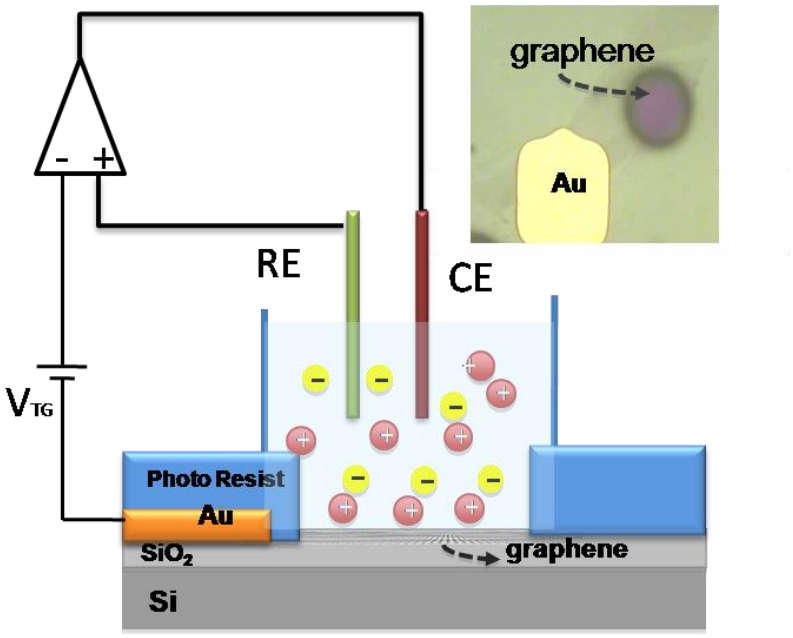

Fig. 1

Figure 4.1. Schematic illustration of quantum capacitance measurement setup in which a graphene sheet on a SiO_2/Si substrate is connected to a Au electrode. The edge of the graphene sheet is covered with insulation layer so that only the top surface is exposed to an ionic liquid electrolyte. The potential of the graphene is controlled and varied with respect to a Pt reference electrode using 3-electrode electrochemical configuration. The inset is an optical micrograph of the graphene device.

4.3 Quantum Capacitance of single layer graphene

Fig.4.1 shows the experimental setup, where a graphene sheet supported on Si/SiO_2(290nm) substrate is connected to a Cr(5nm)/Au(80nm) electrode. The graphene surface is covered by a thick photoresist layer (~4.5 μm) except for a small window with a diameter of 10 μm, exposed to the electrolyte. This configuration minimizes the background capacitance and prevents the exposure of the graphene edges to electrolyte. The interfacial capacitance of the graphene is measured using the standard three electrodes electrochemical cell using a potential-stat in which the potential of graphene is controlled with respect to a reference electrode (a Pt electrode). The inset of Fig.4.1 shows the optical image of the device with one electrode. The distinct color together with Raman spectroscopy provides accurate identification of single layer graphene (or bilayer graphene; see supporting information). Prior to capacitance measurement, each device is cleaned and annealed at 200^0C in Ar/H_2 environment[173, 174] to remove contaminations coming from the device fabrication. An alternative device configuration, in which the graphene is connected to two electrodes, is also used. The alternative configuration provides an additional flexibility to pass a current along the graphene sheet to remove contaminations. Both one- and two-electrode approaches produce similar results.

Fig. 4.2(a) shows the capacitance vs. gate potential measured in 1-butyl-3-methylimidazolium hexafluorophosphate (BMIM-PF_6), an ionic liquid. A Raman spectrum used to verify the thickness is shown in Fig. 4.2(b). Due to the high ionic concentration of the ionic liquid ($2.9\times10^{21} cm^{-3}$), the Debye length

approaches zero, so the measured capacitance consists of only two contributions: interfacial capacitance arising from the double layer at the graphene-ionic liquid interface and the quantum capacitance of graphene. The two can be modeled as two capacitors in series and the one with a smaller value dominates the total capacitance. The double layer arises from the accumulation of a layer of counter ions on a charged electrode, which has been modeled by a parallel plate capacitor whose capacitance per unit area is given by $\varepsilon_0\varepsilon/t$, where $\varepsilon_0=8.85\text{x}10^{-12}$F/m, ε is the dielectric constant of the ionic liquid and t is radius of the counter ions. For BMIM-PF_6 ionic liquid, $\varepsilon=7$[175] and t~0.3 nm, which leads to a double layer capacitance of ~21 $\mu F/cm^2$. We have measured the double layer capacitance directly using the same experimental setup (shown in supporting information). The measured double layer capacitance is ~21 $\mu F/cm^2$ and changes within ±3% within the gate voltage window, which are consistent with the model. These results are also in good agreement with a previous report by S.Baldelli [175]. The double layer capacitance is large comparing to the theoretically predicted quantum capacitance of graphene. Furthermore, the double layer capacitance does not depend on the potential strongly, making it straightforward to extract the quantum capacitance (red line in Fig. 4.2(a)). We have also measured the quantum capacitance of a bilayer graphene using the same procedures. Before discussing the experimental data, we summarize the theoretical prediction of the quantum capacitance for an ideal graphene.

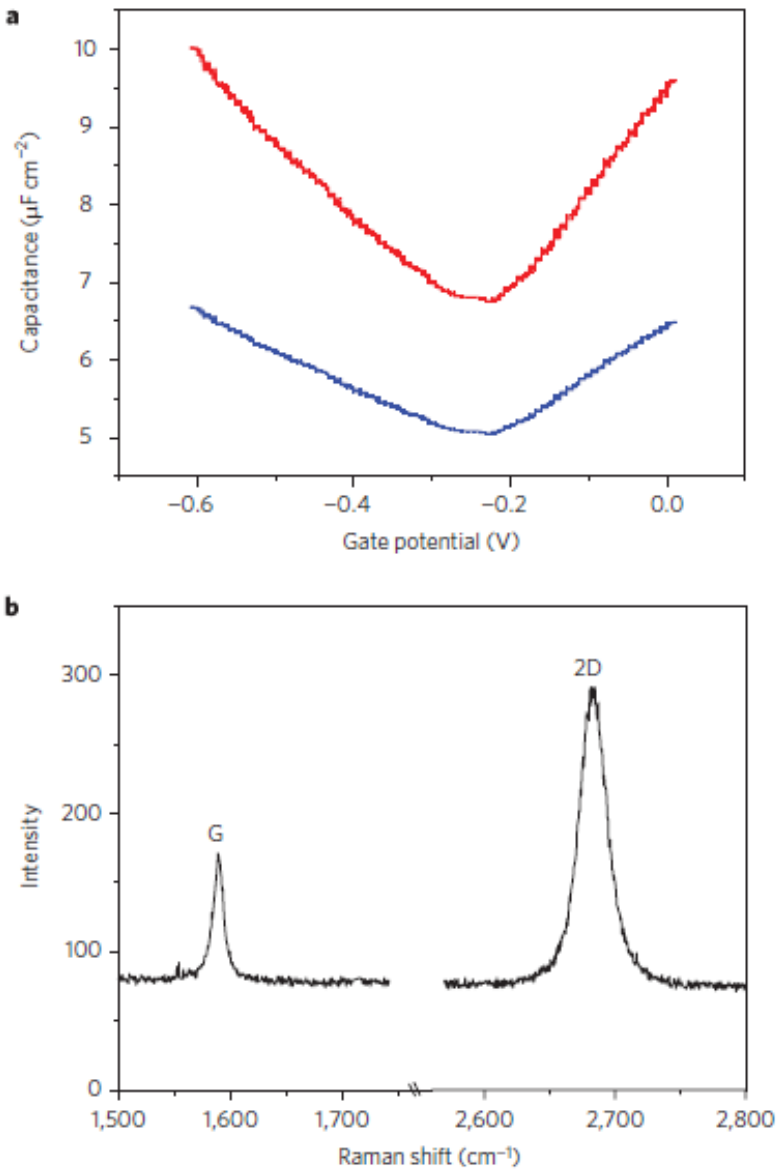

Figure 4.2. Capacitance of graphene as a function of gate potential. (a) Total capacitance (blue line) and quantum capacitance (red line) of graphene measured in ionic liquid ([BMIM]PF_6). The potential is quoted with respect to Pt quasi-reference electrode. (b) Raman spectrum of the single layer graphene device.

The expression of quantum capacitance has been derived based on 2D free electron gas model, which takes the form of[167]

$$C_Q = \frac{2e^2 k_B T}{\pi(\hbar v_F)^2} \ln[2(1+\cosh\frac{eV_{ch}}{k_B T})] \tag{4.1}$$

where $\hbar$ is the Planck constant, e the electron charge, k_B the Boltzmann constant, $v_F \approx c/300$ the Fermi velocity of the Dirac electron, and $V_{ch} = E_F / e$ is the potential of graphene. When $eV_{ch} >> kT$, Equation (4.1) reduces to[172]

$$C_Q \approx e^2 \frac{2}{\pi} \frac{eV_{ch}}{(\hbar v_F)^2} = \frac{2e^2}{\hbar v_F \sqrt{\pi}} \sqrt{n} \tag{4.2}$$

The theory provides a quantitative description of graphene quantum capacitance in terms of Fermi velocity, carrier density temperature and fundamental physical quantities (blue circles in Fig. 4.3(a)). Several important features worth noting: 1) the quantum capacitance has a minimum value at the Dirac point, and 2) the minimum value is close to zero, 3) it increases linearly with V_{ch} with a slope of $23\mu F/cm^2/V$, and 4) it is symmetric with respect to the Dirac point, shown in Fig. 4.3.

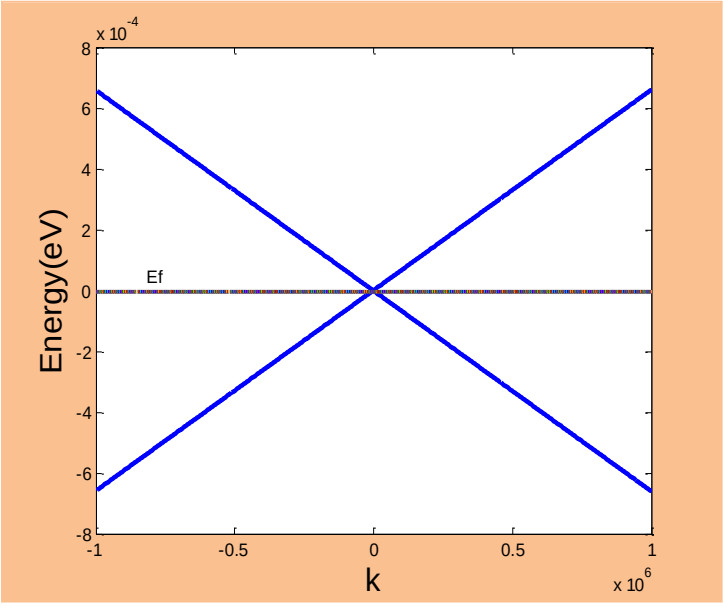

(a)

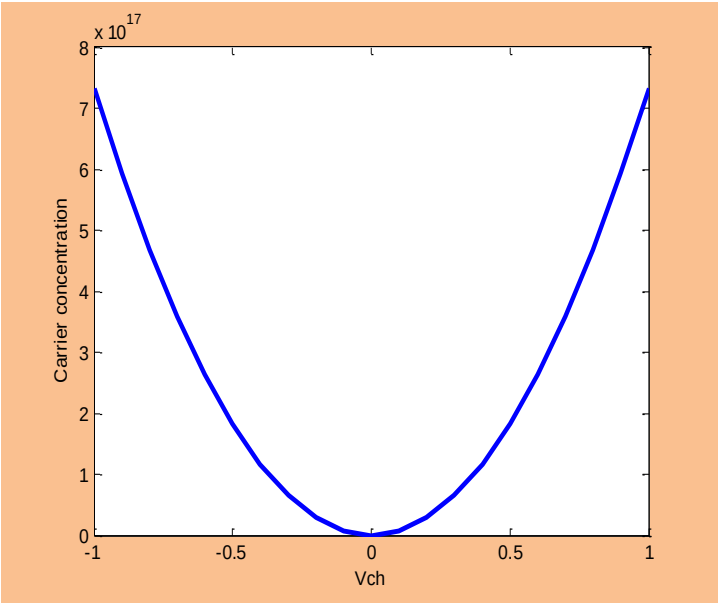

(b)

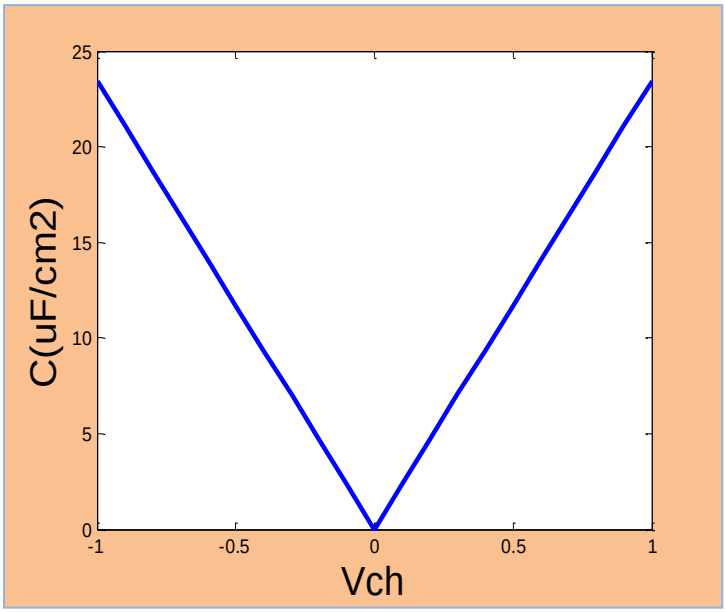

(c)

Figure 4.3. Theoretical calculation of graphene(a) band structure;(b) carrier density; (c)quantum capacitance

In order to compare the measured capacitance with the theory, we re-plot the experimental result in Fig. 4.4(b) (blue dots) in terms of V_{ch} , given by $V_{ch} = V_g C_i /(C_i + C_g)$, where V_g is the gate potential and $C_i = 20\mu F / cm^2$ is the double layer capacitance of the ionic liquid[175]. The measured quantum capacitance displays the "V-shape" and the absolute values are also close to the theoretical prediction. However, there are several distinct discrepancies: 1) the measured quantum capacitance minimum is round, which is more than what thermal smearing at room temperature can possibly produce; 2) the measured minimum is much greater than the predicted value, $C_{Q,\min} = \frac{2e^2 k_B T}{\pi(\hbar v_F)^2}\ln(4) \sim 0.8\mu F / cm^2$ (thermal induced); 3) the measured slope is about $11\mu F / cm^2$/V, which is only about half of the predicted value.

The theoretical model is based on the assumption of a pure and perfect graphene. In reality various impurities and defects exist, and recent theoretical and experimental results have shown that charged impurities play a key role in the transport properties of graphene near the Dirac point.[137, 143] It has been reported that charged impurities in substrates leads to local potential fluctuations and electron/hole puddles in graphene[143,158]. The potential fluctuations based on a self-consistent theory give rise to an additional carrier density, n*, induced by the impurities. While a microscopic capacitance theory including local potential fluctuations is not available, a simple approximation to take into account of the additional carrier density is to express the total carrier concentration as

$$n = |n_G| + |n^*| \tag{4.3}$$

where n_G and n^* are the carrier concentrations caused by the gate potential and charged impurities, respectively. Consequently, the quantum capacitance is given by

$$C_Q = \frac{2e^2}{\hbar v_F \sqrt{\pi}} (|n_G| + |n^*|)^{1/2} \tag{4.4}$$

Note that:[172]

$$n_G = (\frac{eV_{ch}}{\hbar v_F \sqrt{\pi}})^2 \tag{4.5}$$

Combining Equation (4.4) and (4.5), we can calculate the quantum capacitance of graphene as a function of potential of graphene at different impurity densities.

The inclusion of the impurity contribution explains the experimental results well. First at zero potential, $n_G = 0$ and the quantum capacitance is finite and determined by the effective or residual carrier concentration, n^* [143]. Second, the slopes of the linear regimes on both sides of the capacitance minimum are reduced by the charged impurities. Finally, the capacitance minimum regime is round. To further illustrate the importance of the charged impurities, numerical simulation of the quantum capacitance at different impurity densities is performed (Fig. 4.4(a)). The results show that as n^* increases, the minimum capacitance value increases, the minimum region becomes increasingly round, and the slopes decrease. We also fit the experimental results using Equation (4.5) (red line in Fig. 4.4(b)), which gives $n^* \sim 8\times10^{11} cm^{-2}$. Note that a constant representing the

background capacitance from electrodes and leads is included in the fitting, which is $\sim 4\mu F / cm^2$. This value is of the same order of magnitude as the background capacitance estimated using a device containing no graphene. We also note that the position of the measured capacitance minimum occurs at -0.17 V (vs. Pt reference electrode). This value is arbitrary, depending on the reference electrode, and only the potential change relative to the reference electrode is significant.

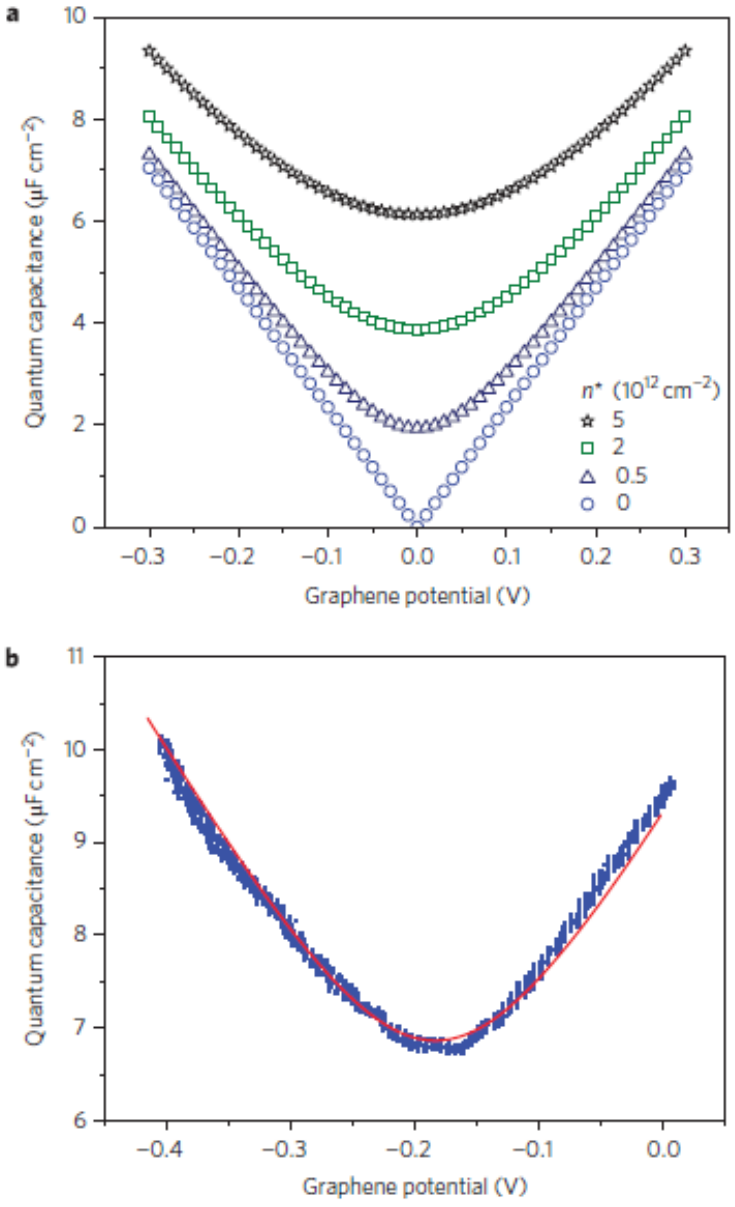

Figure 4.4. Dependence of quantum capacitance on potential of graphene (V_{ch}). (a) Simulated capacitance at different effective charged impurities, n^* (0, 0.5, 2 and $5x10^{12}$ cm^{-2} from bottom to top). (b) Fitting the measured capacitance (blue dots) with the theory (red line).

Based on the self-consistent theory[143], n^* should be effective charged impurity concentration (or induced residual charged impurity concentration), which is related to n_{imp}, the impurity density, and given, according to the self-consistent theory,[139, 143, 154] by

$$n_{imp} = \frac{n^*}{[2r_s{}^2 C_0^{RPA}(r_s, a = 4d\sqrt{\pi n^*})]} \tag{4.6}$$

where $r_s = \frac{2e^2}{\hbar v_F(\varepsilon_1 + \varepsilon_2)}$ and $C_0{}^{RPA}$ is the correlation function from the random phase approximation(RPA), and d (~ 1 nm) is the average distance from the charged impurity to graphene. $\varepsilon_1 = 3.9$ and $\varepsilon_2 = 7$ are the dielectric constants of SiO_2 and ionic liquid [BMIM]PF_6,[175] respectively, which leads to r_s=0.364. Using these parameters and the fitting result, $n^* \sim 8\times10^{11} cm^{-2}$ we determine n_{imp}=8.6 x 10^{12} cm^{-2}. This level of charged impurities is reasonable for graphene supported on SiO_2. [143, 176]

In order to determine if the peculiar interfacial capacitance of the carbon electrodes has a quantum origin, we have measured the capacitance of graphene in aqueous NaF solution. We chose NaF as electrolyte because it is commonly used for interfacial capacitance measurements, both Na^+ and F^- ions are

chemically inert and do not specifically adsorb on graphene surface. Fig. 4.5 shows the capacitance-potential curves at different ionic concentrations of the same device. Both the shape and magnitude of the capacitance measured in the aqueous electrolyte are similar to that in the ionic liquid. An important difference is the dependence of the capacitance on the ionic concentration. In aqueous solution, the double layer capacitance have a value of 10 to 20 $\mu F / cm^2$,[177] independent of ionic concentration. However, different from the ionic liquid, the Debye lengths of the aqueous electrolytes are much greater, which leads to an additional diffuse layer capacitance[178] contribution to the total capacitance. This diffuse layer capacitance is known to depend on the ionic concentration, which is likely the reason of the upward shift of capacitance with the concentration.[177, 179]Increasing ionic concentration also causes a positive shift in the position of the capacitance minimum. We have recently carried out a systematic study of the transport properties of graphene vs. gate voltage at various ionic concentrations, and found that the effective density of charged impurities decreases with the ionic concentration due to screening.[180] The positive shift in the capacitance observed here can be also explained in terms of the ionic screening.

In contrast to metal electrodes, the interfacial capacitance of carbon based electrodes, including single crystal basal plane of graphite, is not only an order of magnitude smaller but also shows greater variability depending on the impurity level of the materials. The unusual capacitance is explained in terms of space charge capacitance.[177, 179] However, the space charge capacitance theory

developed for semiconductors cannot explain the shape of the capacitance curves. Another serious difficulty of the space charge capacitance model is that the Debye length of the graphite is comparable to the lattice dimension due to the high carrier concentrations found in graphite.[177]

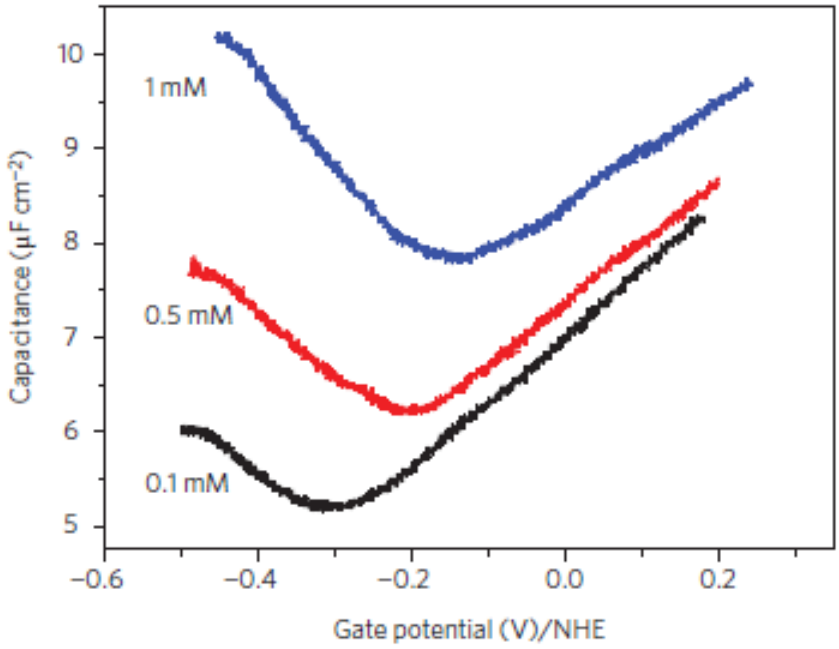

Figure 4.5. Capacitance of graphene in aqueous solution. Capacitance of graphene measured in NaF aqueous solution at different ionic concentrations (0.1, 0.5 and 1mM, from bottom to top). The potential is quoted with respect to the widely used NHE (normal hydrogen electrode) reference electrode.

One of the most carefully measured systems is the basal plane of graphite by Randin and Yeager.[177, 179] Its interfacial capacitance is remarkably similar to the quantum capacitance of a single layer graphene, as well as that of bilayer graphene (see supporting information): 1) All of them have a capacitance minimum and linear increase on both sides of the minimum, 2) the capacitance

values and slopes of the linear regimes are also close, 3) the capacitance curve shifts upward with ionic concentration in both graphene and graphite. This level of similarity suggests that the quantum capacitance model provides a natural and quantitative explanation of the mysterious interfacial capacitance of graphite and other carbon electrodes. The modified quantum capacitance model also explains the sensitive dependence of the carbon electrodes on impurities. Finally, the quantum capacitance model is consistent with the recent observation of Dirac Fermions or two-dimensional electron and hole gases at the surface of graphite.[181] However, a complete interfacial capacitance theory including both the quantum contribution and impurities is yet to be developed.

4.4 Quantum Capacitance of double layer graphene

The capacitive behavior of double layer graphene is also studied with the same setup. Fig. 4.6(a) shows the capacitance vs. potential of a double-layer graphene device measured in ionic liquid ([BMIM]PF_6) and Fig. 4.6(b) shows the Raman spectrum of the device to confirm the graphene thickness.[74] The quantum capacitance of double layer graphene (red line) is determined from the total capacitance (blue line) by subtracting the contribution from the double layer capacitance of the ionic liquid. The overall quantum capacitance vs. gate potential for the bilayer graphene is similar to that of a single layer graphene. A detailed explanation of the observation is discussed in the next section.

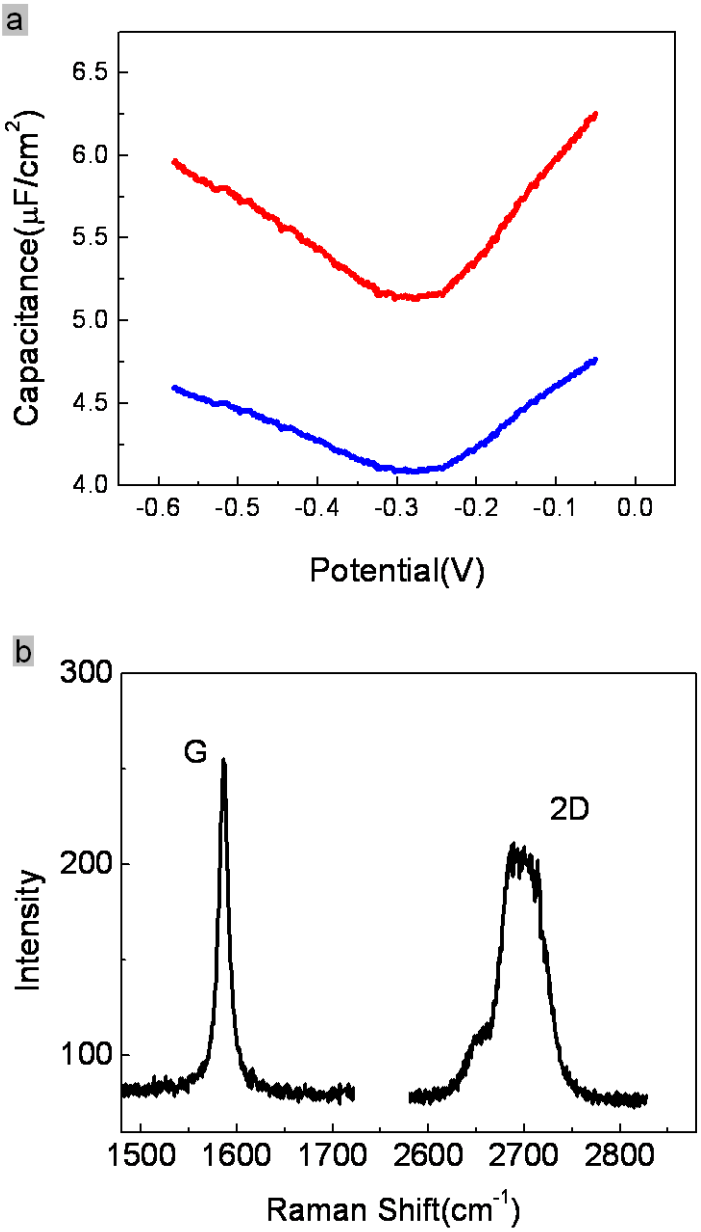

Figure 4.6. Capacitance of bilayer graphene as a function of gate potential. (a). Total capacitance (blue line) and quantum capacitance (red line) of a bilayer graphene measured in ionic liquid ([BMIM]PF_6). (b). Raman Spectrum of the bilayer graphene device.

For a conventional 2D electron gas system, the quantum capacitance is independent of gate voltage and given by $C_Q = \frac{g_v m e^2}{\pi \hbar^2}$ [169], where m is the effective mass, and g_v is the valley degeneracy factor. However, bilayer graphene is different from the conventional 2D electron gas because of its unique band structure. There have been several theoretical calculations [182, 183] on the band structure of double layer graphene. In E.McCann's study[183], the band structure of double layer graphene can be written as:

$$E = \pm \frac{1}{2} \gamma_1 [\sqrt{1 + 4\pi v^2 p^2 / \gamma_1^2} - 1] \qquad (4.7)$$

Here, γ_1 is the interlayer coupling, which equals 0.39eV, v is the Fermi velocity, and $p = \hbar k$. From Eq. 4.7, the band structure of double layer graphene is quadratic at small momenta and becomes linear at high momenta. In other words, bilayer graphene behaves like a conventional 2D electron gas only at very low momenta, and it becomes increasingly like single layer graphene with increasing momentum.

Based on Eq. 4.7 and $k = \sqrt{\pi n}$ for 2D electron gas, we have calculated the quantum capacitance of bilayer graphene (Fig. 4.7). The calculation shows, just as observed experimentally in this work, that the gate dependence of the quantum capacitance of bilayer graphene is similar to that of single layer graphene. One difference, however, is the finite capacitance value of $4.6 \mu F / cm^2$ in the disorder-free bilayer graphene. This minimum quantum capacitance value comes from the quadratic spectrum at low momenta with an effective mass of

$m = \gamma_1 / 2v^2$. Using the conventional 2D electron gas model[169], we have $C_Q = \frac{g_v m e^2}{\pi \hbar^2} = 4.6 \mu F / cm^2$ ($g_v = 2$), which confirms the numerical calculation shown in Fig. 4.7.

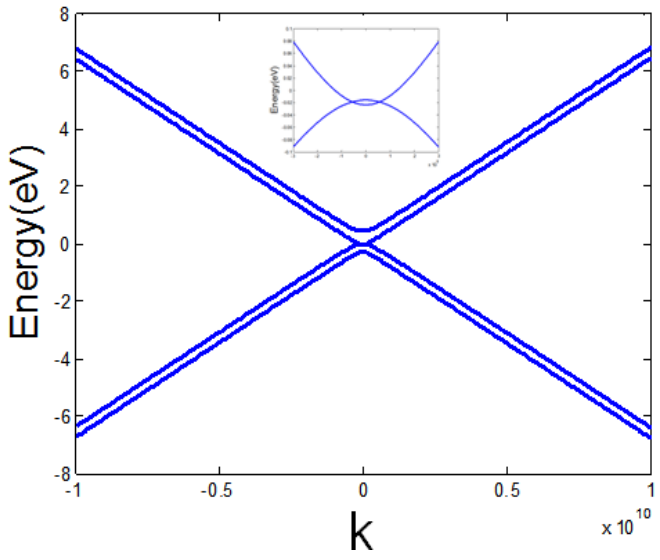

(a)

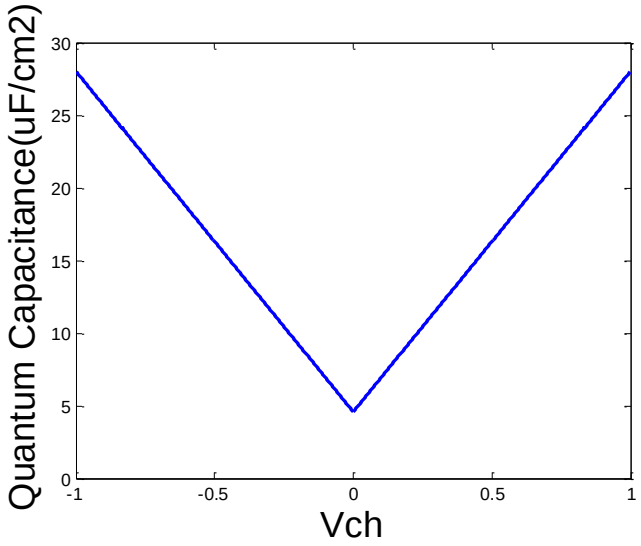

(b)

Figure 4.7. Theoretical calculation of (a) band structure , and (b) quantum capacitance of perfect bilayer graphene.

We note that the theoretical slope is much greater than the measured slope for bilayer graphene. We have shown that impurities can drastically lowered the slope for single layer graphene. The observed small slope for bilayer graphene is also likely due to impurities. However, unlike single layer graphene, a theory for treating impurities in bilayer graphene has not yet been developed. A proper theory would have to consider the effects of impurities on both the first and second layers, which requires a self-consistent theory to include the screening of the impurity field by the carriers in both layers. This is further complicated by the possibility of impurities intercalated between the two layers. Further work will be needed for quantitative understanding of bilayer graphene.

4.5 Conclusions

In summary, we have measured the quantum capacitance of graphene (single and double layers) as a function of gate potential. The quantum capacitance vs. gate potential displays a symmetric V shape with a minimum at the Dirac point which agrees with the theoretical model developed for the ideal graphene. The absolute values of the quantum capacitance are also close to the theoretical prediction. However, there are several significant discrepancies between the disorder-free theory and our experiment: 1) The minimum quantum capacitance at the Dirac point is finite and non-universal which in sharp contrast to the small

value (0.7 $\mu F/cm^2$) predicted by the theory. 2) The minimum capacitance regime is round. 3) The quantum capacitance increases linearly with the potential on both sides of the minimum, but the slopes are smaller than the theoretical prediction. The discrepancies can be explained naturally by including charged impurities in the model. The findings underscore the importance of charged impurities not only in the mobilities but also in the quantum capacitance, and support the local-impurity induced electron and hole puddle picture in graphene. The quantum capacitance measurement is also a good method to determine the impurity concentrations. We have also measured the quantum capacitance of graphene in aqueous solutions at different ionic concentrations. Comparing the results with interfacial capacitance obtained for the basal plane of graphite indicates that the quantum capacitance is the origin of the longstanding puzzling interfacial capacitance of widely used carbon-based electrodes.

Chapter 5

TRANSPORT AND QUANTUM CAPACITANCE PROPERTIES OF EPITAXIAL GRAPHENE

5.1 Introduction

As discussed in Chapter 1, mechanical exfoliated graphene has perfect lattice, however, the low yield limits its real application, making it only suitable for lab research. Fortunately, there are other ways to fabricate graphene in wafer scale, epitaxial graphene is one of them. Epitaxial graphene has good uniformity[46] and compatible with Si fabrication techniques, (shown in Fig. 5.1)making it particularly attractive for device applications. Actually the first 100GHz graphene transistor was fabricated by epitaxial graphene on 3 inch SiC wafer. However, most of the published works are on exfoliated graphene mainly due to the availability of the material via the "magic scotch tape" approach[1, 184]. Although the epitaxial graphene and the exfoliated graphene devices[46, 49, 185]share similarities in transport properties, they are not exactly the same. One of the most important differences between the two materials is the strong interactions of epitaxial graphene with SiC substrate[46], shown in Fig. 5.2. In this letter, we report on the first measurement of both charge transport and capacitance properties[186] on the same epitaxial graphene field effect transistors (FET). We discuss the results in terms of the existing theories, and compare the findings with those from exfoliated graphene devices.

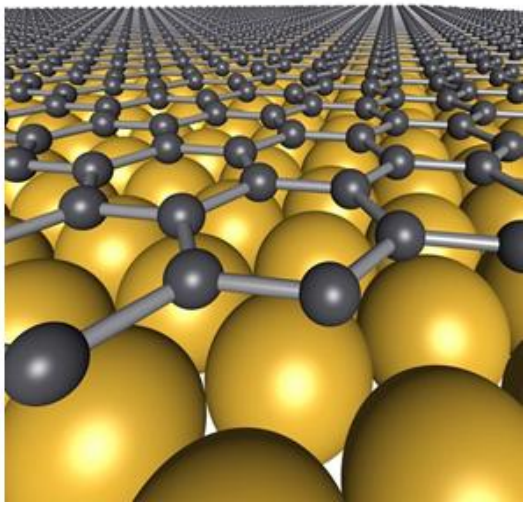

Figure 5.1. Schematic structure of epitaxial graphene

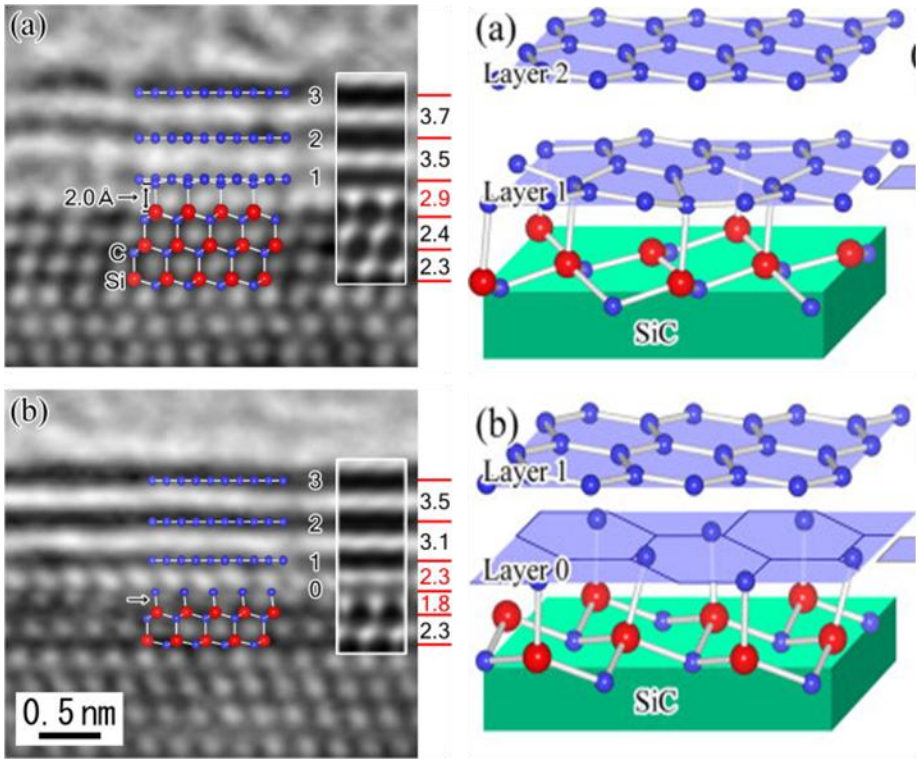

Figure 5.2. TEM images of epitaxial graphene and schematic structure with interlayers[46]

5.2 Experiment Methods

Argon-mediated epitaxial graphene films were grown on 16 x 16 mm^2 substrates sawn from 76.2 mm diameter, chemo-mechanically polished, on-axis (0 ± 0.5^0), semi-insulating Si-face 6H-SiC (II-VI, Inc.) wafers [112], using a variation of the *in-vacuo* epitaxial growth process, which we describe below. The samples were first cleaned *ex situ* using a standard wet chemical cleaning procedure for SiC[187]. After cleaning, the samples were loaded into a commercial available hot-wall chemical vapor deposition reactor (Aixtron/Epigress VP508). The initial reactor push gas was hydrogen with mass flow of 50 standard liters per minute (SLM) at 100 mbar and the temperature of the samples was steadily raised to 1600 ℃. The samples were held at 1600 ℃ for 10 minutes in order to remove at least 500 nm of the SiC, which was sufficient to remove the polishing damage [112]. Following this hydrogen etching step, the reactor push gas was switched to 20 SLM of Ar at 100 mbar Ar. Samples were held at 1600 ℃ for 120 minutes before heating ceased. The samples cooled at a rate of ~9 ℃ min^{-1} while the Ar was removed from the chamber using the process pump (Ebara A25S). Twenty minutes after the Ar was removed the samples continued to cool in a turbo pumped vacuum (~10^{-6} to 10^{-7} mbar, Pfeiffer TMH 521) for several hours, typically overnight, before being removed from the reactor.

After synthesis of the graphene layer, FET devices were fabricated using conventional semiconductor fabrication techniques[137, 186]. The graphene sheet was patterned using oxygen plasma etching to create 15 μm wide and 11 μm long graphene devices. To minimize contact resistance contributions to the transport

data, a four-probe configuration was used, in which the electrodes were 80 nm thick Au with a 5 nm Cr adhesion layer. To minimize the leakage current associated with the use of an electrochemical gate, the device was covered with a ~4.5 μm thick layer of photo-resist, except for a 4.3 μm x 30 μm window that exposed the graphene surface to the electrolyte for electrochemical gating. The thickness of graphene in the channel region was verified by Raman spectroscopy after graphene patterning but before covering it with photo-resist, and the spectrum is shown in Fig. 5.3(a). Different from the exfoliated graphene, the only unambiguous fingerprint in the Raman spectrum to identify the number of epitaxial graphene layers is the line width of the 2D peak.[188] Fitting the 2D peak with a single Lorentzian resulted in a full width at half-maximum (FWHM) of 42.6 cm-1, which indicaties of single layer epitaxial graphene. One thing to be noted here is: the structure of "single" layer epitaxial graphene is different from that of exfoliated graphene, because a carbon interlayer, with atomic density of 1/3 or 2/3 times that of the ideal single layer graphene, may form during the graphitization and thermal decomposition of SiC[189].

The device configuration and experimental setup are shown in Fig. 5.3(b). All the measurements were carried out at room temperature. The electrochemical gate potential was applied with respect to a silver quasi-reference electrode to control the carrier density in graphene. The potential was controlled using a potentiostat (Model 283, Princeton Applied Research) and a platinum wire as counter electrode. 1-butyl-3-methylimidazolium hexaflurophosphate (BMIM-PF6), an ionic liquid was used as electrolyte. The ionic liquid was chose because of its

stability over a wide potential range and high ionic concentration. The four-probe transport experiment was carried out using a Keithley 6221/2182a. For capacitance measurement, only one electrode was used as working electrode, forming the standard three-electrode electrochemical configuration. A small AC modulation (100Hz, 0.01V) was superimposed on the sweeping gate potential ($10mVs^{-1}$) and the AC response was measured using a lock-in amplifier (SR850, Stanford Research System). For more information about the capacitance measurement, see Ref. [186].

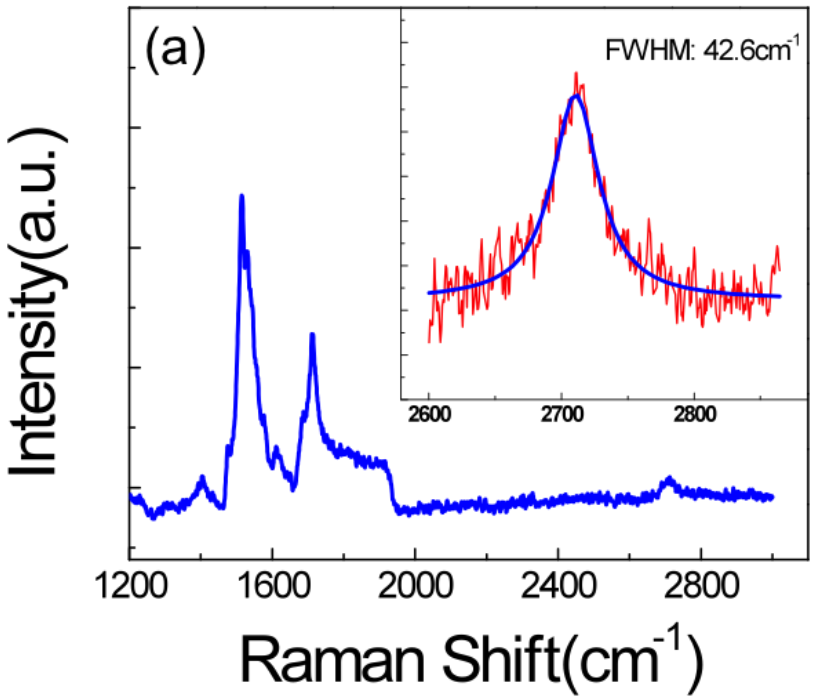

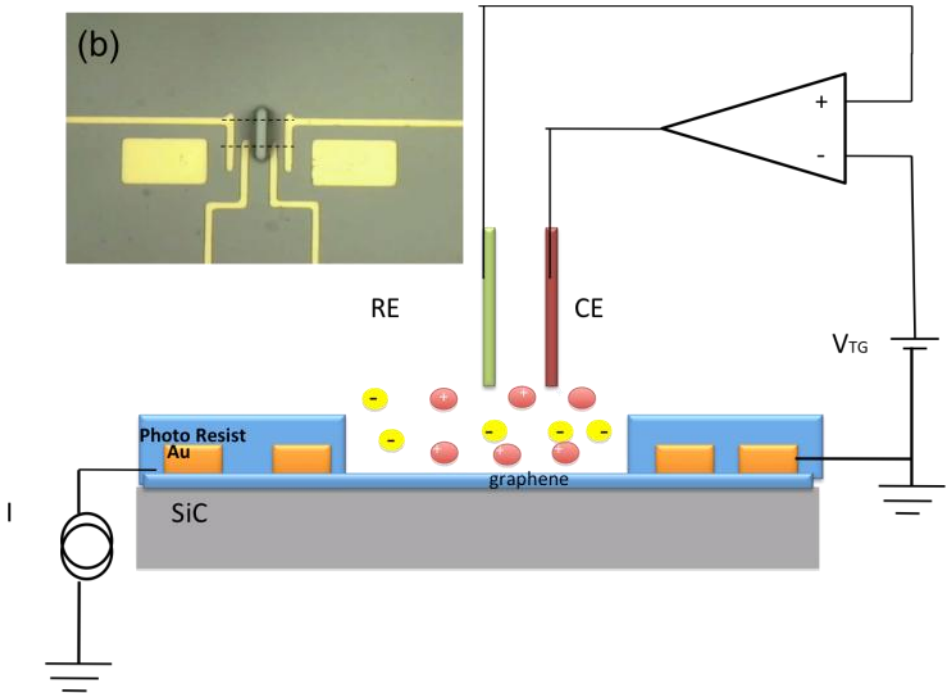

Figure 5.3. (a) Raman spectrum of single layer epitaxial graphene measured in the channel region after FET device fabrication. The inset shows the best fit of the 2D peak by a Lorentzian curve with FWHM of 42.6cm^{-1}. (b) Schematic diagram of the experimental setup. A four-probe configuration was used for the transport measurement, and the standard three-electrode electrochemical configuration for the capacitance measurement. Both measurements were carried out in an ionic liquid at room temperature using electrochemical gate. The inset shows an optical image of the graphene FET, and the dashed line marks the graphene area after etching.

5.3 Results and Discussion

Fig. 5.4 (a) shows the measured capacitance as a function of gate potential. As we have pointed out in a previous work[186], the measured capacitance consists of two parts: interfacial capacitance from a double layer formed by ions at the

graphene-ionic liquid interface and the quantum capacitance of graphene. The double layer capacitance was measured to be 20μF cm^{-2}.[175, 186] By subtracting this double layer capacitance from the total capacitance, the quantum capacitance of epitaxial graphene is determined, shown as the red curve in Fig. 5.4(a). Similar to that of exfoliated graphene, the quantum capacitance of epitaxial graphene also shows a non-zero minimum value, ~7.9 μF cm^{-2}. As discussed previously[18], this finite minimum is contributed to charged impurities and given by

$$C_{Q,\min} = \frac{2e^2}{\hbar v_F \sqrt{\pi}} (|n_0|)^{1/2} \tag{5.1}$$

where $\hbar$ is Planck's constant, e the electron charge, $v_F \approx c/300$, the fermi velocity, and n_0 is called residual carrier density[143], which is $8.5 \times 10^{12} cm^{-2}$ here. However, unlike exfoliated graphene, the quantum capacitance of the epitaxial graphene does not show the well-defined V-shape. Instead, it has an obvious sub-linear dependence at potentials far away from the Dirac point. The origin for this sub-linearity is not clear yet, but the strong interactions of the SiC substrate and the carbon interlayer with the epitaxial graphene, known to change the Raman bands, are likely responsible for the peculiar capacitance behavior[190]. Fig. 5.4 (b) plots the carrier density as a function of gate potential, where the density was determined by $C_{tg}(V_{tg} - V_{Dirac}) = ne$. Note that V_{Dirac} is the Dirac point potential. From the plot, it is clear that the carrier density depends linearly on the gate potential, meaning that the total capacitance depends weakly on the applied gate potential. For simplicity, we treated the total capacitance as a constant, which is ~6.6 μF/cm^2.

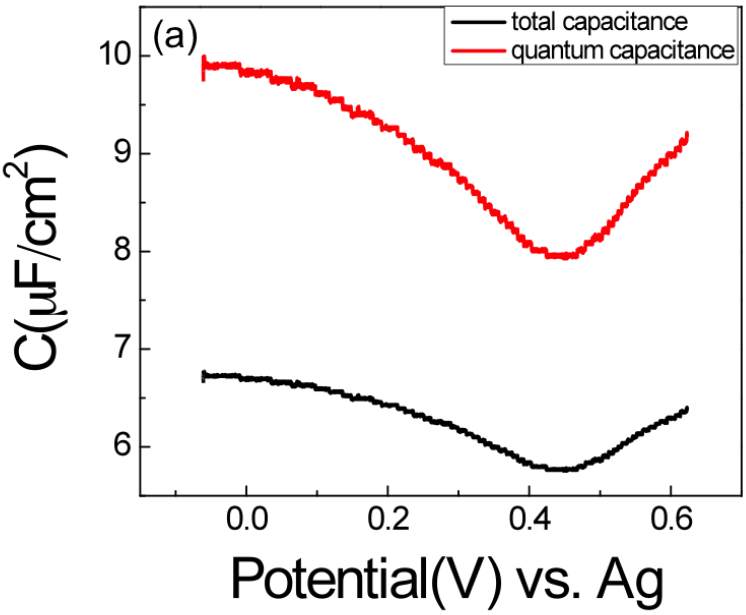

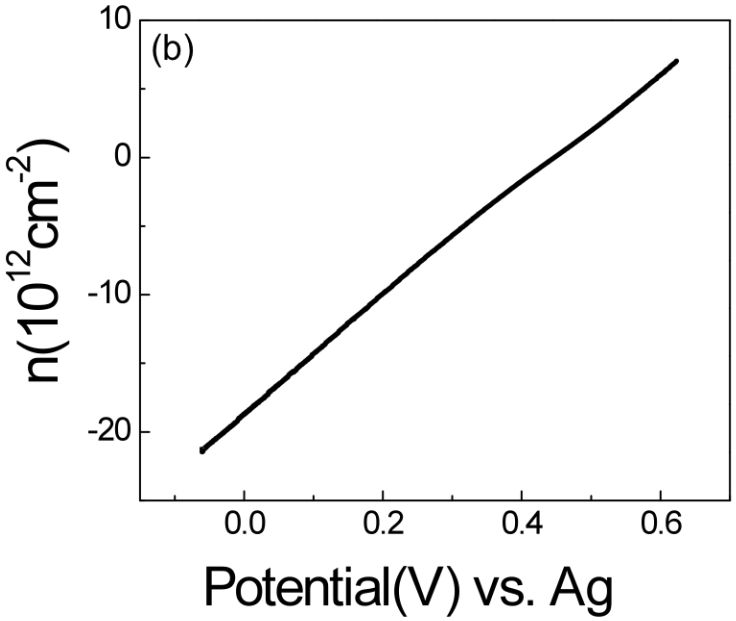

Figure 5.4. (a) Total capacitance (black line) and quantum capacitance (red line) of epitaxial graphene measured in ionic liquid BMIM-PF_6. The potential is

measured with respect to a silver quasi-reference electrode. Note that background capacitance of 4.2 pF obtained from control measurements without graphene is subtracted out to obtain the quantum capacitance. (b) Calculated carrier density as a function of gate potential, showing a linear relation corresponding to a total capacitance of 6.6μF cm^{-2}. The sign indicates different carrier types.

Gate dependent transport properties of the same device were measured, which are shown in Fig. 5.5. The effective channel exposed to the gate electrolyte was 15 μm wide and 4.3 μm long. The measurement was carried out by applying 50 nA constant current between the source and drain electrodes. The total resistance of the device contains two contributions, $R_{channel}$ from the graphene region exposed to the gate electrolyte, and R_c from the region covered by photoresist. The former is controlled by the electrochemical gate potential, while the latter may be regarded as a constant because its carrier density cannot be changed by the gate potential. In this way, we can use the model by Kim *et al.* [106]

$$R_{tot} = R_C + R_{Channel} = R_C + \frac{L/W}{\mu n e} \tag{5.2}$$

$$n = \sqrt{n_0^{\,2} + n_t^{\,2}} = \sqrt{n_0^{\,2} + [C_{tg}(V_{tg} - V_{Dirac})/e]^2} \tag{5.3}$$

$A_{Channel}$ is the area of the channel. By fitting the model to the measured data in Fig. 5.4, using $C_{tg} = 6.6\mu F \cdot cm^{-2}$, we found that $\mu = 478 cm^2 V^{-1} s^{-1}$ and $n_0 = 1.96 \times 10^{12} cm^{-2}$, with an on/off ratio of ~4. The model (red line) fits the experimental data well, and the mobility is consistent with the reported values on epitaxial graphene fabricated using same procedure[17,19].

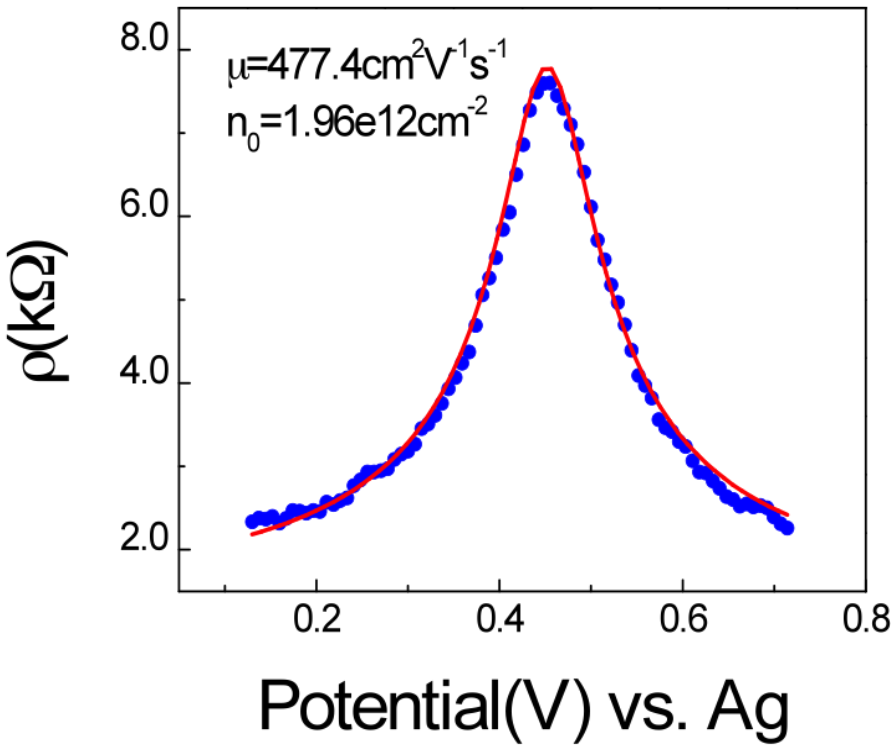

Figure 5.5. Resistivity vs. gate potential (blue symbols) and model fit (red line) using Eq. 5.2.

The self-consistent theory has been developed to explain the dependence of mobility on charged impurities for the exfoliated graphene[143]. We attempted here to apply the theory to the epitaxial graphene. An important parameter in the self-consistent theory is $r_s = \frac{2e^2}{\hbar v_F(\varepsilon_1 + \varepsilon_2)}$, the coupling constant for graphene sandwiched between two dielectric materials with ε_1 and ε_2, which is 0.238 using the dielectric constants of the ionic liquid used here ($\varepsilon_1 = 7$) [175] and SiC ($\varepsilon_1 = 9.66$)[191]. At large carrier densities, the self-consistent theory predicts that

$$\mu = \frac{e}{h}\frac{1}{n_{imp}}\frac{2}{G(2r_s)} \tag{5.4}$$

Where $$\frac{G[x]}{x^2} = \frac{\pi}{4} + 3x - \frac{3\pi x^2}{2} + \frac{x(3x^2-2)\arccos[1/x]}{\sqrt{x^2-1}} \tag{5.5}$$

Based on Eqs. 5.4 and 5.5, the extracted impurity density is about $2.7\times10^{13}cm^{-2}$, much larger than that of exfoliated graphene, which is consistent with the relatively small mobilities in the epitaxial graphene FETs. The impurity density, n_{imp}, and the induced impurity density, n_0, are related by

$$\frac{n_0}{n_{imp}} = 2r_s^2 C_0^{RPA}(r_s, a = 4d\sqrt{\pi n_0}) \tag{5.6}$$

where $C_0^{RPA}$is the correlation function from random phase approximation (RPA), and d is the average distance from the charged impurity to the graphene sheet. For exfoliated graphene, d is ~1nm. In the case of epitaxial grown graphene, $n_0/n_{imp} = 1.96\times10^{12}cm^{-2}/27\times10^{12}cm^{-2} = 0.07$, leading to d=0.55 nm, which is smaller than that found for the exfoliated graphene devices. This difference, as well as the large impurity density found in the epitaxial graphene devices, indicates different origins in the charged impurities in the epitaxial and exfoliated graphene devices. Note also that n_0 determined from the transport data is smaller than that from the capacitance measurement, which also suggests that a better model is needed in order to explain the transport and capacitance data measured for the epitaxial graphene devices.

5.4 Conclusions

In summary, we have measured the transport and capacitance properties of an argon-mediated epitaxial graphene FET using electrochemical gate. The self-consistent theory developed for exfoliated graphene devices provides a reasonable explanation of the transport data of the epitaxial graphene devices. The quantum capacitance of argon-mediated epitaxial graphene shows a sub-linear relation at high carrier densities, which may be due to the contributions from the edge states or the interactions of the graphene with the underlying SiC substrate. The study indicates a need of a complete theory to explain both the transport and capacitance properties of epitaxial grown graphene.

Chapter 6

SUMMARY AND FUTURE

6.1 Summary

In this dissertation, the transport properties of back-gated graphene were studied, especially when covering by high κ medium, to explore the effect of surrounding environment on transport of graphene. Hall measurements were carried out on back-gated graphene field effect transistors (FET) with and without a top dielectric medium. The gate efficiency increased by up to two orders of magnitude in the presence of a high κ top dielectric medium, but the mobility does not change significantly. The measurement further showed that the back-gate capacitance was enhanced dramatically by the top dielectric medium, of which the enhancement increased with the size of the top dielectric medium. The result strongly suggested that the previously reported top dielectric medium-induced charge transport properties of graphene FETs were possibly due to the increase of gate capacitance, rather than enhancement of carrier mobility. The sensitive dependence of the gate capacitance on the top dielectric medium points to the alternative mechanism of graphene FET-based chemical sensor applications.

Quantum Capacitance of graphene was measured using a three-electrode electrochemical configuration. The quantum capacitance showed a non-zero minimum at the Dirac point and a linear increase on both sides of the minimum with relatively small slopes. The findings - which are not predicted by theory for ideal graphene - suggested that the scattering from charged impurities also influences the quantum capacitance. We also measured the capacitance in

aqueous solutions at different ionic concentrations, and our results strongly suggested that the longstanding puzzle about the interfacial capacitance in carbon-based electrodes has a quantum origin.

Epitaxial graphene field effect transistors were fabricated, characterized and studied. Both the capacitance and transport measurements were performed on the same devices using an electrochemical gate. The quantum capacitance of the epitaxial graphene was extracted, which was similar to that of exfoliated graphene near the Dirac point, but it exhibits a large sub-linear behavior at high carrier densities. The recently developed self-consistent theory is found to provide a reasonable description of the transport data, but a more complete theory is needed to explain both the transport and quantum capacitance data for the epitaxial graphene devices.

6.2 Future

Pushed by Moore's Rule, lots of research efforts are seeking electronic materials "beyond Silicon". Carbon based materials have been considered as an excellent candidates, especially after the discovery of carbon nanotube. However, decade has passed, the "carbon age" is still on the way, and there is no clear picture for carbon nanotube yet. Now here comes graphene, will it change this situation? Graphene has attracted so much attention since its discovery, and only after 6 years, Nobel Prize of Physics was awarded to its discoverers. Why graphene, not carbon nanotubes ? If graphene is the one, then when and how is it going to change our lives?

By comparing graphene with carbon nanotubes, as Geim said: “carbon nanotubes were not as successful as graphene, in terms of physics, not application”. Actually, though graphene owns many amazing properties, such as largest surface to weight ratio, strongest material ever measured, excellent conductivity, super mobility, it is still too early to say that the carbon new age is coming. We are still on the way.

REFERENCES

[1] A. K. Geim and K. S. Novoselov, "The rise of graphene," *Nature Materials,* vol. 6, pp. 183-191, 2007.

[2] P. R. Wallace, "The Band Theory of Graphite," *Physical Review,* vol. 71, pp. 622, 1947.

[3] J. W. McClure, "Diamagnetism of Graphite," *Physical Review,* vol. 104, pp. 666, 1956.

[4] R. E. Peierls, "Quelques properietes typique des corpses solides," *Ann.I.H. Poincare,* vol. 5, pp. 177-222, 1935.

[5] L. D. Landau, "Zur Theorie der phasenumwandlungen II.," *Phys.Z.Sowjetunion,* vol. 11, pp. 26-35, 1937.

[6] J. W. McClure, *Physics of Semi-metals and narrow-gap semiconductors*. New York: Pergamon Press, 1971.

[7] S. Iijima, "Helical microtubules of graphitic carbon," *Nature,* vol. 354, pp. 56-58, 1991.

[8] P. Avouris, *et al.*, "Carbon-based electronics," *Nat Nano,* vol. 2, pp. 605-615, 2007.

[9] "Beyond Silicon: Carbon Based Nanotechnology," *MRS Bulletin,* vol. 35, 2010.

[10] T. W. Ebbesen and H. Hiura, "Graphene in 3-dimensions: Towards graphite origami," *Advanced Materials,* vol. 7, pp. 582-586, 1995.

[11] X. Lu, *et al.*, "Patterning of highly oriented pyrolytic graphite by oxygen plasma etching," *Applied Physics Letters,* vol. 75, pp. 193-195, 1999.

[12] M. Y. Xuekun Lu, Hui Huang and Rodney S Ruoff, "Tailoring graphite with the goal of achieving single sheets," *Nanotechnology,* vol. 10, pp. 269, 1999.

[13] Y. Zhang, *et al.*, "Fabrication and electric-field-dependent transport measurements of mesoscopic graphite devices," *Applied Physics Letters,* vol. 86, pp. 073104, 2005.

[14] L. M. Viculis, *et al.*, "A Chemical Route to Carbon Nanoscrolls," *Science,* vol. 299, pp. 1361, 2003.

[15] M. S. Dresselhaus and G. Dresselhaus, "Intercalation compounds of graphite," *Advances in Physics,* vol. 51, pp. 1 - 186, 2002.

[16] K. S. Novoselov, *et al.*, "Electric Field Effect in Atomically Thin Carbon Films," vol. 306, ed, 2004, pp. 666-669.

[17] A. H. Castro Neto, "The carbon new age," *Materials Today,* vol. 13, pp. 12-17, 2010.

[18] C. Rao, *et al.*, "Graphene: The New Two-Dimensional Nanomaterial," *Angewandte Chemie International Edition,* vol. 48, pp. 7752-7777, 2009.

[19] A. H. Castro Neto, *et al.*, "The electronic properties of graphene," *Reviews of Modern Physics,* vol. 81, pp. 109, 2009.

[20] C. N. L. Michael S.Fuhrer, and Allan H. MacDonald, "Graphene: Materially Better Carbon," *MRS Bulletin,* vol. 35, pp. 289-295, 2010.

[21] F. G. Antonio Castro Neto, and Nuno Miguel Peres, "Drawing conclusions from graphene," *Physics World,* vol. 19, pp. 1-5, 2006.

[22] K. S. Novoselov, *et al.*, "Two-dimensional gas of massless Dirac fermions in graphene," *Nature,* vol. 438, pp. 197-200, 2005.

[23] Y. W. Tan, *et al.*, "Measurement of scattering rate and minimum conductivity in graphene," *Physical Review Letters,* vol. 99, pp. 246803, 2007.

[24] Y. B. Zhang, *et al.*, "Experimental observation of the quantum Hall effect and Berry's phase in graphene," *Nature,* vol. 438, pp. 201-204, 2005.

[25] K. S. Novoselov, *et al.*, "Room-Temperature Quantum Hall Effect in Graphene," *Science,* pp. 1137201, 2007.

[26] M. I. Katsnelson, *et al.*, "Chiral tunnelling and the Klein paradox in graphene," *Nat Phys,* vol. 2, pp. 620-625, 2006.

[27] R. R. Nair, *et al.*, "Fine Structure Constant Defines Visual Transparency of Graphene," *Science,* vol. 320, pp. 1308, 2008.

[28] S. V. Morozov, *et al.*, "Two-dimensional electron and hole gases at the surface of graphite," *Physical Review B,* vol. 72, p. 201401, 2005.

[29] K. S. Novoselov, *et al.*, "Unconventional quantum Hall effect and Berry's phase of 2π in bilayer graphene," *Nat Phys,* vol. 2, pp. 177-180, 2006.

[30] M. I. Katsnelson, *et al.*, "Chiral tunnelling and the Klein paradox in graphene," *Nature Physics*, vol. 2, pp. 620-625, 2006.

[31] R. Ruoff, "Graphene: Calling all chemists," *Nat Nano*, vol. 3, pp. 10-11, 2008.

[32] D. J. K.S.Novoselov, F.Schedin, T.J.Booth, V.V.Khotkevich, S.V.Morozov, and A.K. Geim, "Two-dimensional atomic crystals," *Proceeding of the National Academy of Sciences*, vol. 102, pp. 10451-10453, 2005.

[33] J. C. Shelton, *et al.*, "Equilibrium segregation of carbon to a nickel (111) surface: A surface phase transition," *Surface Science*, vol. 43, pp. 493-520, 1974.

[34] M. Eizenberg and J. M. Blakely, "Carbon monolayer phase condensation on Ni(111)" *Surface Science*, vol. 82, pp. 228-236, 1979.

[35] T. A. Land, *et al.*, "STM investigation of single layer graphite structures produced on Pt(111) by hydrocarbon decomposition," *Surface Science*, vol. 264, pp. 261-270, 1992.

[36] A. Nagashima, *et al.*, "Electronic states of monolayer graphite formed on TiC(111) surface," *Surface Science*, vol. 291, pp. 93-98, 1993.

[37] P. R. Somani, *et al.*, "Planer nano-graphenes from camphor by CVD," *Chemical Physics Letters*, vol. 430, pp. 56-59, 2006.

[38] P. W. Sutter, *et al.*, "Epitaxial graphene on ruthenium," *Nat Mater*, vol. 7, pp. 406-411, 2008.

[39] Q. Yu, *et al.*, "Graphene segregated on Ni surfaces and transferred to insulators," *Applied Physics Letters*, vol. 93, pp. 113103, 2008.

[40] X. Li, *et al.*, "Large-Area Synthesis of High-Quality and Uniform Graphene Films on Copper Foils," *Science*, vol. 324, pp. 1312-1314,2009.

[41] Y. Lee, *et al.*, "Wafer-Scale Synthesis and Transfer of Graphene Films," *Nano Letters*, vol. 10, pp. 490-493, 2010.

[42] K. S. Kim, *et al.*, "Large-scale pattern growth of graphene films for stretchable transparent electrodes," *Nature*, vol. 457, pp. 706-710, 2009.

[43] A. Reina, *et al.*, "Large Area, Few-Layer Graphene Films on Arbitrary Substrates by Chemical Vapor Deposition," *Nano Letters*, vol. 9, pp. 30-35, 2008.

[44] S. Bae, *et al.*, "Roll-to-roll production of 30-inch graphene films for transparent electrodes," *Nat Nano,* vol. 5, pp. 574-578, 2010.

[45] E. Acheson. http://web.mit.edu/invent/iow/acheson/html [Online].

[46] T. Seyller, *et al.*, "Epitaxial graphene: a new material," *physica status solidi (b),* vol. 245, pp. 1436-1446, 2008.

[47] C. Berger, *et al.*, "Ultrathin Epitaxial Graphite: 2D Electron Gas Properties and a Route toward Graphene-based Nanoelectronics," *The Journal of Physical Chemistry B,* vol. 108, pp. 19912-19916, 2004.

[48] C. Berger, *et al.*, "Electronic Confinement and Coherence in Patterned Epitaxial Graphene," *Science,* p. 1125925, 2006.

[49] W. A. de Heer, *et al.*, "Epitaxial graphene," *Solid State Communications,* vol. 143, pp. 92-100, 2007.

[50] S. Unarunotai, *et al.*, "Conjugated Carbon Monolayer Membranes: Methods for Synthesis and Integration," *Advanced Materials,* vol. 22, pp. 1072-1077, 2010.

[51] K. V. Emtsev, *et al.*, "Towards wafer-size graphene layers by atmospheric pressure graphitization of silicon carbide," *Nat Mater,* vol. 8, pp. 203-207, 2009.

[52] Y.-M. Lin, *et al.*, "100-GHz Transistors from Wafer-Scale Epitaxial Graphene," *Science,* vol. 327, pp. 662, 2010.

[53] S. Stankovich, *et al.*, "Synthesis and exfoliation of isocyanate-treated graphene oxide nanoplatelets," *Carbon,* vol. 44, pp. 3342-3347, 2006.

[54] S. Stankovich, *et al.*, "Synthesis of graphene-based nanosheets via chemical reduction of exfoliated graphite oxide," *Carbon,* vol. 45, pp. 1558-1565, 2007.

[55] J. R. Lomeda, *et al.*, "Diazonium Functionalization of Surfactant-Wrapped Chemically Converted Graphene Sheets," *Journal of the American Chemical Society,* vol. 130, pp. 16201-16206, 2008.

[56] V. C. Tung, *et al.*, "High-throughput solution processing of large-scale graphene," *Nat Nano,* vol. 4, pp. 25-29, 2009.

[57] S. Gilje, *et al.*, "A Chemical Route to Graphene for Device Applications," *Nano Letters,* vol. 7, pp. 3394-3398, 2007.

[58] Z. Wei, *et al.*, "Nanoscale Tunable Reduction of Graphene Oxide for Graphene Electronics," *Science,* vol. 328, pp. 1373-1376, 2010.

[59] J. I. Paredes, *et al.*, "Graphene Oxide Dispersions in Organic Solvents," *Langmuir,* vol. 24, pp. 10560-10564, 2008.

[60] Y. Hernandez, *et al.*, "High-yield production of graphene by liquid-phase exfoliation of graphite," *Nat Nano,* vol. 3, pp. 563-568, 2008.

[61] G. Wang, *et al.*, "Facile Synthesis and Characterization of Graphene Nanosheets," *The Journal of Physical Chemistry C,* vol. 112, pp. 8192-8195, 2008.

[62] Y. Si and E. T. Samulski, "Synthesis of Water Soluble Graphene," *Nano Letters,* vol. 8, pp. 1679-1682, 2008.

[63] S. Park and R. S. Ruoff, "Chemical methods for the production of graphenes," *Nat Nano,* vol. 4, pp. 217-224, 2009.

[64] C. Xu, *et al.*, "Graphene−Metal Particle Nanocomposites," *The Journal of Physical Chemistry C,* vol. 112, pp. 19841-19845, 2008.

[65] M. D. Stoller, *et al.*, "Graphene-Based Ultracapacitors," *Nano Letters,* vol. 8, pp. 3498-3502, 2008.

[66] D. Wang, *et al.*, "Self-Assembled TiO2–Graphene Hybrid Nanostructures for Enhanced Li-Ion Insertion," *ACS Nano,* vol. 3, pp. 907-914, 2009.

[67] W. Geyer, *et al.*, "Electron-induced crosslinking of aromatic self-assembled monolayers: Negative resists for nanolithography," *Applied Physics Letters,* vol. 75, pp. 2401-2403, 1999.

[68] M. Schnietz, *et al.*, "Chemically Functionalized Carbon Nanosieves with 1-nm Thickness," *Small,* vol. 5, pp. 2651-2655, 2009.

[69] W. Zhang and J. Moore, "Alkyne Metathesis: Catalysts and Synthetic Applications," *Advanced Synthesis & Catalysis,* vol. 349, pp. 93-120, 2007.

[70] P. Siemsen, *et al.*, "Acetylenic Coupling: A Powerful Tool in Molecular Construction," *Angewandte Chemie International Edition,* vol. 39, pp. 2632-2657, 2000.

[71] X. Z. Mitchell *et.al.*, "Synthesis of linked carbon monolayers: Films, balloons, tubes, and pleated sheets," *Proceeding of the National Academy of Sciences,* vol. 105, pp. 7353-7358, 2008.

[72] A. Turchanin, *et al.*, "Thin Films: One Nanometer Thin Carbon Nanosheets with Tunable Conductivity and Stiffness " *Advanced Materials,* vol. 21, pp. 1233-1237, 2009.

[73] P. Blake, *et al.*, "Making graphene visible," *Applied Physics Letters,* vol. 91, pp. 063124, 2007.

[74] A. C. Ferrari, *et al.*, "Raman spectrum of graphene and graphene layers," *Physical Review Letters,* vol. 97, pp. 187401, 2006.

[75] P. Lauffer, *et al.*, "Atomic and electronic structure of few-layer graphene on SiC(0001) studied with scanning tunneling microscopy and spectroscopy," *Physical Review B,* vol. 77, pp. 155426, 2008.

[76] B. Partoens and F. M. Peeters, "From graphene to graphite: Electronic structure around the K point," *Physical Review B,* vol. 74, pp. 075404, 2006.

[77] E. V. Castro, *et al.*, "Biased Bilayer Graphene: Semiconductor with a Gap Tunable by the Electric Field Effect," *Physical Review Letters,* vol. 99, pp. 216802, 2007.

[78] T. Ohta, *et al.*, "Controlling the Electronic Structure of Bilayer Graphene," *Science,* vol. 313, pp. 951-954, 2006.

[79] J. B. Oostinga, *et al.*, "Gate-induced insulating state in bilayer graphene devices," *Nat Mater,* vol. 7, pp. 151-157, 2008.

[80] Y. Zhang, *et al.*, "Direct observation of a widely tunable bandgap in bilayer graphene," *Nature,* vol. 459, pp. 820-823, 2009.

[81] Z. Chen, *et al.*, "Graphene nano-ribbon electronics," *Physica E: Low-dimensional Systems and Nanostructures,* vol. 40, pp. 228-232, 2007.

[82] X. Li, *et al.*, "Chemically Derived, Ultrasmooth Graphene Nanoribbon Semiconductors," *Science,* vol. 319, pp. 1229-1232, 2008.

[83] J. Cai, *et al.*, "Atomically precise bottom-up fabrication of graphene nanoribbons," *Nature,* vol. 466, pp. 470-473, 2010.

[84] D. V. Kosynkin, *et al.*, "Longitudinal unzipping of carbon nanotubes to form graphene nanoribbons," *Nature,* vol. 458, pp. 872-876, 2009.

[85] L. Jiao, *et al.*, "Narrow graphene nanoribbons from carbon nanotubes," *Nature,* vol. 458, pp. 877-880, 2009.

[86] M. Fujita, *et al.*, "Peculiar localized state at zigzag graphite edge," *Journal of the Physical Society of Japan,* vol. 65, pp. 1920-1923, 1996.

[87] K. Wakabayashi, *et al.*, "Electronic and magnetic properties of nanographite ribbons," *Physical Review B,* vol. 59, pp. 8271, 1999.

[88] M. Y. Han, *et al.*, "Energy Band-Gap Engineering of Graphene Nanoribbons," *Physical Review Letters,* vol. 98, pp. 206805, 2007.

[89] Y.-W. Son, *et al.*, "Energy Gaps in Graphene Nanoribbons," *Physical Review Letters,* vol. 97, pp. 216803, 2006.

[90] V. Barone, *et al.*, "Electronic Structure and Stability of Semiconducting Graphene Nanoribbons," *Nano Letters,* vol. 6, pp. 2748-2754, 2006.

[91] J. Bai, *et al.*, "Graphene nanomesh," *Nat Nano,* vol. 5, pp. 190-194, 2010.

[92] X. G. Liang, *et al.*, "Formation of Bandgap and Subbands in Graphene Nanomeshes with Sub-10 nm Ribbon Width Fabricated via Nanoimprint Lithography," *Nano Letters,* vol. 10, pp. 2454-2460, 2010.

[93] M. Kim, *et al.*, "Fabrication and Characterization of Large-Area, Semiconducting Nanoperforated Graphene Materials," *Nano Letters,* vol. 10, pp. 1125-1131, 2010.

[94] R. Martinazzo, *et al.*, "Symmetry-induced band-gap opening in graphene superlattices," *Physical Review B,* vol. 81, 2010.

[95] Y. Zhu, *et al.*, "Graphene and Graphene Oxide: Synthesis, Properties, and Applications," *Advanced Materials,* pp. 3906-3924, 2010.

[96] S. P. Daniel R.Dreyer, Christopher W.Bielawski and Rodney S. Ruoff, "The chemistry of graphene oxide," *Chem.Soc.Rev.,* vol. 39, pp. 228-240, 2010.

[97] C. Gómez-Navarro, *et al.*, "Electronic Transport Properties of Individual Chemically Reduced Graphene Oxide Sheets," *Nano Letters,* vol. 7, pp. 3499-3503, 2007.

[98] I. Jung, *et al.*, "Tunable Electrical Conductivity of Individual Graphene Oxide Sheets Reduced at "Low" Temperatures," *Nano Letters,* vol. 8, pp. 4283-4287, 2008.

[99] J. O. Sofo, *et al.*, "Graphane: A two-dimensional hydrocarbon," *Physical Review B,* vol. 75, pp. 153401, 2007.

[100] D. C. Elias, *et al.*, "Control of Graphene's Properties by Reversible Hydrogenation: Evidence for Graphane," *Science,* vol. 323, pp. 610-613, 2009.

[101] F. Schedin, *et al.*, "Detection of individual gas molecules adsorbed on graphene," *Nature Materials,* vol. 6, pp. 652-655, 2007.

[102] X. Wang, *et al.*, "N-Doping of Graphene Through Electrothermal Reactions with Ammonia," *Science,* vol. 324, pp. 768-771, 2009.

[103] D. Wei, *et al.*, "Synthesis of N-Doped Graphene by Chemical Vapor Deposition and Its Electrical Properties," *Nano Letters,* vol. 9, pp. 1752-1758, 2009.

[104] D. A. Areshkin and C. T. White, "Building Blocks for Integrated Graphene Circuits," *Nano Letters,* vol. 7, pp. 3253-3259, 2007.

[105] X. Du, *et al.*, "Approaching ballistic transport in suspended graphene," *Nature Nanotechnology,* vol. 3, pp. 491-495, 2008.

[106] S. Kim, *et al.*, "Realization of a high mobility dual-gated graphene field-effect transistor with Al_2O_3 dielectric," *Applied Physics Letters,* vol. 94, p. 062107, 2009.

[107] D. B. Farmer, *et al.*, "Utilization of a Buffered Dielectric to Achieve High Field-Effect Carrier Mobility in Graphene Transistors," *Nano Letters,* vol. 9, pp. 4474-4478, 2009.

[108] L. Liao, *et al.*, "Top-Gated Graphene Nanoribbon Transistors with Ultrathin High-k Dielectrics," *Nano Letters,* vol. 10, pp. 1917-1921, 2010.

[109] F. Schwierz, "Graphene transistors," *Nat Nano,* vol. 5, pp. 487-496, 2010.

[110] Y.-M. Lin, *et al.*, "Operation of Graphene Transistors at Gigahertz Frequencies," *Nano Letters,* vol. 9, pp. 422-426, 2008.

[111] Y. M. Lin, *et al.*, "Dual-Gate Graphene FETs With f(T) of 50 GHz," *Ieee Electron Device Letters,* vol. 31, pp. 68-70, Jan 2010.

[112] J. S. Moon, *et al.*, "Epitaxial-Graphene RF Field-Effect Transistors on Si-Face 6H-SiC Substrates," *Electron Device Letters, IEEE,* vol. 30, pp. 650-652, 2009.

[113] J. S. Moon, *et al.*, "Top-Gated Epitaxial Graphene FETs on Si-Face SiC Wafers With a Peak Transconductance of 600 mS/mm," *Electron Device Letters, IEEE,* vol. 31, pp. 260-262, 2010.

[114] B. Standley, *et al.*, "Graphene-Based Atomic-Scale Switches," *Nano Letters,* vol. 8, pp. 3345-3349, 2008.

[115] Y. Li, *et al.*, "Electronic two-terminal bistable graphitic memories," *Nat Mater,* vol. 7, pp. 966-971, 2008.

[116] A. Sinitskii and J. M. Tour, "Lithographic Graphitic Memories," *ACS Nano,* vol. 3, pp. 2760-2766, 2009.

[117] Y. Zheng, *et al.*, "Gate-controlled nonvolatile graphene-ferroelectric memory," *Applied Physics Letters,* vol. 94, 2009.

[118] X. Wang, *et al.*, "Transparent, Conductive Graphene Electrodes for Dye-Sensitized Solar Cells," *Nano Letters,* vol. 8, pp. 323-327, 2007.

[119] X. Li, *et al.*, "Graphene-On-Silicon Schottky Junction Solar Cells," *Advanced Materials,* vol. 22, pp. 2743-2748, 2010.

[120] J. Wu, *et al.*, "Organic solar cells with solution-processed graphene transparent electrodes," *Applied Physics Letters,* vol. 92, pp. 263302, 2008.

[121] P. Blake, *et al.*, "Graphene-Based Liquid Crystal Device," *Nano Letters,* vol. 8, pp. 1704-1708, 2008.

[122] J. Wu, *et al.*, "Organic Light-Emitting Diodes on Solution-Processed Graphene Transparent Electrodes," *ACS Nano,* vol. 4, pp. 43-48, 2009.

[123] S. Vivekchand, *et al.*, "Graphene-based electrochemical supercapacitors," *Journal of Chemical Sciences,* vol. 120, pp. 9-13, 2008.

[124] Y. Wang, *et al.*, "Supercapacitor Devices Based on Graphene Materials," *The Journal of Physical Chemistry C,* vol. 113, pp. 13103-13107, 2009.

[125] S. Chen, *et al.*, "Graphene Oxide−MnO2 Nanocomposites for Supercapacitors," *ACS Nano,* vol. 4, pp. 2822-2830, 2010.

[126] S.-M. Paek, *et al.*, "Enhanced Cyclic Performance and Lithium Storage Capacity of SnO2/Graphene Nanoporous Electrodes with Three-Dimensionally Delaminated Flexible Structure," *Nano Letters,* vol. 9, pp. 72-75, 2008.

[127] K. B. S. Jeong K.Lee, Cary M.Hayner and Harold H.Kung, "Silicon nanoparticles-graphene paper composites for Li ion battery anodes," *Chem.Commun.,* vol. 46, pp. 2025-2027, 2010.

[128] J. T. Robinson, *et al.*, "Reduced Graphene Oxide Molecular Sensors," *Nano Letters,* vol. 8, pp. 3137-3140, 2008.

[129] Y. Dan, *et al.*, "Intrinsic Response of Graphene Vapor Sensors," *Nano Letters,* vol. 9, pp. 1472-1475, 2008.

[130] Y. Ohno, *et al.*, "Electrolyte-Gated Graphene Field-Effect Transistors for Detecting pH and Protein Adsorption," *Nano Letters,* vol. 9, pp. 3318-3322, 2009.

[131] G. g. F. Schneider, *et al.*, "DNA Translocation through Graphene Nanopores," *Nano Letters,* pp. 3163-3167, 2010.

[132] Y. Shao, *et al.*, "Graphene Based Electrochemical Sensors and Biosensors: A Review," *Electroanalysis,* vol. 22, pp. 1027-1036, 2010.

[133] M. Pumera, *et al.*, "Graphene for electrochemical sensing and biosensing," *TrAC Trends in Analytical Chemistry,* vol. 29, pp. 954-965, 2010.

[134] W. Choi, *et al.*, "Synthesis of Graphene and Its Applications: A Review," *Critical Reviews in Solid State and Materials Sciences,* vol. 35, pp. 52-71, 2010.

[135] W. Yang, *et al.*, "Carbon Nanomaterials in Biosensors: Should You Use Nanotubes or Graphene?," *Angewandte Chemie International Edition,* vol. 49, pp. 2114-2138, 2010.

[136] M. C. Lemme, *et al.*, "A Graphene Field-Effect Device," *Electron Device Letters, IEEE,* vol. 28, pp. 282-284, 2007.

[137] J. H. Chen, *et al.*, "Charged-impurity scattering in graphene," *Nature Physics,* vol. 4, pp. 377-381, 2008.

[138] J. Martin, *et al.*, "Observation of electron-hole puddles in graphene using a scanning single-electron transistor," *Nature Physics,* vol. 4, pp. 144-148, 2008.

[139] T. Ando, "Screening effect and impurity scattering in monolayer graphene," *Journal of the Physical Society of Japan,* vol. 75, pp. 074716, 2006.

[140] E. H. Hwang, *et al.*, "Carrier Transport in Two-Dimensional Graphene Layers," *Physical Review Letters,* vol. 98, pp. 186806, 2007.

[141] K. Nomura and A. H. MacDonald, "Quantum Transport of Massless Dirac Fermions," *Physical Review Letters,* vol. 98, pp. 076602, 2007.

[142] V. V. Cheianov and V. I. Fal'ko, "Friedel Oscillations, Impurity Scattering, and Temperature Dependence of Resistivity in Graphene," *Physical Review Letters,* vol. 97, pp. 226801, 2006.

[143] S. Adam, *et al.*, "A self-consistent theory for graphene transport," *Proceedings of the National Academy of Sciences of the United States of America,* vol. 104, pp. 18392-18397, 2007.

[144] V. M. Galitski, *et al.*, "Statistics of random voltage fluctuations and the low-density residual conductivity of graphene," *Physical Review B,* vol. 76, p. 245405, 2007.

[145] L. A. Ponomarenko, *et al.*, "Effect of a High- kappa Environment on Charge Carrier Mobility in Graphene," *Physical Review Letters,* vol. 102, pp. 206603, 2009.

[146] T. O. Wehling, *et al.*, "Local electronic signatures of impurity states in graphene," *Physical Review B,* vol. 75, pp. 125425, 2007.

[147] F. Miao, *et al.*, "Phase-Coherent Transport in Graphene Quantum Billiards," vol. 317, pp. 1530-1533, 2007.

[148] K. I. Bolotin, *et al.*, "Ultrahigh electron mobility in suspended graphene," *Solid State Communications,* vol. 146, pp. 351-355, 2008.

[149] M. I. Katsnelson, "Zitterbewegung, chirality, and minimal conductivity in graphene," *The European Physical Journal B - Condensed Matter and Complex Systems,* vol. 51, pp. 157-160, 2006.

[150] J. Tworzydlo, *et al.*, "Sub-Poissonian Shot Noise in Graphene," *Phys.Rev.Lett.*, vol. 96 , pp. 246802, 2006.

[151] Y.-M. Lin, *et al.*, "100-GHz Transistors from Wafer-Scale Epitaxial Graphene," *Science,* vol. 327, pp. 662, 2010.

[152] L. M. Zhang and M. M. Fogler, "Nonlinear Screening and Ballistic Transport in a Graphene p-n Junction," *Physical Review Letters,* vol. 100, pp. 116804, 2008.

[153] M. I. Katsnelson, "Nonlinear screening of charge impurities in graphene," *Physical Review B,* vol. 74, pp. 201401, 2006.

[154] C. Jang, *et al.*, "Tuning the effective fine structure constant in graphene: Opposing effects of dielectric screening on short- and long-range potential scattering," *Physical Review Letters,* vol. 101, pp. 146805, 2008.

[155] F. Chen, *et al.*, "Dielectric Screening Enhanced Performance in Graphene FET," *Nano Letters,* vol. 9, pp. 2571-2574, 2009.

[156] F. Chen, *et al.*, "Ionic Screening of Charged-Impurity Scattering in Graphene," *Nano Letters,* vol. 9, pp. 1621-1625, 2009.

[157] S. V. Morozov, *et al.*, "Giant intrinsic carrier mobilities in graphene and its bilayer," *Physical Review Letters*, vol. 100, pp. 016602, 2008.

[158] M. G. Victor, *et al.*, "Statistics of random voltage fluctuations and the low-density residual conductivity of graphene," *Physical Review B*, vol. 76, pp. 245405, 2007.

[159] K. Seyoung, *et al.*, "Realization of a high mobility dual-gated graphene field-effect transistor with Al_2O_3 dielectric," *Applied Physics Letter*, vol 94, pp. 062107, 2009.

[160] J. L. Xia, *et al.*, "The transport and quantum capacitance properties of epitaxial graphene," *Applied Physics Letters*, vol. 96, pp. 162101, 2010.

[161] http://www.engineeringarts.com.

[162] T. Lohmann, *et al.*, "Four-Terminal Magneto-Transport in Graphene p-n Junctions Created by Spatially Selective Doping," *Nano Letters*, vol. 9, pp. 1973-1979, 2009.

[163] E. S. Snow, *et al.*, "Chemical Detection with a Single-Walled Carbon Nanotube Capacitor," *Science*, vol. 307, pp. 1942-1945, 2005.

[164] M. Trushin and J. Schliemann, "Minimum electrical and thermal conductivity of graphene: A quasiclassical approach," *Physical Review Letters*, vol. 99, pp.216602, 2007.

[165] C. Zhihong and J. Appenzeller, "Mobility extraction and quantum capacitance impact in high performance graphene field-effect transistor devices," *Electron Devices Meeting, 2008. IEDM 2008. IEEE International*, pp. 1-4, 2008.

[166] D. L. John, *et al.*, "Quantum capacitance in nanoscale device modeling," *Journal of Applied Physics*, vol. 96, pp. 5180-5184, 2004.

[167] T. Fang, *et al.*, "Carrier statistics and quantum capacitance of graphene sheets and ribbons," *Applied Physics Letters*, vol. 91, pp. 092109, 2007.

[168] F. Giannazzo, *et al.*, "Screening Length and Quantum Capacitance in Graphene by Scanning Probe Microscopy," *Nano Letters*, vol. 9, pp. 23-29, 2009.

[169] S. Luryi, "Quantum Capacitance Devices," *Applied Physics Letters*, vol. 52, pp. 501-503, 1988.

[170] http://www.semicorp.com.

[171] L. B. Gao, *et al.*, "Total color difference for rapid and accurate identification of graphene," *Acs Nano,* vol. 2, pp. 1625-1633, 2008.

[172] A. Das, *et al.*, "Monitoring dopants by Raman scattering in an electrochemically top-gated graphene transistor," *Nature Nanotechnology,* vol. 3, pp. 210-215, 2008.

[173] M. Ishigami, *et al.*, "Atomic structure of graphene on SiO2," *Nano Letters,* vol. 7, pp. 1643-1648, 2007.

[174] E. Stolyarova, *et al.*, "High-resolution scanning tunneling microscopy imaging of mesoscopic graphene sheets on an insulating surface," *Proceedings of the National Academy of Sciences of the United States of America,* vol. 104, pp. 9209-9212, 2007.

[175] S. Baldelli, "Surface structure at the ionic liquid-electrified metal interface," *Accounts of Chemical Research,* vol. 41, pp. 421-431, 2008.

[176] S. Cho and M. S. Fuhrer, "Charge transport and inhomogeneity near the minimum conductivity point in graphene," *Physical Review B,* vol. 77, 2008.

[177] J. P. Randin and E. Yeager, "Differential Capacitance Study of Stress/Annealed Pyrolytic Graphite Electrodes," *Journal of the Electrochemical Society,* vol. 118, pp. 711-714, 1971.

[178] J. O. M. Bockris, *Modern Electrochemistry:An Introduction to an Interdisciplinary Area*, 1 ed. New York: Plenum Press, 1970.

[179] J. P. Randin and E. Yeager, "Differential Capacitance Study on Basal Plane of Stress-Annealed Pyrolytic-Graphite," *Journal of Electroanalytical Chemistry,* vol. 36, pp. 257-260, 1972.

[180] F. Chen, *et al.*, "Ionic Screening of Charged-Impurity Scattering in Graphene," *Nano Lett.*, vol. 9, pp. 1621-1625, 2009

[181] S. Y. Zhou, *et al.*, "First direct observation of Dirac fermions in graphite," *Nature Physics,* vol. 2, pp. 595-599, 2006.

[182] B. Partoens and F. M. Peeters, "From graphene to graphite: Electronic structure around the K point," *Physical Review B,* vol. 74, pp. 075404, 2006.

[183] M. Edward and I. F. k. Vladimir, "Landau-Level Degeneracy and Quantum Hall Effect in a Graphite Bilayer," *Physical Review Letter,* vol. 96, pp. 086805, 2006.

[184] A. K. Geim, "Graphene: Status and Prospects," *Science*, vol. 324, pp. 1530-1534, 2009.

[185] J. Kedzierski, *et al.*, "Epitaxial graphene transistors on SIC substrates," *Ieee Transactions on Electron Devices*, vol. 55, pp. 2078-2085, 2008.

[186] J. Xia, *et al.*, "Measurement of the quantum capacitance of graphene," *Nat Nano*, vol. 4, pp. 505-509, 2009.

[187] B. L. V. Kok-Keong Lew, Rachael L.Myers-Ward, Ronald T.Holm, Charles R.Eddy, Jr. and D.Kurt Gaskill, "Etching of 4 and 8 4H-SiC using various hydrogen propane mixtures in a commercial hot wall CVD reactor," *Materials Science Forum*, vol. 556-557, pp. 513-516, 2007.

[188] C. R. Dong Su Lee, Benjamin Krauss, Klaus von Klitzing, Ulrich Starke, and Jurgen H.Smet, "Raman Spectra of Epitaxial Graphene on SiC and of Epitaxial Graphene Transferred to SiO2," *Nano Letters*, vol. 8, pp. 4320-4325, 2008.

[189] W. Norimatsu and M. Kusunoki, "Transitional structures of the interface between graphene and 6H-SiC (0 0 0 1)," *Chemical Physics Letters*, vol. 468, pp. 52-56, 2009.

[190] F. Varchon, *et al.*, "Electronic Structure of Epitaxial Graphene Layers on SiC: Effect of the Substrate," *Physical Review Letters*, vol. 99, pp. 126805, 2007.

[191] L. Patrick and W. J. Choyke, "Static Dielectric Constant of SiC," *Physical Review B*, vol. 2, pp. 2255, 1970.

APPENDIX A

BOLTZMANN TRANSPORT THEORY

In classic Boltzmann theory of semiconductor transport, the electron transport is described by a statistical distribution function, $f(\vec{r},\vec{k},t)$, which describes the probability that an electron is located at a point $\vec{k}$ in the reciprocal space and a point $\vec{r}$ in the real space at a certain time t. The distribution function has to satisfy certain constrains, which is the famous Boltzmann Transport Equation (BTE):

$$\frac{df}{dt} + \vec{v} \cdot \nabla_r f + \vec{F} \cdot \nabla_p f = \left.\frac{\partial f}{\partial t}\right|_{collision} + S(\vec{r}, \vec{p}, t) \tag{A.1}$$

where S is the generation-recombination rate. Once this distribution function is known , the transport properties can be extracted by

$$\begin{aligned} n(\vec{r},t) &= \frac{1}{V}\sum_k f(\vec{r},\vec{k},t) \\ J(\vec{r},t) &= -\frac{e}{V}\sum_k \vec{v}(\vec{k}) f(\vec{r},\vec{k},t) \\ w(\vec{r},t) &= \frac{1}{V}\sum_k E(\vec{k}) f(\vec{r},\vec{k},t) \end{aligned} \tag{A.2}$$

So, the key point is solving the BTE. One important assumption is the Relaxation Time Approximation (RTA), which is:

$$\left.\frac{\partial f}{\partial t}\right|_{collision} = -\frac{f - f_0}{\tau} \tag{A.3}$$

$$\Rightarrow f(t) = f_0 + (f - f_0)e^{-t/\tau} \tag{A.4}$$

where τ is the relaxation time, in this way, we can get(no generation-recombination is involved(S=0), steady state($\frac{df}{dt} = 0$)and uniformly doped($\nabla_r f = 0$), from (A.1),

$$\vec{F}\cdot\nabla_p f = \frac{1}{\hbar}\vec{F}\cdot\nabla_k f = \left.\frac{\partial f}{\partial t}\right|_{collision} \tag{A.5}$$

or
$$-e\vec{E}\nabla_k f = \left.\frac{\partial f}{\partial t}\right|_{collision} \tag{A.6}$$

$$\begin{aligned} f(k) &= f_0(k) - \frac{\tau}{\hbar}\vec{F}\cdot\frac{\partial f(k)}{\partial k} \\ &= f_0(k) - \frac{\tau}{\hbar}\vec{F}\cdot\vec{v}\frac{\partial f(k)}{\partial E} \\ &\approx f_0(k) - \frac{\tau}{\hbar}\vec{F}\cdot\vec{v}\frac{\partial f_0(k)}{\partial E} \end{aligned} \tag{A.7}$$

for the $\left.\frac{\partial f}{\partial t}\right|_{collison}$, it can be described as:

$$\left.\frac{\partial f}{\partial t}\right|_{collison} = \sum_{k'}[(P(\vec{k}',\vec{k})f(\vec{k}')(1-f(\vec{k})) - P(\vec{k},\vec{k}')f(\vec{k})(1-f(\vec{k}')] \tag{A.8}$$

If the scattering is elastic, $E(\vec{k}) = E(\vec{k}')$ and $P(\vec{k}) = P(\vec{k}')$, then

$$\begin{aligned} \left.\frac{\partial f}{\partial t}\right|_{collison} &= -\int d^2 S_{k'} P(\vec{k},\vec{k}')\tau F\cdot(\vec{v}-\vec{v}')\frac{\partial f_0}{\partial E} \\ &= -(f-f_0)\int_{S_{k'}} P(\vec{k},\vec{k}')(1-\cos\theta)d^2 S_{k'} \end{aligned} \tag{A.9}$$

Then the conductivity can be calculated by (A.2) and (A.7) (3D case):

$$\begin{aligned} J &= -e\int d^3 k\rho(k)\vec{v}f(E) = -e\int dE\rho(E)\vec{v}f(E) \\ &= -e\int dE\rho(k)\vec{v}f_0(E) - e^2\int dE\,\tau_m\rho(E)v(\vec{F},\vec{v})\frac{\partial f_0(E)}{\partial \mathrm{E}} \\ &= -eF\int dE\,\tau_m {v_F}^2\frac{\partial f_0(E)}{\partial E} \end{aligned} \tag{A.10}$$

Combined with $n = \int dE\rho(E)f_0(E)$, one can get:

$$J = \frac{ne^2 < \tau_m >}{m^*}E = ne\mu \tag{A.11}$$

Where m^* is the effective mass of electron, μ, defined as $\mu = \frac{e < \tau_m >}{m^*}$, is called mobility. Notes that:

$$< \tau_m >\Big|_{3D} = \frac{\int_0^\infty E^{3/2} \tau_m(E) \frac{\partial f_0(E)}{\partial E} dE}{\int_0^\infty E^{3/2} \frac{\partial f_0(E)}{\partial E} dE} \tag{A.12}$$

which can be extended to every dimension by:

$$< \tau_m >\Big|_{d} = \frac{\int_0^\infty E^{d/2} \tau_m(E) \frac{\partial f_0(E)}{\partial E} dE}{\int_0^\infty E^{d/2} \frac{\partial f_0(E)}{\partial E} dE} \tag{A.13}$$

The above is the BTE for semiconductor materials, as we know graphene is different from traditional semiconductor material, for the massless electron. When applied BTE for graphene, one can use

$$m^* = \frac{E_F}{v_F{}^2} = \frac{k_F}{v_F} \tag{A.14}$$

$$\text{so} \qquad \sigma = ne\mu = ne^2 \frac{< \tau_m >}{m^*} = \frac{k_F{}^2}{\pi} e^2 \frac{v_F}{k_F} < \tau_m >= \frac{2e^2}{h} E_F < \tau_m > \tag{A.15}$$

Then, the question becomes how to solve the relaxation time, which is affected by the scattering center. There are several kinds of scattering centers in graphene, such as charged impurities in graphene/substrate interface, defects in graphene, as well as corrugation of graphene.

APPENDIX B

HYSTERESIS IN GRAPHENE

Just like other carbon materials, such as carbon nanotube, graphene also shows a hysteresis in transport properties, and we observed hysteresis in quantum capacitance too, shown in Fig. B1. The hysteresis was usually attributed to the environment interactions from adsorbates, especially water molecules. And people has observed that this hysteresis depends on sweeping rate of gate voltage, sweeping range of gate voltage, as well as starting voltage[1] and temperature[2]. A recent study[3] indicated that the substrate surface chemistry plays an key role in this hysteresis, which can supply bonding states to water molecules. This SiO2 surface bound water can't be desorbed in vacuum at room temperature, but heating in vacuum can.

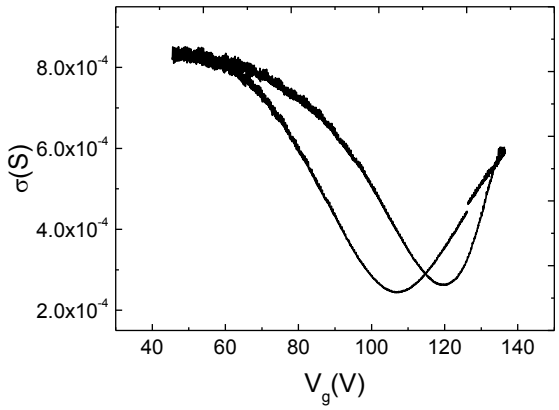

(A)

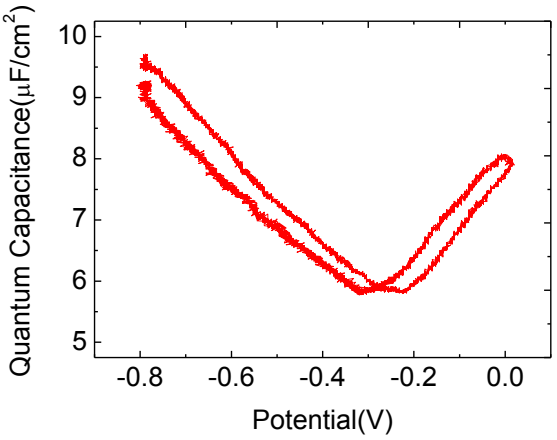

(B)

Figure B1. Hystersis in Graphene: (A) Transport Properties; (B) Quantum Capacitance

A more detailed study on graphene transport hysteresis was reported by Wang et al.[4], who observed two kinds of hysteresis: charge transfer induced positive shift and capacitive gating induced negative shift, shown in Fig. B2. The charge transfer induced positive shift is normally observed, which is due to the adsorption of water molecules described as before. While capacitive gating induced negative shift is new reported, which was observed in electrochemical gate configuration, or with interaction of dipole molecules(water or ice). All these experiments supply additional information about graphene transport, which can help us to understand and use graphene better.

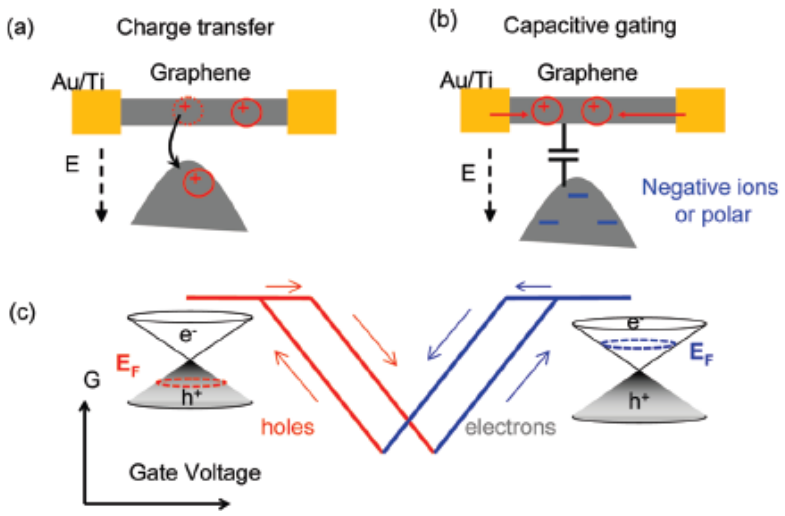

Figure B2. Hystersis in Graphene: (A) Charge Transfer Induced Positive Shift; (B) Capacitive Gating Induced Negative Shift; (c) Schematic diagram of Hysteresis of these two forms[4].

References

[1]Lohmann, T. et al. "Four-Terminal Magneto-Transport in Graphene p-n Junctions Created by Spatially Selective Doping", Nano Nano, vol. 9, pp. 1973-1979, 2009

[2]Liao, Z. et al. "Hystersis reversion in graphene field-effect transistors", *J. Chem. Phys.*, vol.133, pp. 044703, 2010.

[3]Josh, P. et al. "Intrinsic doping and gate hysteresis in graphene field effect device fabricated on SiO2 substrate", *J. Phys.Cond.Matt.* , vol.22 , pp. 334214, 2010.

[4]Wang, H. et al. "Hysteresis of Electronic Transport in Graphene Transistors", *ACS.Nano.* ,published on line, 2010.